

# **Determination of methyl halide emissions from measurements and mesoscale atmospheric model simulations**

**Dissertation  
zur Erlangung des Doktorgrades  
der Naturwissenschaften im Department  
Geowissenschaften  
der Universität Hamburg**

**Vorgelegt von  
Seshagiri Rao Kolusu  
aus  
Maddulaparva, Indien**

**Hamburg  
2013**

Als Dissertation angenommen vom  
Department Geowissenschaften der Universität Hamburg  
auf Grund der Gutachten von

Prof. Dr. K. Heinke Schlünzen  
und  
Dr. Richard Seifert

Hamburg, den 10. Juli 2013

Professor Dr. Christian Betzler  
(Leiter des Department Geowissenschaften)

## Abstract

Methyl chloride ( $\text{CH}_3\text{Cl}$ ) and methylene chloride ( $\text{CH}_2\text{Cl}_2$ ) are known to have natural and anthropogenic sources to the atmosphere. From recent studies it is known that tropical and sub tropical plants are primary sources for atmospheric methyl chloride. The budgets of  $\text{CH}_3\text{Cl}$  and  $\text{CH}_2\text{Cl}_2$  are imbalanced primarily due to large uncertainties in the source estimates for these compounds. In this thesis emissions of the two chlorinated methanes,  $\text{CH}_3\text{Cl}$  and  $\text{CH}_2\text{Cl}_2$  from the tropical Atlantic Ocean and mangrove forest region are quantified.

The variation of  $\text{CH}_3\text{Cl}$  and  $\text{CH}_2\text{Cl}_2$  concentrations in the air and seawater has been analyzed as a function of latitude using Meteor cruise data (M78/2). There is no correlation found between  $\text{CH}_3\text{Cl}$  and  $\text{CH}_2\text{Cl}_2$  concentrations in the seawater. This leads to the suggestion that they may not have a common oceanic source. The diurnal cycle of concentrations, fluxes and sea surface temperature (SST) were studied to determine a dependency of concentrations and fluxes on SST. SST does not show any significant effect on  $\text{CH}_2\text{Cl}_2$  concentrations in surface seawater.  $\text{CH}_3\text{Cl}$  and  $\text{CH}_2\text{Cl}_2$  are supersaturated in the seawater during the cruise. This implies that the tropical Atlantic Ocean emits  $\text{CH}_3\text{Cl}$  and  $\text{CH}_2\text{Cl}_2$  into the atmosphere. The tropical Atlantic Ocean mean fluxes of  $\text{CH}_3\text{Cl}$  and  $\text{CH}_2\text{Cl}_2$  during the cruise were  $150 \text{ nmol m}^{-2} \text{ d}^{-1}$  and  $81 \text{ nmol m}^{-2} \text{ d}^{-1}$ , respectively. Sources of  $\text{CH}_3\text{Cl}$  and  $\text{CH}_2\text{Cl}_2$  were determined by calculating backward trajectories. The backward trajectories revealed that the tropical Atlantic Ocean and the African coast (also inland) were primary and secondary source regions for methyl halides, respectively, during the Meteor cruise.

In order to quantify the biogenic emissions of methyl halides from mangroves, field measurement were conducted in the tropical mangrove forest at the coast of Brazil. A mesoscale atmospheric model, METRAS, was used to simulate passive tracer's concentrations and to study the dependency of concentrations on type of emission function and meteorology. Model simulated concentrations were normalized using the observed field data. With the help of the mesoscale model results and the observed data the mangrove emission were estimated at the local scale. By using this "bottom-up" approach the global emissions of methyl halides from mangroves were quantified. The emission range obtained with different emission functions and different meteorology are  $4\text{--}7 \text{ Gg yr}^{-1}$  for  $\text{CH}_3\text{Cl}$  and  $1\text{--}2 \text{ Gg yr}^{-1}$  for  $\text{CH}_2\text{Cl}_2$ . Based on the present study the mangroves contribute 0.3 percent of  $\text{CH}_2\text{Cl}_2$  and 0.2 percent of  $\text{CH}_3\text{Cl}$  in the global emission budget. Manley et al. (2007)

estimated that the mangroves produce 0.3 percent of CH<sub>3</sub>Cl in the global emission budget. This study supports the Manley et al. (2007) study. From the detailed analyses of the model results it can be concluded that meteorology has a larger influence on the variability in the concentrations than constant emissions or humidity dependent emission functions.

## Zusammenfassung

Es ist bekannt, dass die Quellen von Methylchlorid ( $\text{CH}_3\text{Cl}$ ) und Dichlormethan ( $\text{CH}_2\text{Cl}_2$ ) in der Atmosphäre sowohl natürlichen als auch anthropogenen Ursprungs sind. Aktuelle Studien nennen tropische und subtropische Pflanzen als primäre Quelle des atmosphärischen Methylchlorids. Die Unsicherheiten in den Bilanzen von  $\text{CH}_3\text{Cl}$  und  $\text{CH}_2\text{Cl}_2$  werden größtenteils durch Unsicherheiten in der Bestimmung der Quellstärken verursacht. In dieser Arbeit werden die Emissionen aus dem tropischen Atlantischen Ozean und aus einem Mangrovenwald für zwei chlorierte Methane,  $\text{CH}_3\text{Cl}$  und  $\text{CH}_2\text{Cl}_2$ , quantifiziert.

Die Variabilität der  $\text{CH}_3\text{Cl}$  und  $\text{CH}_2\text{Cl}_2$  Konzentrationen in der Luft und im Meerwasser wurden als Funktion der geographischen Breite unter Verwendung von Daten, die auf der der Fahrt M78/2 des Forschungsschiffes Meteor gesammelt wurden, analysiert. Es konnten keine Korrelationen zwischen  $\text{CH}_3\text{Cl}$  und  $\text{CH}_2\text{Cl}_2$  Konzentrationen im Meerwasser gefunden werden. Dies deutet darauf hin, dass sie keine gemeinsame Quelle im Ozean besitzen. Der Tagesgang der Konzentrationen, der Flüsse und der Meeresoberflächentemperatur (sea surface temperature (SST)) wurde untersucht, um die Abhängigkeit der Konzentrationen und Flüsse von der SST zu bestimmen. Die SST zeigt keinen signifikanten Effekt auf die  $\text{CH}_2\text{Cl}_2$  Konzentrationen im Meerwasser.  $\text{CH}_3\text{Cl}$  und  $\text{CH}_2\text{Cl}_2$  waren während der Fahrt M78/2 im Meerwasser übersättigt. Das impliziert, dass der tropische Atlantische Ozean  $\text{CH}_3\text{Cl}$  und  $\text{CH}_2\text{Cl}_2$  in die Atmosphäre emittiert. Der mittlere Fluss von  $\text{CH}_3\text{Cl}$  und  $\text{CH}_2\text{Cl}_2$  aus dem tropischen Atlantischen Ozean war  $150 \text{ nmol m}^{-2} \text{ d}^{-1}$  und  $81 \text{ nmol m}^{-2} \text{ d}^{-1}$  während der Fahrt M78/2. Quellen von  $\text{CH}_3\text{Cl}$  und  $\text{CH}_2\text{Cl}_2$  wurden durch die Berechnung von Rückwärtstrajektorie bestimmt. Die Berechnung der Rückwärtstrajektorien ergab, dass der tropische Atlantische Ozean die primäre und die Afrikanische Küste (auch Inland) die sekundäre Quellregion für halogeniertes Methan während der Fahrt M78/2 waren.

Um die biogene Emission halogener Methane von Mangroven zu quantifizieren wurden Feldmessungen im Mangrovenwald an der Küste von Brasilien durchgeführt. Das mesoskalige Atmosphärenmodell METRAS wurde verwendet, um die Konzentrationen der passiven Tracer und die Abhängigkeit der Konzentrationen von der Wahl der Emissionsfunktion und der Meteorologie zu untersuchen. Die mit METRAS simulierten Konzentrationen wurden mit den Daten aus den Feldmessungen normalisiert. Mit der Hilfe der Modellergebnisse und der Feldmessung wurden die Emissionen der Mangroven auf einer lokalen Skala bestimmt. Unter Verwendung dieses "bottom-up" Ansatzes wurde die globale

Emission von halogenierten Methane aus Mangroven quantifiziert. Die erhaltenen Ergebnisse für die Emission unter der Nutzung unterschiedlicher Emissionsfunktionen und unterschiedlicher Meteorologie liegen im Bereich von 4–7 Gg yr<sup>-1</sup> für CH<sub>3</sub>Cl und 1–2 Gg yr<sup>-1</sup> für CH<sub>2</sub>Cl<sub>2</sub>. Basierend auf Daten der vorgestellten Studie liegt der Anteil von Mangroven am globalen Emissionshaushalt bei 0.3 Prozent für CH<sub>2</sub>Cl<sub>2</sub> und 0.2 Prozent für CH<sub>3</sub>Cl. Manley et al. (2007) sehen den Anteil von Mangroven am globalen Emissionshaushalt bei 0.3 Prozent für CH<sub>3</sub>Cl. Diese Studie bekräftigt das Ergebnis von Manley et al. (2007). Aus einer detaillierten Analyse der Modellergebnisse kann geschlossen werden, dass die Meteorologie einen größeren Einfluss auf die Variabilität der Konzentrationen hat als die zeitliche Variationen der Emission.

# Contents

Abstract.....	i
Zusammenfassung.....	iii
1 Introduction.....	1
1.1 Sources and sinks of methyl halides in the atmosphere.....	1
1.1.1 Sources and sinks of methyl chloride.....	2
1.1.2 Sources and sinks of methyl bromide.....	3
1.1.3 Sources and sinks of methylene chloride.....	5
1.1.4 Summary of the atmospheric global budgets of methyl halides.....	6
1.2 Importance of methyl halides in the atmosphere.....	7
1.2.1 Chapman mechanism.....	8
1.2.2 Catalytic destruction of ozone by chlorine and bromine.....	8
1.3 Aims of this thesis.....	9
2. Background concentrations and emissions of methyl halides over the tropical Atlantic Ocean 11	
2.1 Introduction.....	11
2.2 Variation of methyl chloride and methylene chloride in air and seawater.....	12
2.3 Quantifying emissions of methyl halides from the tropical Atlantic Ocean.....	17
2.3.1 Flux calculation of methyl chloride and methylene chloride.....	17
2.3.2 Diurnal cycle of concentrations and fluxes over the tropical Atlantic Ocean ..	23
2.3.3 Significance of sea surface temperature on concentrations and fluxes of methyl halides	25
2.4. Identification of methyl halides source regions using HYSPLIT back trajectories. 27	
2.4.1 HYSPLIT model setup.....	27
2.4.2 HYSPLIT results for the Meteor cruise.....	28
2.5 Conclusions.....	31
3. Observational data.....	33
3.1 Introduction.....	33
3.2 Data from the literature survey.....	33
3.3 Field experiment in Braganca.....	34
3.3.1 Experimental setup and data to be measured.....	35
3.3.2 Observed concentrations from Braganca.....	39
3.4 Conclusions.....	41
4. Adaptation and application of METRAS to the Braganca region.....	42
4.1 Relevant qualities of the model METRAS.....	42

4.2	Selected model domain and input data.....	43
4.3	Adaptation of METRAS land-use classes to the tropical region of Braganca .....	46
4.3.1	Adaptation of land-use class water .....	48
4.3.2	Adaptation of land-use class mudflats to wetland with mangroves.....	49
4.3.3	Adaptation of land-use class savannas.....	52
4.3.4	Adaptation of mixed land-use class .....	54
4.3.5	Adaptation of land-use class meadows .....	55
4.3.6	Adaptation of land-use class heath to shrubs .....	57
4.3.7	Adaptation of land-use class bushes .....	59
4.3.8	Adaptation of land-use class mixed forests .....	60
4.3.9	Adaptation of land-use class coniferous forest .....	63
4.3.10	Adaptation of urban land-use class .....	64
4.4	Meteorology results from METRAS over the tropical Braganca region .....	66
4.4.1	Qualitative analyses .....	67
4.4.2	Quantitative comparison .....	73
4.5	Conclusions .....	77
5.	Role of meteorology and emission functions for concentration values .....	79
5.1	Introduction .....	79
5.2	Emissions in the model domain and emission functions used .....	80
5.3	Determination of the different impacts on concentrations .....	84
5.3.1	Impact of meteorology on concentrations of methyl halides in a coastal mangrove region .....	84
5.3.2	Impact of time dependent emission functions on concentrations .....	90
5.3.3	Frequency distributions to quantify impacts.....	95
5.4	Contribution of different emission sources to the coastal concentrations.....	98
5.5	Determination of methyl halide emissions from mangroves .....	106
5.6	Conclusions .....	107
6.	Conclusions and future work .....	109
	Acknowledgements.....	112
	Acronyms.....	114
	References.....	116

## **1 Introduction**

Halocarbons (where one or more hydrogen atoms are replaced by a halogen atom, i.e. fluorine (F), chlorine (Cl), bromine (Br) and iodine (I)), such as methyl chloride (chloromethane) ( $\text{CH}_3\text{Cl}$ ), methyl bromide (bromomethane) ( $\text{CH}_3\text{Br}$ ), and methylene chloride ( $\text{CH}_2\text{Cl}_2$ ) are precursors of reactive halogens, which contribute to the destruction of stratospheric ozone (Clerbaux and Cunnold, 2007), and in the case of methyl iodide (iodomethane) ( $\text{CH}_3\text{I}$ ), also to the formation of aerosols in the marine boundary layer (Carpenter, 2003). To date, there are still large uncertainties concerning their atmospheric budgets. This particularly holds true for  $\text{CH}_3\text{Br}$ , whose known sinks exceed the known sources by more than 20% (Yvon-Lewis et al., 2009). Though recent modeling and field studies suggest that the atmospheric budget of  $\text{CH}_3\text{Cl}$  can be closed by large emissions from tropical forests (Gebhardt et al., 2008; Saito and Yokouchi, 2008), the strength of the known distinct sources are assigned with large uncertainties. Even less is known about the natural sources of methylene chloride.

These methyl halides play a very important role in the atmospheric chemical processes. Their present globally surface averaged mixing ratios are 545 pptv (parts per trillion) for  $\text{CH}_3\text{Cl}$  and 7.5 pptv for  $\text{CH}_3\text{Br}$  (WMO, 2010). In the case of  $\text{CH}_2\text{Cl}_2$  average mixing ratios in the atmosphere range from 8.7 pptv at Cape Grim (Tasmania) to 30.2 pptv at Mace Head (Ireland) (Simmonds et al., 2006). The  $\text{CH}_3\text{I}$ , mixing ratio in the atmosphere is within the range of 0.1 - 3 pptv over the open ocean (Singh et al., 1983; Yokouchi et al., 2001 and reference therein). The estimated atmospheric life times are 1.0 yr, 0.8 yr and 0.5 yr for  $\text{CH}_3\text{Cl}$ ,  $\text{CH}_3\text{Br}$  and  $\text{CH}_2\text{Cl}_2$  respectively (WMO, 2010). These atmospheric life times are large enough that they can be transported into the stratosphere via convective processes in the Intertropical Convergence Zone (ITCZ) (Gebhardt et al., 2008).

### **1.1 Sources and sinks of methyl halides in the atmosphere**

This section provides a brief overview of the different sources and sinks of mono methyl halides, namely methyl chloride, methyl bromide and methylene chloride as quantified and outlined in the Scientific Assessment for Ozone Depletion (WMO, 2007; 2010) and some additional references in the literature.

### 1.1.1 Sources and sinks of methyl chloride

Methyl chloride is known to have both, natural as well as industrial sources. The most important industrial use of methyl chloride is the production of silicon polymers. However, industrial processes are responsible for only a minor portion of the atmospheric CH<sub>3</sub>Cl (Clerbaux and Cunnold, 2007) while the majority of atmospheric CH<sub>3</sub>Cl has natural sources. The known natural sources are oceans, tropical and subtropical plants, biomass burning, wet lands, rice paddies, salt marshes, biogenic production by vascular plants, abiotic release from dead or senescent plant material, decay of organic matter in topsoil, tropical wood-root fungi, and mangroves (WMO, 2007; 2010 and reference therein). The known sinks of methyl chloride are oxidation by hydroxyl radicals (OH), loss to the stratosphere, reaction with chlorine radicals in the marine boundary layer, oceanic uptake to the cold waters (i.e. polar oceans) and the uptake by soils. The estimated global sources of CH<sub>3</sub>Cl are summarized in Table 1.1 and Table 1.2, respectively.

Table 1.1 Current best estimated known source strengths (Gg yr<sup>-1</sup>) for atmospheric methyl chloride.

Ecosystem	Emissions (Gg yr <sup>-1</sup> )		Reference
	Range	Best estimate	
Tropical and subtropical plants	820 - 8200	2640*	WMO, 2007 and reference therein.
Biomass burning	655 - 1125	911	Lobert et al., 1999; Keppler et al., 2005
Salt marshes	65 - 440	170	WMO, 2007 and reference therein.
Fungi	43 - 470	160	WMO, 2007 and reference therein.
Coastal oceans	19 - 98	50	Hu et al., 2010
Incineration	15 - 75	45	Keppler et al., 2005
Rice paddy	2.4 - 4.9	5	WMO, 2007 and reference therein.
Peat lands	0.9 - 43.4	5.5	Dimmer et al., 2001
Leaf litter <sup>□</sup>	-5.2 - 1900	320	Blei et al., 2010
Salt marshes including mangroves	n.q.	49	Manley et al., 2006
Wetlands	n.q.	34.7	Dimmer et al., 2001
Mangroves	n.q.	12	Manley et al., 2007
Industrial processes	n.q.	10	WMO, 2007 and reference therein
Decay of organic matter in topsoil	n.q.	n.q.	Keppler et al., 2005

\* average values based on model studies (Lee-Taylor et al., 2001; Yoshida et al., 2004), n.q. not quantified. <sup>□</sup> source was estimated from measurements of net fluxes and may be influenced by sink.

Table 1.2 Current best estimated known sink strengths ( $Gg\ yr^{-1}$ ) for atmospheric methyl chloride.

Ecosystem	Range ( $Gg\ yr^{-1}$ )	Best estimate ( $Gg\ yr^{-1}$ )	Reference
OH reaction	3800 – 4100	3180	WMO, 2007 and reference therein.
Oceans (loss to polar cold ocean waters)	93 – 145	75	WMO, 2007 and reference therein.
Cl reaction	180 – 550	370	WMO, 2007 and reference therein.
Soil	100 – 1600	1600	WMO, 2007 and reference therein.
Loss to stratosphere	100 – 300	200	WMO, 2007 and reference therein.

Until 1996, the oceans were thought to be the largest natural source of methyl chloride to the atmosphere. Later studies have demonstrated that the terrestrial sources are more important for the atmospheric budget (Moore et al., 1996; Harper and Hamilton, 2003; Montzka and Fraser, 2003; Keppler et al., 2005; WMO, 2010).

### 1.1.2 Sources and sinks of methyl bromide

Methyl bromide ( $CH_3Br$ ) also has both, natural and anthropogenic sources. Methyl bromide is an important ozone-depleting substance (ODS) and contributes about 34% of the total stratospheric bromine (Montzka et al., 2011). In the past, methyl bromide was widely used as an agricultural fumigant for different crops. However,  $CH_3Br$  production and trade was reduced according to the amendments made to the Montreal Protocol (UNEP, 1995), and the phase out began in 1998. The globally averaged surface mixing ratio of  $CH_3Br$  thus reduced from ~9.2 pptv in 1996 – 1998 to ~7.4 pptv in 2008 (Yokouchi et al., 2002b; Montzka et al., 2003; Yvon-Lewis et al., 2009). Therefore, a significant portion of  $CH_3Br$  is emitted from natural sources. The relative significance of natural  $CH_3Br$  emissions will play more and more important roles in stratospheric ozone depletion due to reduction of anthropogenic emissions of methyl bromide to the atmosphere. Table 1.3 and Table 1.4 describe the known sources and sinks of methyl bromide based on the WMO (2010) report.

Table 1.3 Current best estimated known source strengths ( $Gg\ yr^{-1}$ ) for atmospheric methyl bromide.

Ecosystem	Emissions ( $Gg\ yr^{-1}$ )		Reference
	Range	Best estimate	
Ocean	34 – 49	42	WMO, 2010 and reference therein.
Biomass Burning	10 – 40	29	WMO, 2010 and reference therein.
Based on California saltmarshes	7 – 29	14	WMO, 2010 and reference therein.
Fumigation-quarantine/pre-shipmen	7.1 – 8.1	7.6	WMO, 2010 and reference therein.
Fumigation-dispersive (soils)	4.6 – 9.0	6.7	WMO, 2010 and reference therein.
Rapeseed	4 – 6.1	5.1	WMO, 2010 and reference therein.
Mangroves	1.2 – 1.3	1.3	WMO, 2010 and reference therein.
Coastal salt marshes*	0.6 – 14	7	WMO, 2010 and reference therein.
Based on Scottish salt marsh	0.5 – 3.0	1	WMO, 2010 and reference therein.
Fungus (litter decay)	0.5 – 5.2	1.7	WMO, 2010 and reference therein.
Based on Tasmania saltmarsh	0.2 – 1.0	0.6	WMO, 2010 and reference therein.
Rice paddies	0.1 – 1.7	0.7	WMO, 2010 and reference therein.
Shrublands*	0 – 1	0.2	WMO, 2010 and reference therein.
Temperate peatlands*	-0.1 – 1.3	0.6	WMO, 2010 and reference therein.
Leaded gasoline	n.q.	<5.7	WMO, 2010 and reference therein.
Fungus (leaf-cutter ants)	n.q.	0.5	WMO, 2010 and reference therein.
Tropical trees	n.q.	18	Blei et al., 2010
Temperate woodlands	n.q.	n.q.	WMO, 2010 and reference therein.

\* sources were estimated from measurements of net fluxes and may be influenced by sinks within them, n. q. not quantified.

Table 1.4 Current best estimated known sink strengths ( $Gg\ yr^{-1}$ ) for atmospheric methyl bromide.

Ecosystem	Range ( $Gg\ yr^{-1}$ )	Best estimate ( $Gg\ yr^{-1}$ )	Reference
Ocean	49 – 52	49	WMO, 2010 and reference therein.
OH and Photolysis	n.q.	63.6	WMO, 2010 and reference therein.
Soils	19 – 44	32	WMO, 2010 and reference therein.

*n. q. is not quantified.*

Rhew et al. (2007) suggests that the Arctic tundra is a major source and sink of carbon-containing gases, but the biogeochemical cycle of halocarbons in this ecosystem is largely unexplored. They observed that the smallest net uptake rates or largest net emissions of  $CH_3Cl$  and  $CH_3Br$  are at the flooded sites, while the largest net uptake rates or smallest net emissions are at the drained sites. A study by Teh et al. (2009) suggests the Arctic tundra acting as a net sink for  $CH_3Cl$  and  $CH_3Br$ . Swanson et al. (2007) measured over polar and mid-latitude regions and confirmed a significant production of methyl halides associated with all snow or ice environments. The above authors have not up scaled the results. Therefore, the values are not shown in the Table 1.1, 1.2, 1.3 and 1.4. Rhew (2011) has shown that the tall grass prairie acts both, as a source and a sink for  $CH_3Br$  and  $CH_3Cl$ . The tall grass prairie covers 68 million hectares of North America, but only 4% remains today due to the widespread conversion to agricultural and grazing lands (Samson and Knopf, 1994). Therefore, tall grass prairie is not likely to be a globally important source or sink of methyl halides. Thus, the values are not included in Table 1.3 and 1.4.

### 1.1.3 Sources and sinks of methylene chloride

Methylene chloride or dichloromethane ( $CH_2Cl_2$ ) is used as a paint remover in foam production and fumigation. Industrial sources of methylene chloride were estimated by McCulloch et al. (1999) from audited sales data to about 580 Gg in 1990. 70% of methylene chloride emissions into the atmosphere were attributed to anthropogenic sources by Cox et al. (2003). The atmospheric life time of  $CH_2Cl_2$  is about 0.5 yr (WMO, 2010). Methylene chloride is not regulated by the Montreal Protocol due to the low impact on the stratospheric ozone destruction. A study by Moore (2004) based on cruise measurements in the North Atlantic and the Labrador Sea suggests that methylene chloride has also a marine source. Ooki and Yokouchi (2011) found indications of a  $CH_2Cl_2$  production by phytoplankton in the sea surface water between 10°S and 40°S. Another source of  $CH_2Cl_2$  is biomass burning

(Lobert et al., 1999). However, the natural sources of CH<sub>2</sub>Cl<sub>2</sub> are not well understood, hence it is not possible to provide a global budget for methylene chloride. The annual Northern Hemisphere (NH) mean concentration of CH<sub>2</sub>Cl<sub>2</sub> in air was 30.8±0.2 pptv at Mace Head, Ireland (1998-2004), and in the Southern Hemisphere (SH) 8.74±0.03 pptv at Cape Grim, Tasmania (1998-2004) (Simmonds et al., 2006). The major atmospheric removal process for CH<sub>2</sub>Cl<sub>2</sub> is destruction by the hydroxyl radical (OH) (WMO, 2007).

This study mainly focuses on the CH<sub>3</sub>Cl and CH<sub>2</sub>Cl<sub>2</sub>. Hence, source and sinks of CH<sub>3</sub>I are not explained in this thesis.

#### 1.1.4 Summary of the atmospheric global budgets of methyl halides

Significant uncertainties remain in the detailed atmospheric budget of methyl halides. Natural terrestrial ecosystems can be both, a source and a sink for methyl halides. Global budgets for methyl halides are still tainted with considerable uncertainties. Table 1.5 summarizes the global budgets of methyl halides taken from WMO (2007, 2010) and own estimates based on the above literature reviews. Methylene chloride is not yet fully explored (Section 1.1.3). Hence, a global budget of CH<sub>2</sub>Cl<sub>2</sub> is not given in the Table 1.5.

Table 1.5 Imbalance in the global budgets of methyl chloride and methyl bromide.

	Methyl bromide				Methyl chloride			
	Best estimate (Gg yr <sup>-1</sup> )		Range (Gg yr <sup>-1</sup> )		Best estimate (Gg yr <sup>-1</sup> )		Range (Gg yr <sup>-1</sup> )	
	WMO 2010	Own estimates	WMO 2010	Own estimates	WMO 2007	Own estimates	WMO 2007	Own estimates
Sources	111.5	140	69.7 – 169.7	69.7 – 142.7	4098	4413.7	1743 – 13,578	1614.8 – 12356
Sinks	147.6	144.6	64 – 96	68 – 96	4106	5425	4273 – 6695	4273 – 6695
Net	36.1	4.6	5.7 – 73.7	1.7 – 46.7	8	1012	2530 – 6883	2658.2 – 5661

The source and sink strengths for methyl halides as shown in Tables 1.1, 1.2, 1.3, 1.4 and 1.5 clearly shows that the known sinks are larger than the known sources. In the case of methyl bromide known sinks still outweigh known sources by 36.1 Gg yr<sup>-1</sup>. This large missing source for CH<sub>3</sub>Br is assumed to be of terrestrial and nonindustrial origin (Lee-Taylor et al., 1998; Reeves, 2003; Warwick et al., 2006). However, the 3D-global chemical transport

modeling study for CH<sub>3</sub>Br by Warwick et al. (2006) suggested to perform more measurements in the continental mid-to-high latitudes, the central-Southern Africa and South America to constrain the terrestrial source of methyl halides.

In the case of methyl chloride, 3D-modeling studies were performed to explain the missing sources. A first modeling study of the global tropospheric budget for CH<sub>3</sub>Cl was carried out by Lee-Taylor et al. (2001). They found that the imbalance of the methyl chloride budget was due to the missing sources, which are likely to be terrestrial emissions. Another modeling study of Yashida et al. (2004) found that a biogenic source could be located at 30°N - 30°S and they constrained this region in the model. They calculated that biogenic emissions between 30°N - 30°S account for 93% of the global CH<sub>3</sub>Cl sources using the GEOS-Chem chemical transport model. This is in agreement with the estimates by Khalil and Rasmussen (1999) who suggested that 85% of the emission of CH<sub>3</sub>Cl comes from tropical and subtropical regions. Further modeling results by Xiao et al. (2010a) indicate that about 50% of the CH<sub>3</sub>Cl comes from tropical terrestrial sources that vary with global temperature changes.

## **1.2 Importance of methyl halides in the atmosphere**

Halocarbons from anthropogenic and natural sources represent a large source of reactive chlorine (Cl) and bromine (Br) to the stratosphere. These are formed when chlorofluorocarbons (CFCs) or methyl halides enter the stratosphere. Methyl chloride and methyl bromide can reach the stratosphere where their halogen atoms, released through photolysis, catalytically destroy ozone. It is estimated that the natural sources of CH<sub>3</sub>Cl and CH<sub>3</sub>Br currently contribute about 17% of the chlorine and 30% of the bromine in the stratosphere, respectively (Fahey, 2010). With the phase out of chlorofluorocarbons, which are currently recognized as the most important carriers of reactive halogens, the relative importance of naturally produced methyl halides as a source for reactive halogens will increase. Only in the past decade methyl halides received attention with respect to the stratospheric ozone destruction. Methyl bromide is the single largest carrier of bromine to the stratosphere. It has also been determined that it is 50 to 60 times more effective than chlorine in depleting ozone on a per atom basis (Butler, 2000). Furthermore, naturally produced halocarbons are important contributors to the global warming with an estimated combined radiative forcing of 0.01 W m<sup>-2</sup> ppb<sup>-1</sup> for CH<sub>3</sub>Cl and 0.03 W m<sup>-2</sup> ppb<sup>-1</sup> for CH<sub>2</sub>Cl<sub>2</sub> (IPCC, 2007).

### 1.2.1 Chapman mechanism

The stratosphere which begins at about 10 km - 16 km above the earth's surface and extends up to about 50 km high is the region of the atmosphere that contains 90% of the earth's ozone. The understanding of ozone photochemistry was proposed by Sydney Chapman in 1930. He hypothesized that the solar ultraviolet radiation and the oxygen molecule ( $O_2$ ) are responsible for ozone production and destruction. The elementary reactions given below describe the Chapman mechanism.

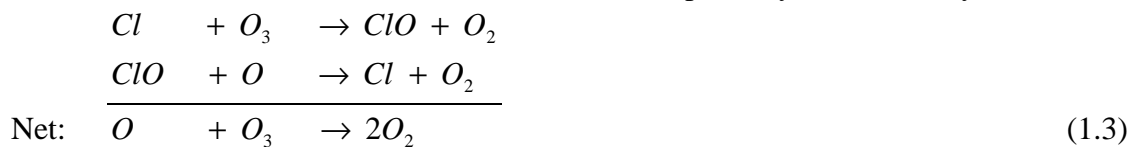


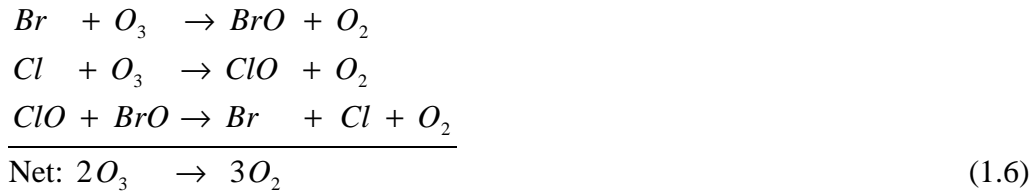
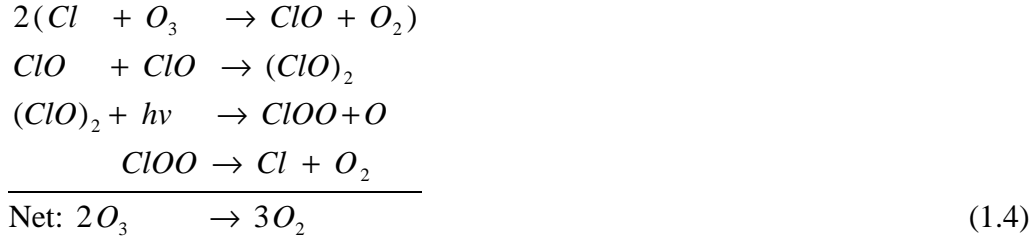
In the production equations, molecular oxygen absorbs solar radiation ( $h\nu$ ) of wavelengths smaller than 242 nm and the molecular oxygen photodissociates. The oxygen atoms (O) formed, react rapidly with  $O_2$  in presence of a third body (M). Here M is any chemically inert collision atom or molecule which removes energy to stabilize an adduct product. As  $N_2$  and  $O_2$  are the most abundant gases in the air, M, therefore, is most likely  $N_2$  or  $O_2$ .

In the second part of the mechanism ozone absorbs solar radiation in the wavelength range of 240 nm to 320 nm and decomposes to  $O_2$  and an oxygen atom. Finally, ozone reacts with atomic oxygen to regenerate two molecules of  $O_2$ . The above cycle occurs usually in the stratosphere.

### 1.2.2 Catalytic destruction of ozone by chlorine and bromine

The Chapman cycle stated in Section 1.2.1 overestimates the stratospheric ozone. Measurements indicate that the actual amount of ozone in the stratosphere is about a factor of two smaller than explained by the Chapman mechanism (Warneck, 1998). The chlorine and bromine radicals that destruct ozone follow reaction pathways described by Crutzen (1974):





The net results of the above reactions are to convert ozone molecule into oxygen molecules. In each cycle, chlorine and bromine act as a catalyst. It is estimated that one chlorine atom can destroy up to tens of thousands of ozone molecules during the total time of its stay in the stratosphere.

### 1.3 Aims of this thesis

Methyl halides ( $CH_3Cl$ ,  $CH_3Br$  and  $CH_2Cl_2$ ) are green house gases in the atmosphere (IPCC, 2007). Since, it is important to study emissions of methyl halides from different sources in the atmosphere. A typical example is determination of the global methyl halide emissions from coastal salt marshes (Rhew et al., 2000). Field measurements were conducted in the coastal salt marshes site and then extrapolating local measurements to global scale by multiplying the unit area flux with an estimated global salt marsh area. This is so named “bottom-up” study. Another method is “top-down” or inverse modeling approach. Manley et al. (2007) found methyl halide emissions from mangroves in a greenhouse experiment. They obtained data from a single mangrove grown in a greenhouse in the laboratory. A more accurate field experiment should be conducted on the natural populations of mangroves to determine emissions more generally. An overall aim of this study is to determine the methyl halide emissions from mangroves. In order to fulfill these goals, observations were

performed and analyzed. In addition, numerical simulations were performed using the mesoscale atmospheric model METRAS.

The thesis aims

- To quantify the emissions of methyl halides from the tropical Atlantic Ocean.
- To determine methyl halide emissions from mangroves.
- To determine the impact of meteorology and emission functions on concentrations of methyl halides.

Chapter 2 gives the background concentrations of methyl halides observed during the Meteor cruise. It also determines emissions of methyl halides from the ocean to the atmosphere and identifies the possible source regions of methyl halides (methyl chloride and methylene chloride only) by using the Hybrid Single Particle Lagrangian Integrated Trajectory Model (HYSPLIT). Chapter 3 describes the observations in the tropical Braganca mangrove forest region. It also shows the methyl halides data that are used in this study from the literature. Chapter 4 describes the model METRAS used in the thesis, the model adaptation and application over the tropical Braganca region and its results. Chapter 5 presents the model sensitivity studies on the role of meteorology on constant concentrations and impact of emissions function on concentrations. Chapter 5 also gives the determined global emission of methyl halides from mangrove region. Chapter 6 presents a brief summary of the thesis with the main results and the overall conclusions.

## **2. Background concentrations and emissions of methyl halides over the tropical Atlantic Ocean**

### **2.1 Introduction**

The ocean plays an important role in the global biogeochemical cycle of methyl halides. Previous studies have shown that methyl chloride ( $\text{CH}_3\text{Cl}$ ) in the ocean is supersaturated (exceeding the equilibrium concentration in the atmosphere) in middle and low latitudes and undersaturated in high latitudes (Moore et al., 1996; Yvon-Lewis et al., 2004). Methyl bromide ( $\text{CH}_3\text{Br}$ ) is undersaturated in the open ocean (Lobert et al., 1995; 1996, 1997; Groszko and Moore 1998; King et al., 2000, 2002; Yvon-Lewis et al., 2004; Tokarczyk and Moore 2006), and supersaturated in the temperate waters (Lobert et al., 1996; Groszko and Moore 1998; Baker et al., 1999). Methylene chloride ( $\text{CH}_2\text{Cl}_2$ ) is not fully explored in the ocean. Moore (2004) suggested that the ocean is an apparent source of methylene chloride in the North Atlantic and the Labrador Seawaters based on the Poseidon and the Hudson cruise data. Another study by Ooki and Yokouchi (2011) confirmed the in-situ production of methylene chloride in the seawater between  $10^\circ$  south and  $40^\circ$  south. They also suggested that more measurements are required covering all seasons to evaluate the global oceanic emission of methylene chloride.

This chapter presents methyl chloride and methylene chloride concentrations in the air and seawater from the Meteor cruise M78/2 over the tropical Atlantic Ocean. The objectives of this chapter are to understand the variation of methyl chloride and methylene chloride in the air and the tropical Atlantic Ocean water for different latitudes. Furthermore, the possible nonlocal source regions shall be identified and methyl halide fluxes from the tropical Atlantic Ocean to the atmosphere shall be quantified. An additional aim is to determine a relation of sea surface temperature (SST) and concentration and fluxes of  $\text{CH}_3\text{Cl}$  and  $\text{CH}_2\text{Cl}_2$ .

The chemistry data are provided by the Institute for Biogeochemistry and Marine Chemistry (IfBM), University of Hamburg. The air and seawater concentrations of methyl chloride and methylene chloride were determined using Gas Chromatography (GC).

The samples were collected along a transect which began after leaving the Exclusive Economic Zone (EEZ) of Guyana at  $10^\circ 13.07' \text{N}$ ,  $56^\circ 38.16' \text{W}$  and ended with entering the EEZ of Brazil at  $23^\circ 9.6' \text{S}$ ,  $39^\circ 40.2' \text{W}$ . Figure 2.1 shows the locations of the samples and

methylene chloride concentrations in the air from M78/2 during the period of 5 April 2009 – 9 May 2009.

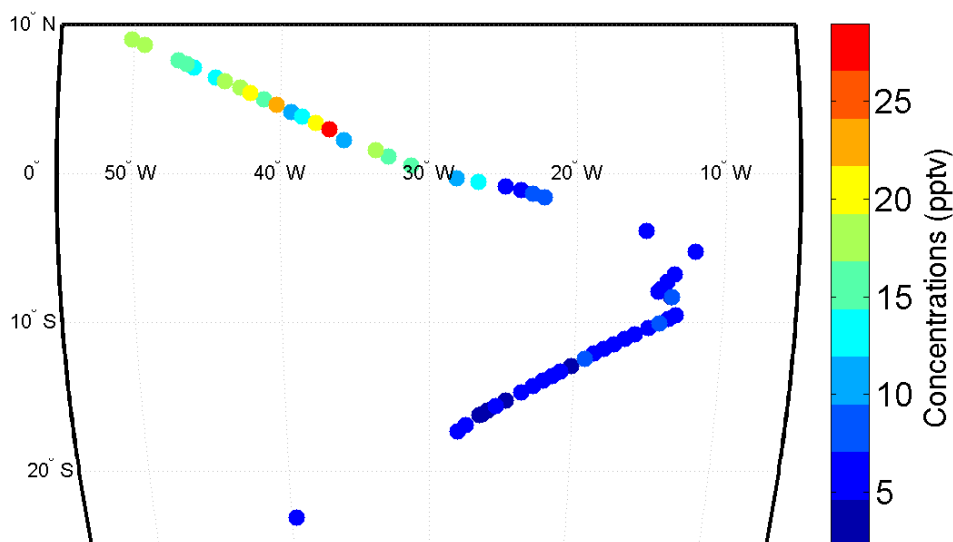


Figure 2.1 Geographical location of sampling sites and methylene chloride concentrations (colors) in the air during the meteor cruise.

## 2.2 Variation of methyl chloride and methylene chloride in air and seawater

The latitudinal distribution of the methyl chloride and methylene chloride concentrations in the air measured are shown in Figure 2.2. Figures 2.2c, d show the normalized concentrations. The normalized concentrations have been calculated as the ratio of the single concentration measurement to the average concentration. Normalized concentration is represented as a percentage.

The average concentration of methyl chloride determined in the air from the cruise data is 825 pptv. Earlier studies determined the annual (1981–1997) average global concentration of methyl chloride in the marine region to be 606 pptv, with a range of 570–620 pptv (Koppmann et al., 1993; Khali et al., 1999; Li et al., 1999; Yokouchi et al., 2000). Methyl chloride mean concentration in the air is also higher than hourly mean (547 pptv) from the NOAA/ESRL data of halocarbon in-situ program at Cape Matatulu 14.3°S 170.6°W during 5<sup>th</sup> April to 9<sup>th</sup> May 2009. Thus, the observed average methyl chloride concentration in the air from the Meteor cruise is higher than the average value of the global marine air concentration as in previous studies and NOAA observational site.

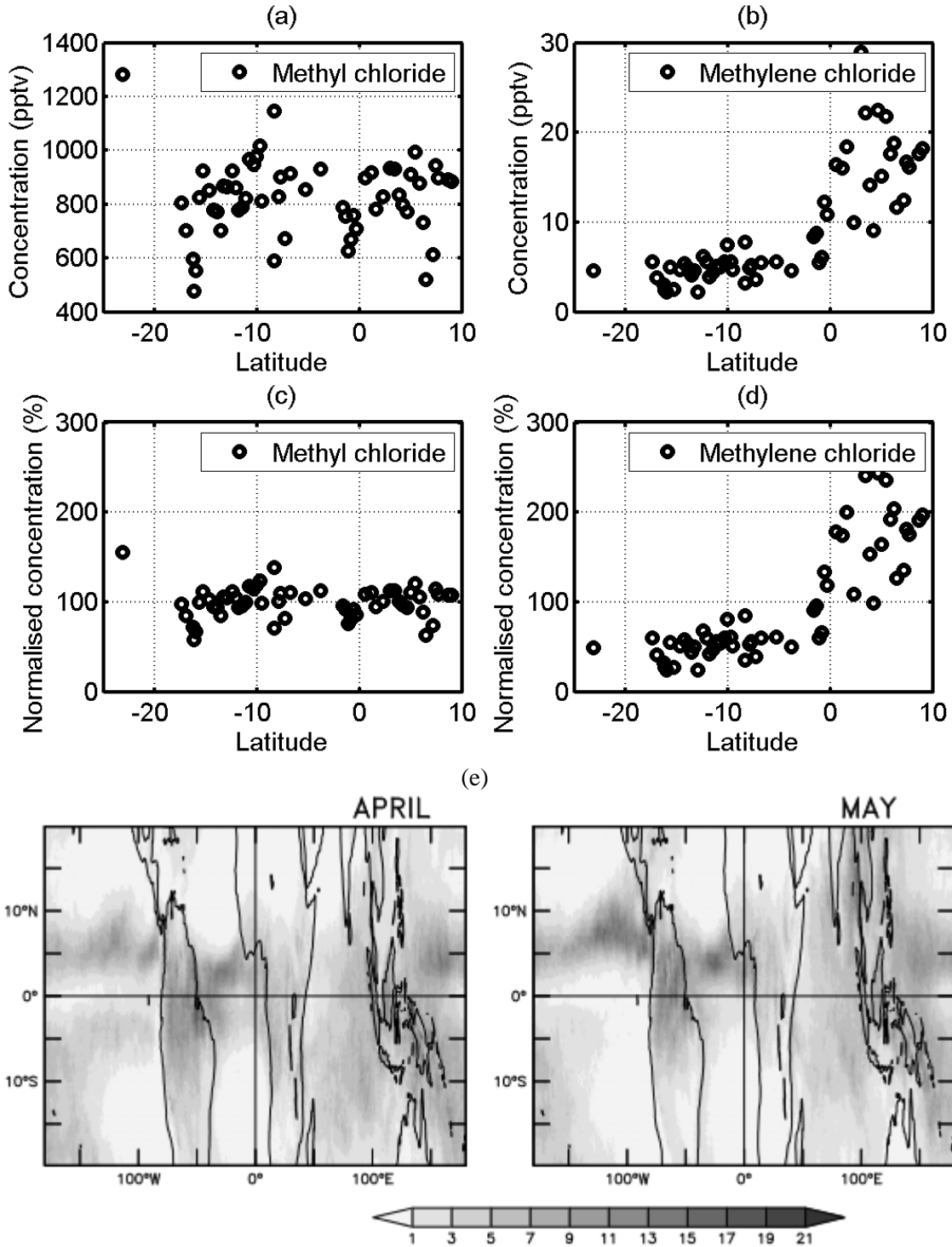


Figure 2.2 Latitudinal variation of concentrations in air (a) methyl chloride, (b) methylene chloride, (c) normalized methyl chloride, (d) normalized methylene chloride, (e) TRMM rainfall climatology (mm/day).

Latitudinal variation of atmospheric (air) concentration (Figure 2.2c) is very small, mostly below  $\pm 50\%$ . The analytical error of concentration in the air and seawater was  $\pm 9\%$  during

the cruise (Personal communication with Dr. Seifert, IfBM, University of Hamburg, 2012). This analytical error is also applicable to normalized concentrations. Methyl chloride concentrations are slightly enhanced in the air at about 10°S. The maximum observed concentration is 1282 pptv for CH<sub>3</sub>Cl in the air near to the Brazil coast (latitude 23° 16'S, longitude 39° 67'W). The increase in concentration nearer to the coast suggests it is likely influenced by coastal or land bound sources of CH<sub>3</sub>Cl.

In the case of methylene chloride very few measurements are available. The first measurements of CH<sub>2</sub>Cl<sub>2</sub> were reported by Cox et al. (1976). They found an average mixing ratio of 35±19 pptv in December 1974 and January 1975 in Wiltshire, England. The average concentration of CH<sub>2</sub>Cl<sub>2</sub> determined in the air from the current cruise data is 9 pptv. The average concentration (9 pptv) for CH<sub>2</sub>Cl<sub>2</sub> during the cruise is lower than the annual mean concentration in air 30.8 pptv (dry air mole fraction) at Mace Head, Ireland (1998-2004). However, there is an excellent agreement, with the annual mean concentration of 8.74 pptv (dry air mole fraction) found in the Southern Hemisphere (SH) at Cape Grim, Tasmania (1998 - 2004) (Simmonds et al., 2006).

The concentrations of CH<sub>2</sub>Cl<sub>2</sub> do not vary with latitude in the Southern Hemisphere (Figures 2.2b, d) and are found to increase linearly just north of the equator (0.5°N) to 7°N. The concentrations are mostly constant in the tropical South Atlantic Ocean. Koppmann et al. (1993) found that the concentrations of CH<sub>2</sub>Cl<sub>2</sub> over the Atlantic Ocean decreased linearly from 45°N to the northern boundary of the Intertropical Convergence Zone (ITCZ) around 10°N and were almost constant over the South Atlantic Ocean. The gradient found here is similar to the one described by them. However, the satellite pictures show a convective cloud band over the high concentration region. (Satellite pictures from Dundee web site <http://www.sat.dundee.ac.uk/auth.html>).

In order to understand the location of ITCZ in the month of April and May, the climatological rainfall data of TRMM satellite is shown in the Figure 2.2 (e). The climatology is calculated from 1998 – 2008 data in mm/day. The ITCZ is located in the ±5° in the Northern Hemisphere and Southern Hemisphere in April. The ITCZ is mostly in the Northern Hemisphere during May. Higher concentrations of CH<sub>2</sub>Cl<sub>2</sub> in the NH are due to more sources and emissions. The gradient in the concentrations shows inter hemispheric mixing in the ITCZ.

The concentration in the seawater is determined in picomole per liter ( $\text{pmol l}^{-1}$ ). The seawater from the Meteor cruise showed mean concentrations of methyl chloride and methylene chloride to be around  $120 \text{ pmol l}^{-1}$  and  $28 \text{ pmol l}^{-1}$ , respectively. Figure 2.3 shows the latitudinal variation of concentrations and normalized concentrations of  $\text{CH}_3\text{Cl}$  and  $\text{CH}_2\text{Cl}_2$  in the seawater. Unlike in the air, the concentrations of  $\text{CH}_3\text{Cl}$  and  $\text{CH}_2\text{Cl}_2$  in the seawater show a large variability, but hardly a systematic change with latitude as found for  $\text{CH}_2\text{Cl}_2$  in the air (Figure 2.2d).

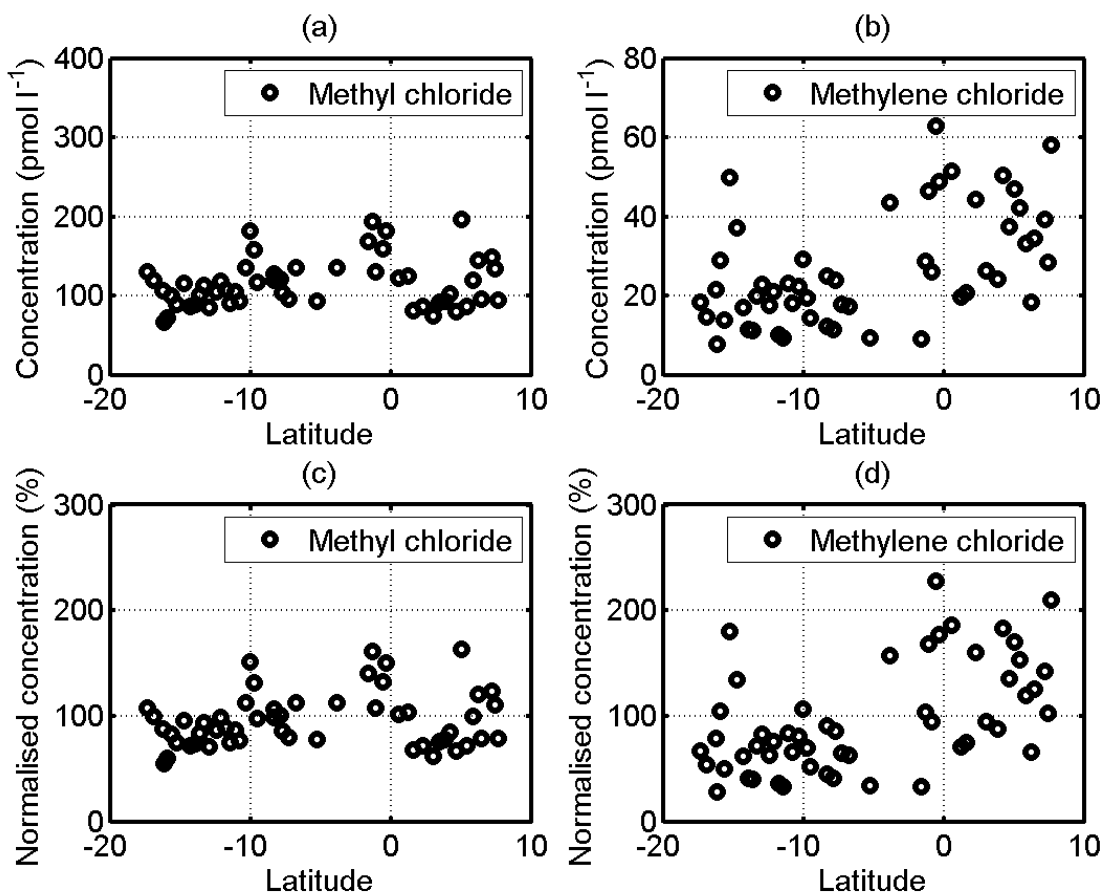


Figure 2.3 Latitudinal variation of concentrations in seawater of (a) methyl chloride, (b) methylene chloride, (c) normalized methyl chloride, (d) normalized methylene chloride (All concentrations are given in  $\text{pmol l}^{-1}$ ).

The Meteor cruise data are subdivided into two groups: the Northern Hemisphere (NH) data ( $0.55^\circ \text{ N} - 9.04^\circ \text{ N}$ ) and the Southern Hemisphere ( $0.3^\circ \text{ S} - 23.16^\circ \text{ S}$ ). Table 2.1 and Table 2.2 summarize the mean and standard deviation of  $\text{CH}_3\text{Cl}$  and  $\text{CH}_2\text{Cl}_2$  concentrations in the air and seawater. The analytical uncertainty of  $\pm 9\%$  is given in the parentheses. Table 2.1 and Table 2.2 show that  $\text{CH}_3\text{Cl}$  concentrations in the air have a slightly higher hemispheric difference than in seawater. In the case of  $\text{CH}_2\text{Cl}_2$ , the concentrations in the air also have a

larger hemispheric difference than in seawater, which may indicate an influence of anthropogenic sources in the NH.

*Table 2.1 Mean and standard deviation of methyl chloride and methylene chloride in the air (n is number of observations).*

<b>Air</b>	<b>methyl chloride (pptv)</b>	<b>methylene chloride (pptv)</b>
Mean concentration (n=57)	825 ± 144 (±9%)	9 ± 6 (±9%)
Northern Hemisphere (n=19)	840 ± 118	17 ± 5
Southern Hemisphere (n=38)	818 ± 157	5 ± 2

*Table 2.2 Mean and standard deviation of methyl chloride and methylene chloride in the seawater (n is number of observations).*

<b>Seawater</b>	<b>methyl chloride [pmol l<sup>-1</sup>]</b>	<b>methylene chloride [pmol l<sup>-1</sup>]</b>
Mean concentration (n=54)	120 ± 46 (±9%)	28 ± 15 (±9%)
Northern Hemisphere (n=17)	111 ± 32	38 ± 15
Southern Hemisphere (n=37)	125 ± 50	23 ± 13

It is known that methyl halides are produced by marine algae and phytoplankton in the ocean. Singh et al. (1983) found a strong correlation between CH<sub>3</sub>Cl and CH<sub>3</sub>Br concentrations in seawater. The authors concluded a common oceanic source for CH<sub>3</sub>Cl and CH<sub>3</sub>Br. Here an attempt is made to find a significant correlation between CH<sub>3</sub>Cl and CH<sub>2</sub>Cl<sub>2</sub> in the seawater. Figure 2.4 shows the relation between CH<sub>3</sub>Cl and CH<sub>2</sub>Cl<sub>2</sub> concentrations in the seawater with the correlation coefficient value denoted by R. Figure 2.4 suggests that there is no significant relation between CH<sub>3</sub>Cl and CH<sub>2</sub>Cl<sub>2</sub> concentrations in seawater. The correlation between CH<sub>3</sub>Cl and CH<sub>2</sub>Cl<sub>2</sub> concentrations in the air is slightly better with R=0.198. Although the exact mechanisms for the production of CH<sub>3</sub>Cl and CH<sub>2</sub>Cl<sub>2</sub> in the ocean are not clear, some studies show phytoplankton production of CH<sub>2</sub>Cl<sub>2</sub> (Ooki et al., 2011) and CH<sub>3</sub>Cl (Tait and Moore, 1995). Based on the above discussion, it is concluded that CH<sub>3</sub>Cl and CH<sub>2</sub>Cl<sub>2</sub> might not have a common oceanic source.

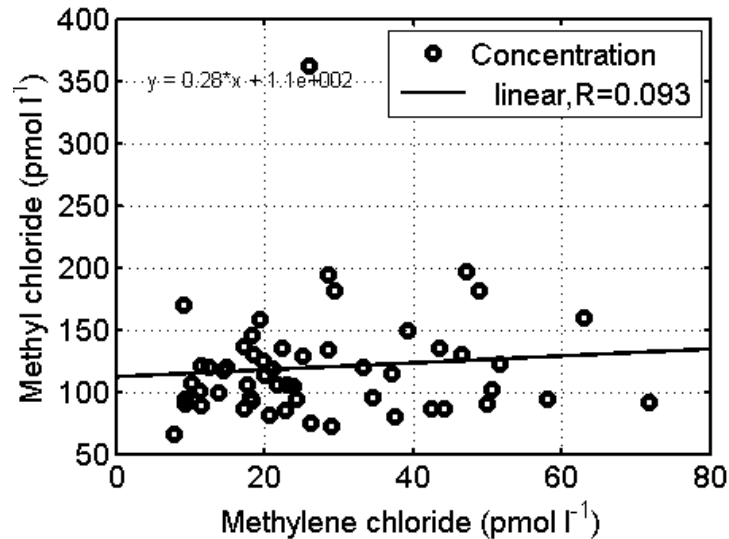


Figure 2.4 Relationship between methyl chloride and methylene chloride concentrations in the seawater.

## 2.3 Quantifying emissions of methyl halides from the tropical Atlantic Ocean

The study of sea to air flux of methyl halides is very important for understanding their global budgets. Liss and Slater (1974) first described the classical and most widely used two layer film model, which proposes that the transfer process is by molecular diffusion through a thin layer of water at the air water interface. According to this model, a net flux is driven by the concentration gradient between seawater to air and the transfer velocity or piston velocity ( $K$ ). The transfer velocity depends on several factors such as wind speed, friction velocity, bubble formation, temperature and small-scale waves (Liss and Merlivat, 1986; Wanninkhof, 1992; McGillis et al., 2001a; 2001b; Nightingale et al., 2000). Many factors can affect the transfer velocity, but over the open ocean wind forcing has a dominant effect. There are many ways for flux measurements such as the covariance or eddy correlation technique, relaxed eddy accumulation, profile method, mass balance techniques. The following describes the flux calculation procedure used in this study.

### 2.3.1 Flux calculation of methyl chloride and methylene chloride

The fluxes of  $\text{CH}_3\text{Cl}$  and  $\text{CH}_2\text{Cl}_2$  from the sea to the air can be defined as the product of transfer velocity ( $K$ ) and the concentration difference between seawater and air ( $\Delta C$ ).

$$F = K (C_w - C_a H^{-1}) \quad (2.1)$$

Here  $F$  is the flux from the sea in  $\text{nmol m}^{-2} \text{d}^{-1}$ .  $C_w$  is the concentration ( $\text{pmol l}^{-1}$ ) of  $\text{CH}_3\text{Cl}$  and  $\text{CH}_2\text{Cl}_2$  in the seawater,  $C_a$  is the concentration ( $\text{pmol l}^{-1}$ ) of  $\text{CH}_3\text{Cl}$  and  $\text{CH}_2\text{Cl}_2$  in the air.  $H$  is the Henry constant, which is nondimensional and adapted from Moore (2000) for  $\text{CH}_3\text{Cl}$  and  $\text{CH}_2\text{Cl}_2$ .  $H$  is calculated by the following expression:

$$H = \exp(A - B/T) \quad (2.2)$$

Here  $A$  and  $B$  are constants that are specific for each compound and obtained from Moore (2000) for  $\text{CH}_2\text{Cl}_2$  and from Khalil et al. (1999) for  $\text{CH}_3\text{Cl}$ . The adopted values are  $A=8.75$ ,  $B=2834\text{K}$  for  $\text{CH}_3\text{Cl}$ ,  $A=11.09$ ,  $B=3935\text{K}$  for  $\text{CH}_2\text{Cl}_2$ .  $T$  is the sea surface temperature in Kelvin, as measured during the Meteor cruise.

The transfer velocity  $K$  is an important term in the calculation of the fluxes. There have been several attempts or estimates made to calculate  $K$ . Many of the studies parameterize  $K$  as a function of wind speed (Liss and Merlivat, 1986; Wanninkhof, 1992; McGillis et al., 2001) because it is a major factor and also easy to measure. In this study, an empirical quadratic and cubic relation between the transfer velocity and wind speed from Wanninkhof (1992), hereafter called (W92), and McGillis et al. (2001), hereafter called (Mc01), are used to calculate the fluxes.

The W92 formula for  $K$  uses wind speeds of ship bound anemometers. The W92 relationship was derived from laboratory studies. The W92 relationship (eq.2.3) is used most often to determine the fluxes.

$$K_{W92} = 0.31 u^2 \left[ \frac{Sc}{660} \right]^{-1/2} \quad (2.3)$$

The Mc01 formula is similar and given by eq. (2.4)

$$K_{Mc01} = (3.3 + 0.026 u^3) \left[ \frac{Sc}{660} \right]^{-1/2} \quad (2.4)$$

The transfer velocities from eq. (2.3) and eq. (2.4) are given in  $\text{cm h}^{-1}$  with  $u$  being the wind speed at 10 m. However, the wind speed was measured on the ship at a height of 45.5 m. Therefore, the wind speed has to be recalculated to a height of 10 m. Under neutral conditions, Prandtl's solution shows that the horizontal flow over the ocean surface follows the logarithmic wind profile in the vertical direction. A logarithmic wind profile is calculated as follows:

$$u_z = \frac{u_*}{k} \ln \left[ \frac{z}{z_0} \right] \quad (2.5)$$

Here  $u_z$  is the wind speed at the height  $z$ ,  $u_*$  is the friction velocity and can not be measured directly,  $k$  is the von Kármán constant (0.40) and  $z_0$  is the roughness length which dependence on wind speed (about 0.0001 m for the smooth ocean). The above formula is used to calculate the 10 m wind speed from the values at 45 m.

The boundary layer over the ocean is not necessarily neutral, it could be stable or unstable. The tropical Atlantic Ocean is more unstable as was during the Meteor cruise observed. A stability dependent logarithmic wind profile given by Monin-Obukhov similarity theory as follows (Schlünzen et al., 1996):

$$u_z = \frac{u_*}{k} \left[ \ln \left\{ \frac{z}{z_0} \right\} - \psi \left\{ \frac{z}{L} \right\} \right] \quad (2.6)$$

Here  $L$  is the Monin-Obukhov length. The  $\psi$  function is derived for unstable conditions using the approach by Dyer (Schlünzen et al., 1996), again using 10 m wind speed values. In addition, the Large and Pond (1981) empirical formula is also used. These two different approaches give similar 10 m wind speeds with a difference from only 0.01 to 0.1  $\text{ms}^{-1}$  for the Meteor cruise. Hence, the logarithmic profile calculated wind speed is used in the eq. (2.3) and eq. (2.4).

In the eq. (2.3) and eq. (2.4),  $Sc$  denotes the Schmidt number and the constant 660 is the value of  $Sc$  for  $\text{CO}_2$  in seawater at 20°C. The Schmidt number is defined as the ratio of the kinematic viscosity ( $\nu$ ) to the molecular diffusivity of the trace gas in air ( $D^{-1}$ ) ( $Sc = \nu D^{-1}$ ). The temperature dependency of the Schmidt number is estimated by Khalil and Rasmussen (1999) as follows:

$$Sc = 335.6 M^{1/2} (1 - 0.065 T + 0.002043 T^2 - 2.6 \cdot 10^{-5} T^3) \quad (2.7)$$

$M$  is the molecular weight of the compound and  $T$  is the sea surface temperature (SST) in degree Celsius.

Figure 2.5 shows the transfer velocity for  $\text{CH}_2\text{Cl}_2$  and  $\text{CH}_3\text{Cl}$  calculated for different wind speeds. The transfer velocities are in centimeter per hour. It needs to be converted into meter per day for flux calculations. The concentrations  $\text{pmol l}^{-1}$  is converted in to  $\text{g cm}^{-3}$ . Finally fluxes are calculated in  $\text{nmol m}^{-2} \text{d}^{-1}$ . To determine the difference between the W92 and

Mc01 relationships, transfer velocity is plotted against the wind speed. Figure 2.5 shows that the Mc01 relation gives higher transfer velocities below 4  $\text{ms}^{-1}$  wind speed than the W92 relation. For larger wind speeds the W92 relation gives higher transfer velocities. These are about 120% higher than that received with Mc01 for both compounds. However, the two relations show the similar pattern with wind speed for both compounds.

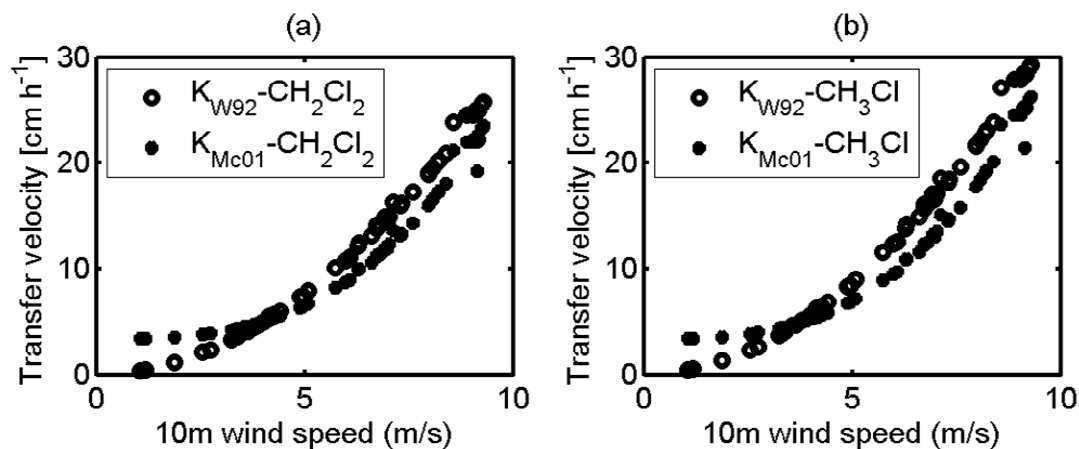


Figure 2.5 Dependency of transfer velocity on wind speed W92 and Mc01 formula for (a)  $\text{CH}_2\text{Cl}_2$  and (b)  $\text{CH}_3\text{Cl}$ .

The fluxes are calculated from the W92 and Mc01 formula at every sampling location. The sampling time is 30 minutes for atmospheric and seawater samples. Hence, the meteorological parameters such as the corrected 10 m wind speed and air temperature are taken as 30 minutes average with respect to their sampling time.

The  $\text{CH}_2\text{Cl}_2$  fluxes are shown in Figure 2.5 using both relationships. The variations of fluxes from both relationships are similar, only the magnitude differs. The Mc01 relation gave lower fluxes than the W92 formula. The mean calculated fluxes are  $81 \pm 81.72 \text{ nmol m}^{-2} \text{ d}^{-1}$ ,  $73 \pm 70 \text{ nmol m}^{-2} \text{ d}^{-1}$  from the W92 and Mc01, respectively. As to be expected from Figure 2.6, the mean flux calculated from Mc01 is slightly lower than W92 in the tropical Atlantic Ocean during the Meteor cruise. According to Ooki and Yokouchi (2011) the average calculated oceanic emission of  $\text{CH}_2\text{Cl}_2$  derived from the region between  $10^\circ\text{S}$  and  $40^\circ\text{S}$  in the Indian ocean was  $0.29 \mu\text{g m}^{-2} \text{ d}^{-1}$  -  $0.43 \mu\text{g m}^{-2} \text{ d}^{-1}$ . The calculated average emissions during the Meteor cruise in the tropical Atlantic Ocean are  $6.87 \mu\text{g m}^{-2} \text{ d}^{-1}$  and  $6.2 \mu\text{g m}^{-2} \text{ d}^{-1}$  using W92 and Mc01, respectively. Thus the values are higher than in the other study. The maximum and minimum calculated fluxes of  $\text{CH}_2\text{Cl}_2$  in the tropical Atlantic Ocean are  $330 \text{ nmol m}^{-2} \text{ d}^{-1}$  and  $0.72 \text{ nmol m}^{-2} \text{ d}^{-1}$  using W92 relation. Figure 2.7 also shows

that calculated fluxes are higher in the NH, lower at the equator and then increased at 15°S. Moreover, the SH fluxes are more or less similar.

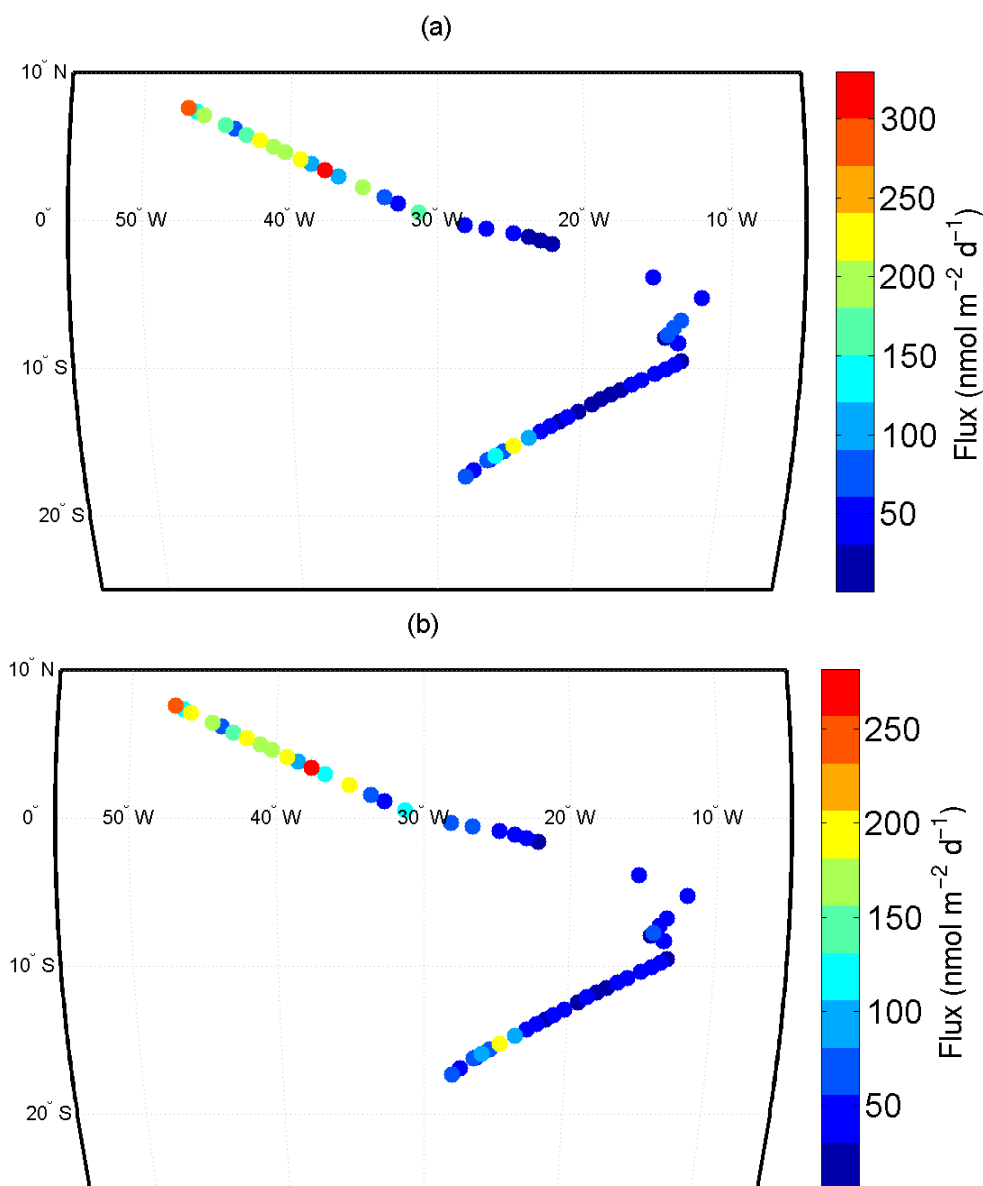


Figure 2.6 Calculated fluxes of  $\text{CH}_2\text{Cl}_2$  in the tropical Atlantic Ocean using (a) W92 and (b) Mc01 relationships.

$\text{CH}_3\text{Cl}$  calculated fluxes are shown in Figure 2.7. The Mc01 calculated fluxes are not shown in this figure because it shows a similar pattern except their somewhat smaller values. The average calculated fluxes of  $\text{CH}_3\text{Cl}$  in the tropical Atlantic Ocean are  $150 \pm 150 \text{ nmol m}^{-2} \text{d}^{-1}$  and  $134 \pm 129 \text{ nmol m}^{-2} \text{d}^{-1}$  from the W92 and Mc01, respectively. The flux ranges of  $\text{CH}_3\text{Cl}$  using W92 relationship ( $-16.5 \text{ nmol m}^{-2} \text{d}^{-1}$  to  $683 \text{ nmol m}^{-2} \text{d}^{-1}$ ) are larger than those

determined by Hu et al. (2010) ( $-5.9 \text{ nmol m}^{-2} \text{ d}^{-1}$  -  $348 \text{ nmol m}^{-2} \text{ d}^{-1}$ ) and lower than those of Lu et al. (2010) ( $-185 \text{ nmol m}^{-2} \text{ d}^{-1}$  to  $1791 \text{ nmol m}^{-2} \text{ d}^{-1}$ ). The W92 mean calculated  $\text{CH}_3\text{Cl}$  flux ( $150 \text{ nmol m}^{-2} \text{ d}^{-1}$ ) in the tropical Atlantic Ocean is less than that by Singh et al. (1983) who determined mean flux of  $705 \text{ nmol m}^{-2} \text{ d}^{-1}$ . Our average sea to air flux of  $\text{CH}_3\text{Cl}$  ( $150 \text{ nmol m}^{-2} \text{ d}^{-1}$ ) in the tropical Atlantic Ocean is higher than the annual global oceanic mean flux of  $48 \text{ nmol m}^{-2} \text{ d}^{-1}$  -  $98.4 \text{ nmol m}^{-2} \text{ d}^{-1}$  (Khalil et al., 1999; Moore, 2000; Yoshida et al., 2004). The annual global oceanic mean fluxes are influenced by the seasonal variations and sinks. Hence, calculated  $\text{CH}_3\text{Cl}$  flux is higher than the global values. The calculated  $\text{CH}_3\text{Cl}$  fluxes are within the range of previous studies. It is also noted that fluxes are higher where the wind speed is higher. The  $\text{CH}_3\text{Cl}$  fluxes are higher in the NH and slightly lower in the SH. There is a negative flux ( $-16.5 \text{ nmol m}^{-2} \text{ d}^{-1}$ ) calculated at  $3.02^\circ\text{N}$  and  $36.70^\circ\text{W}$ , which means flux from atmosphere to the sea, and the ocean is acting as a local sink.

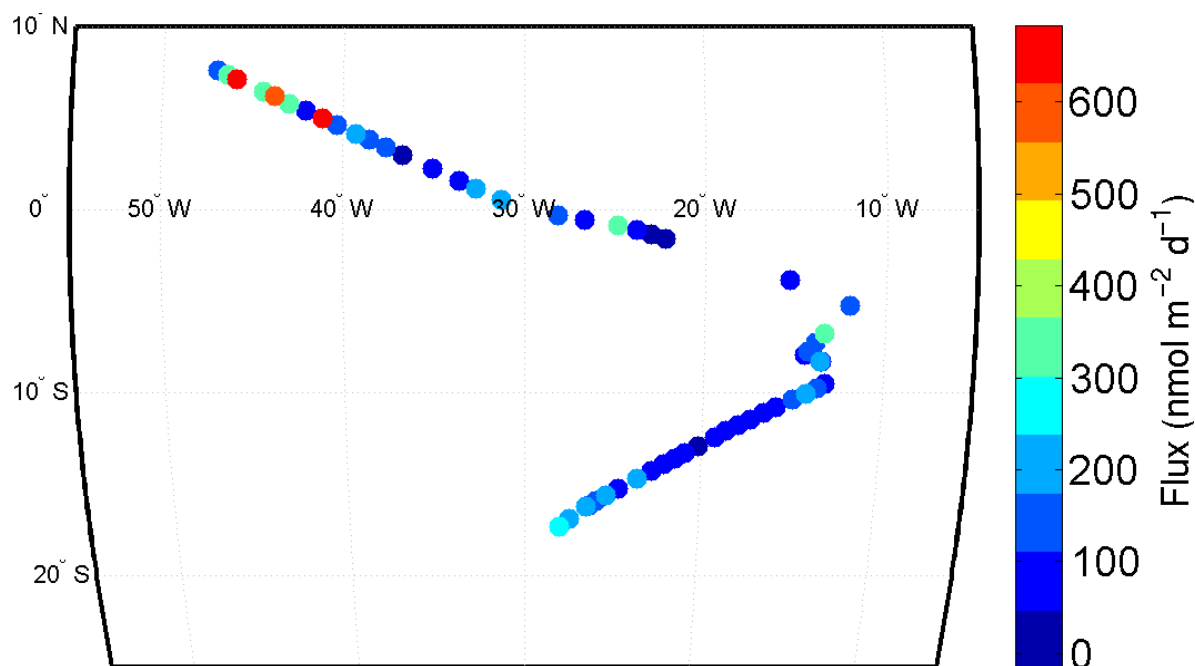


Figure 2.7 Calculated fluxes of  $\text{CH}_3\text{Cl}$  in the tropical Atlantic Ocean using the W92 relationship.

The  $\text{CH}_3\text{Cl}$  fluxes show similar variations as the  $\text{CH}_2\text{Cl}_2$  fluxes, but higher values were found for the tropical Atlantic Ocean. The variations of fluxes of the two compounds are caused by wind speed and seawater concentration. Saturation anomalies were calculated for  $\text{CH}_3\text{Cl}$  and  $\text{CH}_2\text{Cl}_2$  during the meteor cruise. Saturation anomaly is defined as the percentage departure from the expected equilibrium between gas concentrations in surface seawater and the atmosphere (Hughes et al., 2009). Saturation anomaly is calculated by eq. (2.8).

$$\text{Saturation anomaly (\%)} = 100 (C_w - \frac{C_a}{H}) / \frac{C_a}{H} \quad (2.8)$$

Here  $C_w$  is the concentration in seawater,  $C_a$  is the concentration in air and  $H$  is the nondimensional temperature dependency Henry's Law coefficient as calculated by eq. (2.2).

The saturation anomaly maximum and minimum values for  $\text{CH}_3\text{Cl}$  are 477 percent, -3 percent in the tropical Atlantic Ocean. In the case of  $\text{CH}_2\text{Cl}_2$  the maximum and minimum saturation anomaly are found to 205 percent and 6190 percent. Higher saturation anomaly values of  $\text{CH}_3\text{Cl}$  and  $\text{CH}_2\text{Cl}_2$  suggest that the tropical Atlantic Ocean is an important source for these compounds.

The positive saturation anomalies indicate the supersaturation of  $\text{CH}_3\text{Cl}$  and  $\text{CH}_2\text{Cl}_2$  in the seawater. The saturation anomalies of both compounds are positive (supersaturation) in the tropical Atlantic Ocean during the Meteor cruise. Supersaturation implies a net flux from the ocean to the atmosphere. Hence,  $\text{CH}_3\text{Cl}$  and  $\text{CH}_2\text{Cl}_2$  are emitted from the tropical Atlantic Ocean to the atmosphere during the Meteor cruise.

### 2.3.2 Diurnal cycle of concentrations and fluxes over the tropical Atlantic Ocean

Figure 2.8 shows the diurnal variations of  $\text{CH}_3\text{Cl}$  (a, d) and  $\text{CH}_2\text{Cl}_2$  (b, e) normalized concentrations in the air (a, b) and seawater (d, e) as well as ambient air temperature (c) and wind speed (f) during 4 - 6 May 2009. X-axis is the sample local sun time based on the sample location. The air temperature is measured at 28.3 m above the sea level (Figure 2.8c). There is a diurnal cycle of air temperature on May 6<sup>th</sup> observed over the tropical Atlantic Ocean. Higher wind speeds are observed on May 5<sup>th</sup> and 6<sup>th</sup> May from noon compared to May 4<sup>th</sup> 2009. The Relative humidity is about 70% observed during the three days period. Meteorological conditions have been changing with position of the ship. Measured concentrations are also not from the same water mass in one day.

The concentrations of  $\text{CH}_3\text{Cl}$  and  $\text{CH}_2\text{Cl}_2$  in the air do show a little variation with time of day. There is also clear diurnal cycle of  $\text{CH}_3\text{Cl}$  concentrations visible in the seawater.  $\text{CH}_2\text{Cl}_2$  concentration in the seawater has a maximum at night, minimum at noon and a second maximum in the evening. The above mentioned patterns are observed during the Meteor cruise. Lu et al. (2010) studied diurnal variation of  $\text{CH}_3\text{Cl}$  in seawater in the East China Sea and the Southern Yellow Sea and found different diurnal patterns at both sites. They found

maximum concentration at noon in the East China Sea and in the evening in the Southern Yellow Sea and lowest concentration at night for both locations. It indicates that different regions show different diurnal cycle patterns. Ooki and Yokouchi (2011) determined the oceanic emission of  $\text{CH}_2\text{Cl}_2$  by the phytoplankton production in the South Indian Ocean. Maximum concentrations of chlorophyll-a were determined in the subsurface layer (20 – 150 m), as were maximum concentrations of dihalomethanes ( $\text{CH}_2\text{I}_2$ ,  $\text{CH}_2\text{ClI}$  and  $\text{CH}_2\text{Cl}_2$ ) in the South Indian ocean between 5°S and 30°S. They concluded that maximum concentration of  $\text{CH}_2\text{Cl}_2$  in the subsurface layer was derived from direct and indirect productions by phytoplankton, indirect productions of  $\text{CH}_2\text{Cl}_2$  mean photolysis and chloride substitution of  $\text{CH}_2\text{ClI}$ .

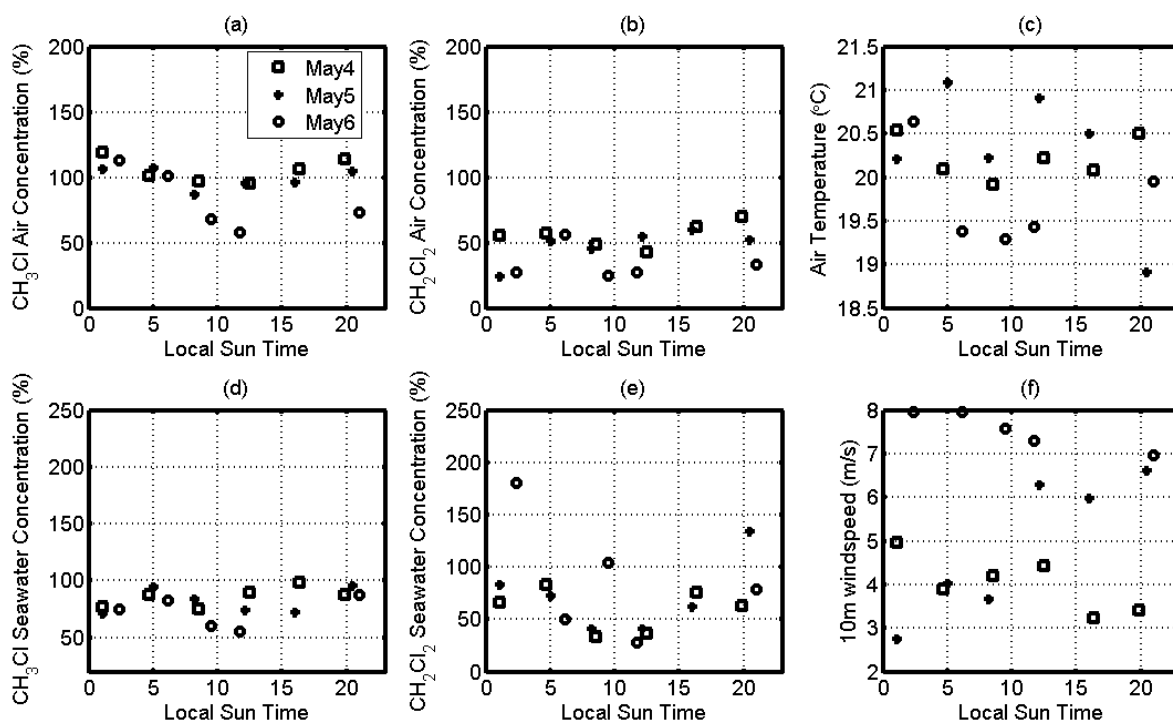


Figure 2.8 Diurnal variation of (a), (d) normalized methyl chloride and (b), (e) normalized methylene chloride concentrations in (a), (b) air and (d), (e) seawater, of (c) air temperature and (f) wind speed over the tropical Atlantic Ocean.

In order to understand the biological processes influencing concentration, high resolution satellite chlorophyll-a data downloaded from the National Aeronautics and Space Administration (NASA) website (<http://oceancolor.gsfc.nasa.gov/cgi/l3?per=DAY>) is used. The data set has 4 km spatial resolution and daily time scale. The chlorophyll-a data have, however, many gaps due to clouds over the sampling locations. The satellite data can not be

used during the cruise period. Unfortunately, no usable chlorophyll-a data were obtained during the Meteor cruise. Thus, the biological influence on concentration can not be studied.

The diurnal cycles of calculated normalized fluxes of both compounds are shown in Figure 2.9.  $\text{CH}_3\text{Cl}$  fluxes calculated are mostly lower at night and slightly higher at day time. However, the overall maximum of  $\text{CH}_3\text{Cl}$  flux is about 150% found on 6 May at around 20 hrs. The night time maximum of  $\text{CH}_3\text{Cl}$  flux may be caused by biological activity such as respiration. The  $\text{CH}_2\text{Cl}_2$  fluxes calculated are slightly higher in the late night, lower at noon and thereafter constant. The overall maximum of  $\text{CH}_2\text{Cl}_2$  flux is about 270% found on May 6 at 02hrs local sun time. Both compounds do not show consistent diurnal cycle in the fluxes over the tropical Atlantic Ocean from 4 to 6 May 2009. Wind speed is the most driving factor for the diurnal variations of fluxes in the tropical Atlantic Ocean.

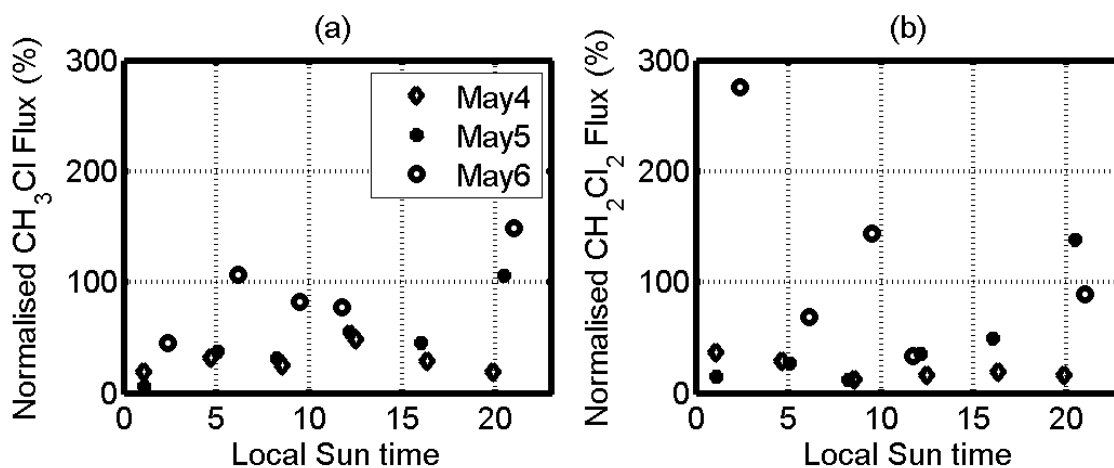


Figure 2.9 Diurnal variation of (a)  $\text{CH}_3\text{Cl}$  and (b)  $\text{CH}_2\text{Cl}_2$  normalized fluxes in the tropical Atlantic Ocean.

### 2.3.3 Significance of sea surface temperature on concentrations and fluxes of methyl halides

Previous studies have reported existence of a relationship between the concentration anomalies and concentration for  $\text{CH}_3\text{Cl}$  in the seawater and sea surface temperature (SST) for the open ocean (MacDonald and Moore, 2007; Ooki et al., 2010). Lu et al. (2010) found no correlation between concentration anomalies of  $\text{CH}_3\text{Cl}$  and SST in the East China sea while others (like Ooki et al., 2010) found strong correlations. Similarly, an attempt is made to find the correlation of concentration and flux of methyl halides with SST. The in-situ measurement of seawater temperatures were taken along the Meteor cruise at 2.1 m depth in the tropical Atlantic Ocean. The measured SST varied from 26°C to 28.5°C during the

Meteor cruise. The measurement values are in the same range as NOAA weekly SST data for the cruise period.

The results are shown in the Figure 2.10. The scatter plots show that the concentrations of  $\text{CH}_3\text{Cl}$  are less scattered than the concentrations of  $\text{CH}_2\text{Cl}_2$  and increase with SST. There is a positive correlation  $R=0.4$  found between concentrations of  $\text{CH}_3\text{Cl}$  and SST. This suggests the dependency of  $\text{CH}_3\text{Cl}$  concentration on SST in the tropical Atlantic Ocean.

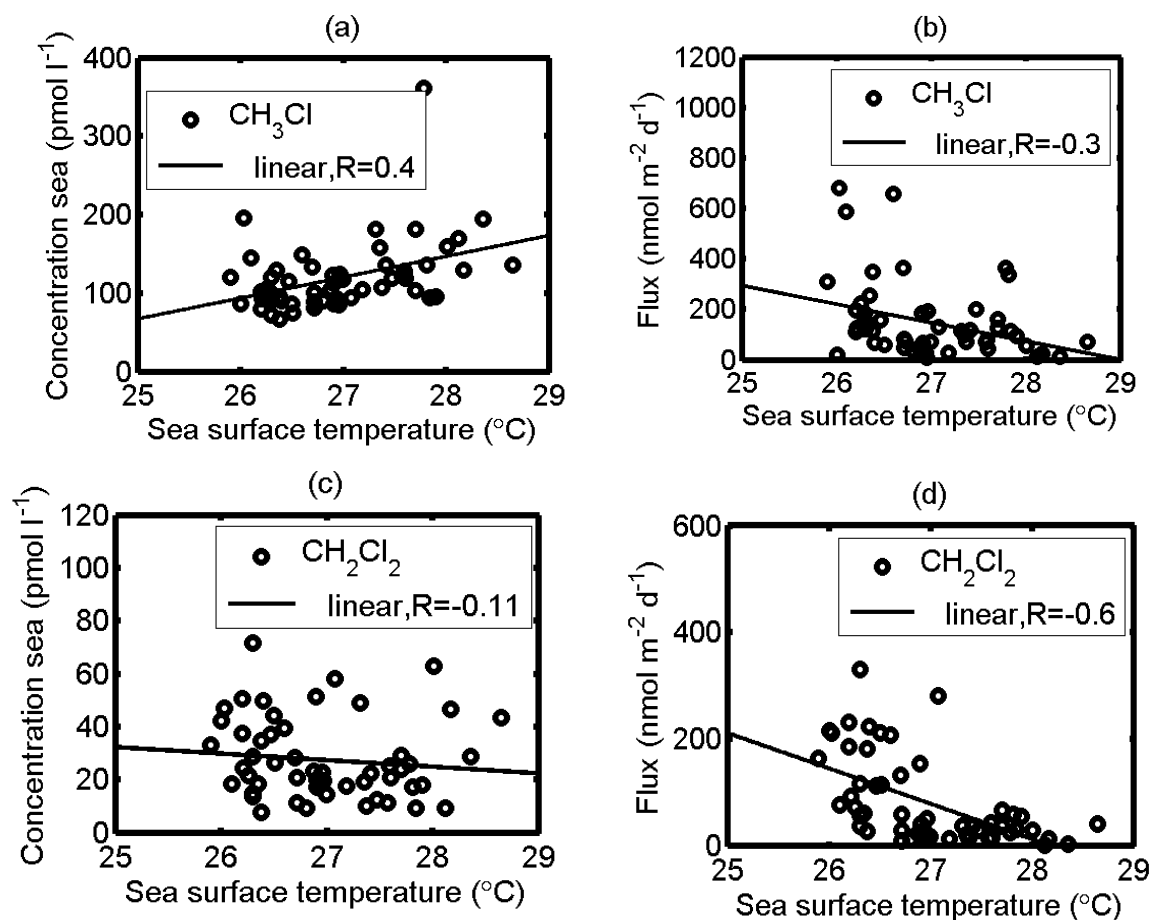


Figure 2.10 Comparison of (a),  $\text{CH}_3\text{Cl}$  and (c),  $\text{CH}_2\text{Cl}_2$  concentrations in the seawater against SST, and of (b)  $\text{CH}_3\text{Cl}$  and (d)  $\text{CH}_2\text{Cl}_2$  fluxes against SST.

In the case of  $\text{CH}_2\text{Cl}_2$  the concentrations are less dependent on SST. There is a small negative correlation ( $R=-0.11$ ) found between concentration of  $\text{CH}_2\text{Cl}_2$  and SST. Thus,  $\text{CH}_2\text{Cl}_2$  does not solely depend on the SST in the tropical Atlantic Ocean. There is a higher relation of SST to  $\text{CH}_3\text{Cl}$  concentrations than for  $\text{CH}_2\text{Cl}_2$  concentrations.

The correlation between the fluxes of both the compounds and SST is negative. There is a high negative correlation found between  $\text{CH}_2\text{Cl}_2$  flux and SST of 0.6. The scatter plot shows that the fluxes of both the compounds are scattered more about for temperatures of 26°C to 27°C. Overall, fluxes are negatively correlated with SST in the tropical Atlantic Ocean. The inverse relation of SST and fluxes are mainly due to the flux equation.

## **2.4. Identification of methyl halides source regions using HYSPLIT back trajectories**

The air mass source regions for the concentrations that were measured over the tropical Atlantic Ocean region during the Meteor cruise are determined by simulating backward trajectories. The Hybrid Single Particle Lagrangian Integrated Trajectory Model (HYSPLIT) was used to calculate the back trajectories for the probed air masses.

### **2.4.1 HYSPLIT model setup**

The HYSPLIT model was downloaded from the Air Resources Laboratory (ARL) web site. The model code version used was HYSPLIT - 4.9. The HYSPLIT model can be run interactively on the web or on a PC. For the current studies the HYSPLIT model has installed on a windows XP laptop and run using a graphical user interface (GUI).

Lagrangian particle models compute trajectories of a large number of so-called particles to describe the transport and diffusion of tracers in the atmosphere. The main advantage of Lagrangian models is that, unlike in Eulerian models, there is no numerical diffusion. This study used a simple approach of ensemble trajectories by using HYSPLIT.

HYSPLIT requires meteorological data of the horizontal wind (u), (v), the vertical wind (w), temperature (T) and surface pressure (P<sub>surf</sub>). Relative humidity or specific humidity (Q) is optional. The meteorology data of the Global Data Assimilation System (GDAS) from the National Centers for Environmental Prediction (NCEP's) providing a 0.5° horizontal resolution are used as input for the HYSPLIT backward trajectory calculation. There are many uncertainties in the calculation of trajectories arising from the possible errors in input meteorological fields and the numerical methods. To reduce uncertainties associated with a single trajectory, HYSPLIT is run in an ensemble mode to generate multiple trajectories from a single meteorological field (Draxler, 2003). Each ensemble member is computed from the same location starting for the same time. The model configuration used 27 ensemble members with each member having the same probability. All backward trajectories were

simulated in accordance with the sample time of the measurements performed at 20 meters above sea level. A total of 57 air samples were collected during the Meteor cruise. For each of them an ensemble of backward trajectories was computed. Draxler and Hess (1997) gave a more detailed model description. A brief description to model the trajectory equation follows. If we assume that a particle passively follows the wind, then its trajectory is just the integration of the particle position vector in space and time (t). The final position is computed from the average velocity (V) at the initial position (P) and first-guess position (P'). The first-guess and final positions are as follows:

$$P'(t + \Delta t) = P(t) + V(P, t) \Delta t \quad (2.8)$$

$$P(t + \Delta t) = P(t) + 0.5[V(P, t) + V(P', t + \Delta t)] \Delta t \quad (2.9)$$

The integration time step ( $\Delta t$ ) can vary during the simulation. It is computed from the requirement that the advection distance per time step should be less than the grid spacing. Time steps can vary from 1 minute to 1 hour.

Backward trajectories were calculated for the time period 5 April to 9 May 2009. Backward trajectories have been calculated for a week and displayed at 00,06,12,18 Universal Time Coordinated (UTC), starting at sampling time and sampling location.

#### 2.4.2 HYSPLIT results for the Meteor cruise

The ensemble of trajectories was classified according to the region in which they were most often present. In one such backward trajectory case, three to five days were spent adjacent to the African coast, thus defining this trajectory as among those of the African coast source region. Based on this assumption, trajectories were categorised and their probable source region was identified. The following are the probable sources regions for methyl halides:

- (i) The Open ocean air mass source region
- (ii) The African coast air mass source region
- (iii) The African coast (also inland) air mass source region
- (iv) The South American coast (off shore) air mass source region

Examples of HYSPLIT model results are shown in Figure 2.11 and Figure 2.12 for the different sampling positions thereby depicting days with different probable source regions. The average concentrations of methyl chloride and methylene chloride were calculated based on the backward trajectory analysis of assigned source regions. The mean concentration of

methyl chloride and methylene chloride in air from the African coast air mass were 830 pptv and 11 pptv respectively. The African coast (also inland) air mass source region concentrations were 817 pptv for  $\text{CH}_3\text{Cl}$  and 13 pptv for  $\text{CH}_2\text{Cl}_2$ . The South American coast (off shore) air mass source region concentrations were 717 pptv for  $\text{CH}_3\text{Cl}$  and 4 pptv for  $\text{CH}_2\text{Cl}_2$ . The open ocean air mass source region concentrations were 863 pptv for  $\text{CH}_3\text{Cl}$  and 5 pptv for  $\text{CH}_2\text{Cl}_2$ .

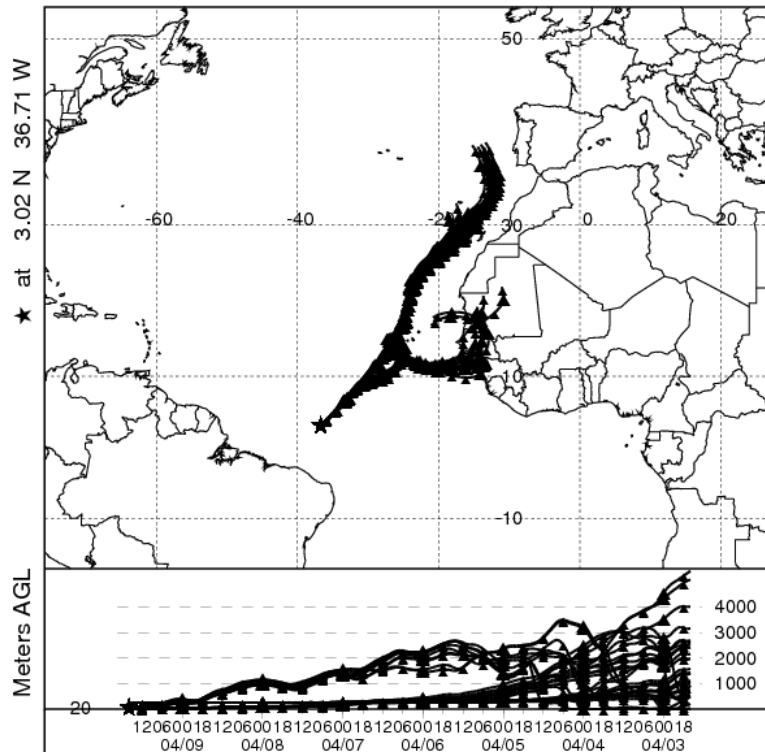


Figure 2.11 Calculated ensemble backward trajectories using 0.5 resolution meteorological data on 9 April 2009, receptor at 15.30 UTC.

\* denotes the receptor. The vertical momentum of the air mass from the source region to the receptor (sample location) is given in meters above the ground level (AGL).

$\text{CH}_3\text{Cl}$  concentration for the open ocean air mass source region was higher than the African coast (also inland) and the South American coast (off shore) air mass source region. There was a negative flux of  $\text{CH}_3\text{Cl}$  calculated at 3.02°N, 36.7°W, which comes from the African coast (also inland) air mass source region. Figure 2.11 shows an example of the assigned African coast (also inland) air mass source regions at 3.02°N, 36.7°W sample location. The negative flux of  $\text{CH}_3\text{Cl}$  at this sample location may be influenced by the African coast (also inland) air mass transport. Since, also  $\text{CH}_2\text{Cl}_2$  concentrations were found to be higher in the African coast (also inland) air mass source region compared to other source regions, this could be a hint for either anthropogenic or ocean sources.

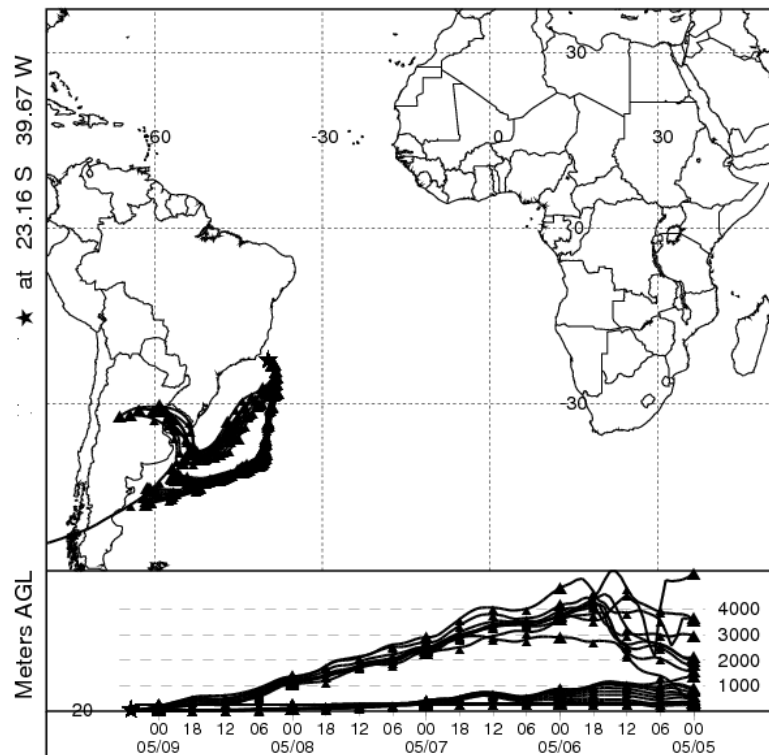


Figure 2.12 Calculated backward trajectories assigned for the South American coast (also inland) sources regions on 9 May 2009, receptor at 05.00 UTC. \* denotes the receptor. The vertical momentum of the air mass from the source region to the receptor (sample location) is given in meters above the ground level (AGL).

To speculate on possible source regions one can argue, that biomass burning is the second largest source for methyl chloride. Biomass burning activity is widespread, most often in the tropical farmlands in South America and Africa. The most active biomass burning geographical region is between 10°S and 30°S. Most of the biomass burning in South America occurs south of 10°S during the August - October period with peak activity in September. Unlike in South America, the central Africa biomass burning starts in June with peak activity in August (Torres et al., 2010). Higher concentration of CH<sub>3</sub>Cl and negative flux associated with African coast (also inland) indicates a second probable source region for CH<sub>3</sub>Cl. Thus, tropical Atlantic Ocean could be the primary source region for the CH<sub>3</sub>Cl during the Meteor cruise. In the case of CH<sub>2</sub>Cl<sub>2</sub> higher concentration and lower fluxes were calculated for the African coastal (also inland) air mass source region. There is no negative flux calculated for CH<sub>2</sub>Cl<sub>2</sub>. Thus, the tropical Atlantic Ocean was primary, the African coast (also inland) air mass source region secondary probable source regions for CH<sub>2</sub>Cl<sub>2</sub> during the Meteor cruise.

The peak concentration of CH<sub>3</sub>Cl associated with the South American coast (also inland) (Figure. 2.12) air mass source was observed to be 1282 pptv (Figure 2.2) (23.15°S 39.67°W). Figure 2.12 shows only 5 days backward trajectories due to missing meteorological data input file. Similarly, large concentrations of methyl chloride [1500 pptv at Cape Hedo, Okinawa island (26.9°N, 128.3°W) (Japan) and spot measurement at Jakarta (6.2°S 106.8°E, in a forest of Bandung (6.9°S 107.6°E on tropical Java (Indonesia) ranging from 1000 pptv to 2000 pptv] have been measured by Yokouchi et al. (2000). They suggest a land source of CH<sub>3</sub>Cl may be responsible for higher concentrations. Most of the South America coastal region consists of a mangrove forest. With tropical and subtropical vegetation being the largest source, it is much more likely that tropical forests act as the main source for methyl chloride. The backward trajectory analysis supports the higher concentration of methyl chloride might result from the South American coast (also inland) air mass source region.

## 2.5 Conclusions

The average concentrations of methyl chloride and methylene chloride in the air and seawater during the Meteor cruise are 825±144 pptv, 9±6 pptv and 120±46 pmol l<sup>-1</sup>, 28±15 pmol l<sup>-1</sup>, respectively. Observed concentrations of methyl chloride are higher in the air compared to earlier studies performed in other regions of the world.

There are significant calibration differences between research groups reporting data on CH<sub>3</sub>Cl and CH<sub>2</sub>Cl<sub>2</sub>. The analytical uncertainty of ±9% also needs to be considered for further studies of the global budget and in modeling studies. There is no correlation between the concentrations of methyl chloride and methylene chloride in the seawater. Thus, methyl chloride and methylene chloride may not have a common oceanic source.

The quantified average methyl chloride and methylene chloride emission from the tropical Atlantic Ocean are 150±150 nmol m<sup>-2</sup> d<sup>-1</sup> and 81±81.72 nmol m<sup>-2</sup> d<sup>-1</sup>. The global coastal ocean emission of CH<sub>3</sub>Cl and CH<sub>2</sub>Cl<sub>2</sub> using a global coastal ocean area of 27.123×10<sup>6</sup> km<sup>2</sup> (Menard and Smith, 1966) are 75 Gg yr<sup>-1</sup> and 68 Gg yr<sup>-1</sup>, respectively. Thus, the ocean may be an important source for CH<sub>3</sub>Cl and CH<sub>2</sub>Cl<sub>2</sub> emissions.

The diurnal cycle of methyl chloride and methylene chloride concentrations and fluxes were studied. Slightly higher concentrations of CH<sub>3</sub>Cl and CH<sub>2</sub>Cl<sub>2</sub> in seawater and higher fluxes of

$\text{CH}_3\text{Cl}$  and  $\text{CH}_2\text{Cl}_2$  at night time were may be due to the biological processes in the tropical Atlantic Ocean. However, the reason for high concentrations at night-time remains unknown. The higher fluxes during night time may be due to meteorological conditions.

A high correlation was found between the  $\text{CH}_3\text{Cl}$  concentration in seawater and SST, suggesting that the  $\text{CH}_3\text{Cl}$  concentration depends on the SST in the study area during the Meteor cruise. On the other hand, no correlation was found between the  $\text{CH}_2\text{Cl}_2$  concentration in seawater and SST implying that the  $\text{CH}_2\text{Cl}_2$  concentration may not depend on the SST in the study area. For the future modeling study, it has to be considered that there are measurement uncertainties in the concentration data.

The backward trajectory results of the HYSPLIT model show that mainly the air masses came from the African coast (also inland) as well as the South American coast (off shore) and the open ocean. The backward trajectories revealed that the tropical Atlantic Ocean and the African coast (also inland) were primary and secondary source regions for methyl chloride, respectively, during the Meteor cruise. This could be either due to natural or anthropogenic emissions to the atmosphere.

The trajectory results support the findings of other studies such as Yokouchi et al. (2000) and Rhew et al. (2000) that coastal terrestrial sources are significant in the global budget of  $\text{CH}_3\text{Cl}$ . Moreover, high concentrations nearer to the South America coast (also inland) source region suggest that the (may be mangrove) forest is most likely to be a source of methyl chloride.

### **3. Observational data**

#### **3.1 Introduction**

The observations of the important gases like chlorofluorocarbons, hydrochlorofluorocarbons and methyl halides are available from the Advanced Global Atmospheric Gases Experiment (AGAGE). The AGAGE has been measuring the composition of the atmosphere since 1978 at a number of high frequency stations (Prinn et al., 2000). These data will give a background global concentration value for these compounds. However, the AGAGE do not give the local emissions of a particular forest. Thus, more local observations are needed.

This study focuses on mangrove forest emissions. In order to accomplish this study, a field experiment was conducted in the tropical Braganca mangrove forest region. It is an arduous task to do observations in the field, because of a large number of possible technical and human errors. Also, observations are costly and time consuming. To the best of our knowledge these field measurements were the first of its kind conducted in the tropical Braganca mangrove ecosystem. Manley et al. (2007) studied greenhouse-grown mangroves emissions of methyl halides in the laboratory. However, their study could not consider the tidal activity, rainfall and biogeochemical processes that would occur in naturally grown mangroves forest. Also the emissions from roots and stems or the possibility of enhanced emissions during flowering were not considered during their study.

This chapter will present the measurement area and the observed methyl halides data from the tropical mangrove forest region.

#### **3.2 Data from the literature survey**

In mangrove forests typically two different natural sources exist for methyl halides, namely the mangrove and the ocean. Manley et al. (2007) conducted laboratory studies for different types of mangroves like *Rhizophora mangle* (Red mangrove), and *Avicennia germinans* (Black mangrove) and quantified emissions of methyl halides. In the case of the ocean, calculated emissions are based on results of Chapter 2 of this thesis. Table 3.1 shows the quantified methyl halide emissions from different sources.

Table 3.1 Quantified methyl halide emissions from the mangroves and Oceans.

Plant Species	Time of incubation	Methyl chloride	Methylene chloride	Reference
A. germinans*	>240 days (Laboratory)	82 mg m <sup>-2</sup> yr <sup>-1</sup>	n.q.	[1]
A. germinans*	~1.5years (Laboratory)	27 mg m <sup>-2</sup> yr <sup>-1</sup>	n.q.	[1]
R. Mangle*	>240 days (Laboratory)	29 mg m <sup>-2</sup> yr <sup>-1</sup>	n.q.	[1]
R.Mangle*	~1.5years (Laboratory)	97 mg m <sup>-2</sup> yr <sup>-1</sup>	n.q.	[1]
Ocean	Field	2.8 mg m <sup>-2</sup> yr <sup>-1</sup>	2.5 mg m <sup>-2</sup> yr <sup>-1</sup>	[2]

\* based on LAI = 5. n.q. not quantified. [1] Manley et al. (2007), [2] Chapter 2 of this thesis.

### 3.3 Field experiment in Braganca

The tropical Braganca coastal region was chosen for field sampling. Braganca encompasses a mangrove ecosystem at the Atlantic coast that reaches from the state of Para in the eastern Amazonia, northern Brazil. Braganca is 210 km away from the city of Belem. The general local classification is “Region Bragantina” which is a part of the “Amazon Oriental” (Krause et al., 2001). The Bragantiana mangrove ecosystem is integral part of the 2340 square kilometer area of the municipality of Braganca. Brazil has an area of 8500 square kilometer of coastal mangrove region, and is the second largest mangrove forest on the earth (Kjerfve et al., 1997). Hereafter the Bragantina mangrove ecosystem is referred to as the Braganca mangrove ecosystem. The Braganca coastal mangrove forest is dominated by three species namely, *Rhizophora mangle* (Red mangrove), *Avicennia germinans* (Black mangrove) and *Laguncularia racemosa* (White mangrove) (Krause et al., 2001). The mangrove forest also consists of grass area. The growth of the mangroves depends on different environmental factors such as soil type, salinity and tidal activity in that region. The average height of a mangrove tree is about 20 m - 25 m in the Braganca. Also, it was observed that there was less than 1 m tall mangrove trees in the forest. Figure 3.1 shows the mangroves trees in the Braganca forest.



*Figure 3.1 Mangrove forest in the tropical Bragança. (Foto by the author of this thesis).*

### **3.3.1 Experimental setup and data to be measured**

The field equipment consisted of well equipped weather stations and Chemistry instruments such as a Gas Chromatography (GC). Observations related to the chemical samples were carried out by Dr. habil. Frank Laturus from the Institute for Biogeochemistry and Marine Chemistry (IfBM), University of Hamburg. However, the campaign in the mangrove forest had to be done with a very limited instrumentation. Due to custom security clearance problems, only very few instruments were available. The following are the list of instruments:

- 1) Flow meter for adjusting and correcting air flow rates.
- 2) Adsorption tubes to collect air samples.
- 3) Timer.
- 4) Portable generator.
- 5) Thermometer.
- 6) Anemometer.

The meteorological parameters and air samples were measured at the coastal and inland location. Meteorological parameters such as temperature, wind speed and wind direction are

important factors to determine the emission from the forest. Basic equipments were used for collecting the air samples in the metallic tubes. The air samples were processed at the Federal University of Pará (UFPA). These processed air samples were later analyzed in the Institute for Biogeochemistry and Marine Chemistry, University of Hamburg by Dr. habil. Frank Laturus using well equipped GC. Data were reviewed by Dr. Bahlmann from the same group.

Wind speed was measured at a height of 1.5 m from the ground level using an Instrutherm AD-155 portable anemometer. A simple thermometer was used to measure the ambient air temperature. The thermometer was not covered with an instrument shelter or a thermometer shelter. Thus, it takes the direct heat radiation into consideration as well. Figure 3.2 shows the observational setup in the field with the available limited instruments.

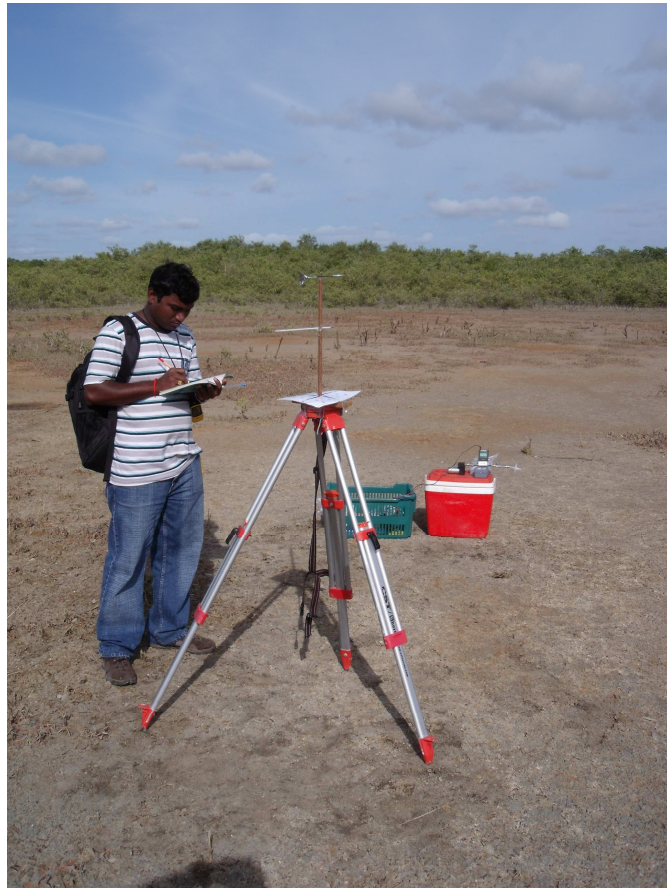


*Figure 3.2 Instruments used in the mangrove forest (Foto by Dr. Frank Laturus).*

A survey was conducted in the tropical mangrove region for the best possible upwind and downwind sites. Braganca beach position with the co-ordinates of  $0^{\circ} 49' 29.9''$  S,  $46^{\circ} 36' 56.5''$  W had been chosen as upwind location. Braganca region is in the equatorial belt.

The wind direction is mostly north-easterly, the trade winds from the equatorial Atlantic are most prominent. Hence, the beach region of Braganca is the most suitable place for an upwind measurement location.

The downwind position was located at the end of the mangrove forest. The coordinates of the downwind location were  $0^{\circ} 54' 04.5''$  S,  $46^{\circ} 40' 37.9''$  W. The north-easterly air mass then is advected over the mangrove ecosystem thus, a downwind position is chosen at the end of the forest. The downwind location was inundated during the high tide time. Both places are easily accessible in the forest. The distance between the upwind and the downwind location is about 8 kilometers. In general, the Braganca mangrove ecosystem is flooded regularly during high tide.

Some few additional observations were taken in the centre of the forest, which has a concrete bridge of 100 m length. The coordinates of the centre wind location are  $0^{\circ} 50' 41.9''$  S,  $46^{\circ} 38' 36.7''$  W. The sampling instruments were placed in the middle of the bridge.

The experimental procedure follows the simple Lagrangian approach. In this method, concentration differences essential to determine forest emission are calculated as the difference between the measured upwind and downwind concentration. The upwind site at the beach is called upwind. The site situated after the wind passed through the forest region is called downwind. Figure 3.3 shows the upwind and downwind locations in the tropical Braganca mangrove forest. Figure 3.3 is downloaded from NASA website (<http://landsat.usgs.gov/>) during field work from Prof. Dr. Nils Edvin Asp lab.

A southerly wind was measured on 15 December 2012. In that case the upwind and downwind positions were reversed (Figure 3.3). The gradient across the forest is calculated as difference between upwind and downwind concentrations across the space. It is expressed by equation (3.3).

$$E = (C_{upwind} - C_{downwind}) / \Delta X \quad (3.1)$$

Here  $C_{upwind}$  and  $C_{downwind}$  are the concentrations of methyl halides at upwind and downwind locations, respectively.  $\Delta X$  is the distance between upwind and downwind location in the mangrove forest.



Figure 3.3 Upwind and downwind positions of a mangrove forest area at Braganca (yellow color arrow shows the north direction of mangrove forest site).

Field work was carried out from 11 December 2010 to 17 December 2010. To add more information, the automatic meteorological weather station data from the Brazilian National institute of Meteorology (INMET) in Braganca ( $1.04522^{\circ}\text{S}$ ,  $46.7827^{\circ}\text{W}$ ) were collected. The INMET automatic weather station data are stored in one hourly intervals. These data can be downloaded from the INMET website ([http://www.inmet.gov.br/sonabra/maps/pg\\_automaticas.php](http://www.inmet.gov.br/sonabra/maps/pg_automaticas.php)) and are available for complete duration of the field campaign. These data were used for a better understanding of the observed field data. Figure 3.4 shows the time series of air temperature, wind speed and wind direction from the INMET automatic weather station and observed data in the field. The measured field temperature at the coast, inland and the centre wind well matched with the INMET weather station on 12 December 2010. Higher temperature and wind speed are observed during 15 to 17 December 2010 in the field compared to weather station location. It also shows a clear diurnal cycle in

temperature and wind speed during 11 to 13 December 2010 and thereafter cloudy conditions. Wind directions are excluded for wind speeds below  $0.5 \text{ ms}^{-1}$ , from the field as well as the INMET weather station data. The wind direction observed in the forest region was more likely constant easterly. The wind direction was mostly northerly on 11 – 13 December at the INMET station and thereafter variation was observed. The wind direction and wind speed show more variation on 14 – 15 December and higher wind speeds. It was also noted that there was thunderstorm activity in the field on 15 December. The rainfall was observed on 15 December after the morning samples. Overall, clear diurnal cycles of temperature and wind speed were seen from 11 December to 13 December and thereafter cloudier and thunderstorm activities occurred. Despite the limited meteorological instruments available in the field, reasonable weather data were collected. The anemometer was not available during 11 – 14 December 2010. Hence, wind speed and wind direction data are not shown in Figure 3.4 for that period.

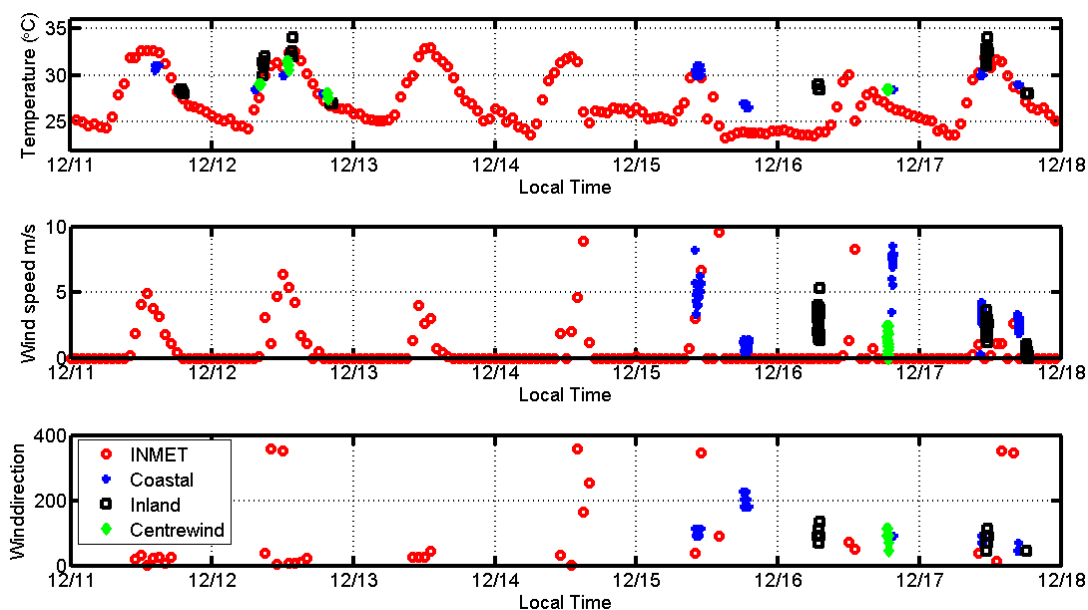


Figure 3.4 Observed meteorological parameters compared with INMET weather station data.

### 3.3.2 Observed concentrations from Braganca

This section describes the observed chemistry data in the mangrove field. Air samples were collected at the upwind, downwind and the centre wind region from the mangroves. In addition, the stable carbon isotope ratio of methyl halides from the air samples was measured in the isotope laboratory at the IfBM. Twenty ambient air samples were taken at the downwind, centre wind and the upwind from 11 to 17 December 2010. The sampling system

inlet was placed 50 centimeters above the ground. The duration of air sampling in the forest was 20 minutes and was done in the morning, noon and in the evening. Most of the samples had errors due to the interaction with humidity in the sample processing. Only one day of data for concentrations for methyl halides were valid from the field work due to difficulties in the sampling process.

Out of the twenty samples, four samples were taken for the stable carbon isotope analysis. The sampling duration for the stable carbon isotope analysis was 40 minutes.

The stable carbon isotope ratios are usually expressed in the  $\delta$ -notation (in ‰) relative to the Vienna Pee Dee Belemnite (V-PDB) standard:

$$\delta^{13}\text{C} = \left[ \frac{(^{13}\text{C}/^{12}\text{C})_{\text{sample}} - (^{13}\text{C}/^{12}\text{C})_{\text{standard}}}{(^{13}\text{C}/^{12}\text{C})_{\text{standard}}} \right] \times 1000 \quad (3.2)$$

A brief description of the configuration and validation of the sampling analysis for isotopic determination is given by Bahlmann et al. (2011), in which they have discussed the total sampling system. This study followed the above author's methodology for the chemistry analysis of air samples.

Table 3.2 shows the observed concentration and stable carbon isotope ratio of methyl halides from the mangrove ecosystem for the remaining samples. Sampling date, and time and the mixing ratios of different compounds at the upwind and downwind locations are given. Mixing ratios are expressed in pptv (parts per trillion by volumes). The sample time is in the local time of Brazil (BRT) and it is the starting time for sample collection. The stable carbon isotope ratios are in parts per mil (‰). Measured air samples at the centre of the forest are not obtained due to large errors. Hence, neither the concentration nor the carbon isotope ratio is available at the centre wind. The concentration difference between upwind and downwind is 744 pptv for  $\text{CH}_3\text{Cl}$ . In the case of  $\text{CH}_2\text{Cl}_2$  the difference is 178 pptv. The calculated concentration gradient is 93 pptv  $\text{km}^{-1}$  for  $\text{CH}_3\text{Cl}$  from the equation 3.1. In the case of  $\text{CH}_2\text{Cl}_2$  the concentration gradient is 22.25 pptv  $\text{km}^{-1}$  above the mangrove forest. The calculated gradient and concentration difference may suggest that mangroves may emit methyl chloride as well as methylene chloride. The stable carbon isotope ratios were smaller at the downwind location suggesting biological emission of methyl chloride (Table 3.2) from the tropical mangroves forest.

*Table 3.2 Observed mixing ratios and the isotope ratios of methyl halides at upwind and downwind location from mangrove ecosystem, n/a is not available.*

Compound	Mixing ratios (pptv)		Stable carbon isotope ratios (‰)	
	Upwind	Downwind	Upwind	Downwind
Sample location	Upwind	Downwind	Upwind	Downwind
Sample date time (BRT)	17.12.2010 16:40	17.12.2010 18:05	11.12.2010 14:15	11.12.2010 18:30
Methyl chloride	707	1451	-39.6 -37.8	-79.0 -63.2
Methylene chloride	38	216	n/a	n/a

### 3.4 Conclusions

This chapter provides the first field data of methyl halides from the tropical mangrove ecosystems. Due to all the problems involved with the field study and drawbacks due to not available instruments and problems in analyses of the concentration data, only very limited ambient air samples were obtained in this study. A simple Lagrangian approach has been used in this study. This approach may since be recommended for field studies in the forest region.

Observed meteorological parameters in the field are well matched with the INMET automatic weather station data. The measured concentrations show that methyl chloride and methylene chloride concentrations increase downwind over a forest. These high concentration differences suggest that mangrove forest may emit methyl chloride and methylene chloride in the tropical Braganca. The stable carbon isotope ratios of methyl chloride have larger negative values downwind indicating biogenic emission of methyl chloride from the tropical mangrove forest. The calculated stable carbon isotope ratio at the downwind position is similar to that of salt marsh and tropical plants. Hence, with the help of the stable carbon isotope ratios and concentrations data it has been concluded that mangroves emit methyl chloride and methylene chloride.

## 4. Adaptation and application of METRAS to the Braganca region

The atmospheric MEsoscale TRAnsport and fluid (Stream) model (METRAS) is adopted to simulate the meteorological conditions and transport of methyl halides over the tropical Braganca region.

### 4.1 Relevant qualities of the model METRAS

METRAS is based on the primitive equations, ensuring the conservation of momentum, mass and energy. The three dimensional equations are solved in a terrain-following coordinate system. Wind, temperature, humidity, cloud and rain water content as well as concentrations are derived from prognostic equations, whereas density and pressure are calculated from diagnostic equations (Schlünzen et al., 2012). METRAS has already been used to simulate atmospheric phenomena in different regions and for different applications (Dierer et al., 2005; Lüpkes et al., 1996; Niemeier et al., 1993; Schlünzen et al., 2003). However, this is the first study where METRAS has been applied for the Braganca region.

The concentrations of passive tracers are calculated in METRAS on an Eulerian grid by solving the conservation of mass equation in flux form:

$$\underbrace{\frac{\partial \bar{C}_s}{\partial t}}_{(a)} = - \underbrace{\frac{1}{\rho_0} \nabla(\rho_0 \bar{C} \bar{v})}_{(b)} - \underbrace{\frac{1}{\rho_0} \nabla(\rho_0 \overline{C'v'})}_{(c)} + \underbrace{Q_{source}}_{(d)} + \underbrace{Q_{sink}}_{(e)} \quad (4.1)$$

Equation (4.1) gives the rate of change of the average concentration (a), of different source regions resulting from the advection (b), turbulent diffusion (c), the sources (d) and the sinks (e). Chemical reactions and deposition of tracers are neglected in our present study, because the chemical species have long life times in the atmosphere of about a year. Furthermore, measured deposition velocity data are unavailable in the literature. Hence, wet and dry deposition calculations have been neglected in this study. Hence, in the eq. (4. 1) the sink term (e) can be neglected.

A biogenic emission has already been defined for pollen emission (Schueler and Schlünzen, 2006). There are six different types of passive tracers defined in the model which are used here to study the biogenic emissions in the Braganca region (Table 4.1). Out of the six, two are point sources at a fixed site corresponding to e.g. a few mangroves; T1 is at the

downwind position of the observational site, T2 at the upwind location (Figure 3.3). Passive tracer T3 is calculated for a constant emission rate that covers the entire mangrove region. Passive tracer T4 is the same as the third but the emission depends on humidity. T5 is used in the present study to represent emissions from the water, as a constant passive tracer, and T6 is the same as the fifth one, but emission depends on humidity. Table 4.1 summarizes the different types of passive tracer emission regions.

*Table 4.1 Different type of passive tracers in the model METRAS*

<b>Tracers</b>	<b>Source area</b>	<b>Emission function</b>
T1	Single stand downwind of measurement site	Constant
T2	Single stand upwind of measurement site	Constant
T3	Mangroves	Constant
T4	Mangroves	Depends on humidity
T5	Water	Constant
T6	Water	Depends on humidity

## **4.2 Selected model domain and input data**

The model METRAS is a limited area model. Therefore, boundary values are needed from a coarser resolved domain. The following describes the METRAS model domain, initial conditions and boundary values of the simulation setup.

The study region is located in the north eastern coastal part of Brazil, South America (Chapter 3). The model domain is setup for this region. The MODIS land cover data are used, which have a horizontal resolution of 500 m. The MODIS data can be downloaded from this webpage ([https://lpdaac.usgs.gov/get\\_data](https://lpdaac.usgs.gov/get_data)). These data were processed to a METRAS model readable format. The Shuttle Radar Topography Mission (SRTM) orography data of 100 m resolution are used for the tropical Braganca domain. The data can be downloaded from the webpage (<http://srtm.csi.cgiar.org>). Figure 4.1 shows the different land-use classes and the topography for the tropical Braganca region. Figure 4.1 (a) shows that meadows, mixed forest and mangroves are the most abundant land-use classes in the domain. The maximum orography height is about 115 m in the south west of the domain (Figure 4.1 b). The minimum orography can be seen along the coastal Braganca region.

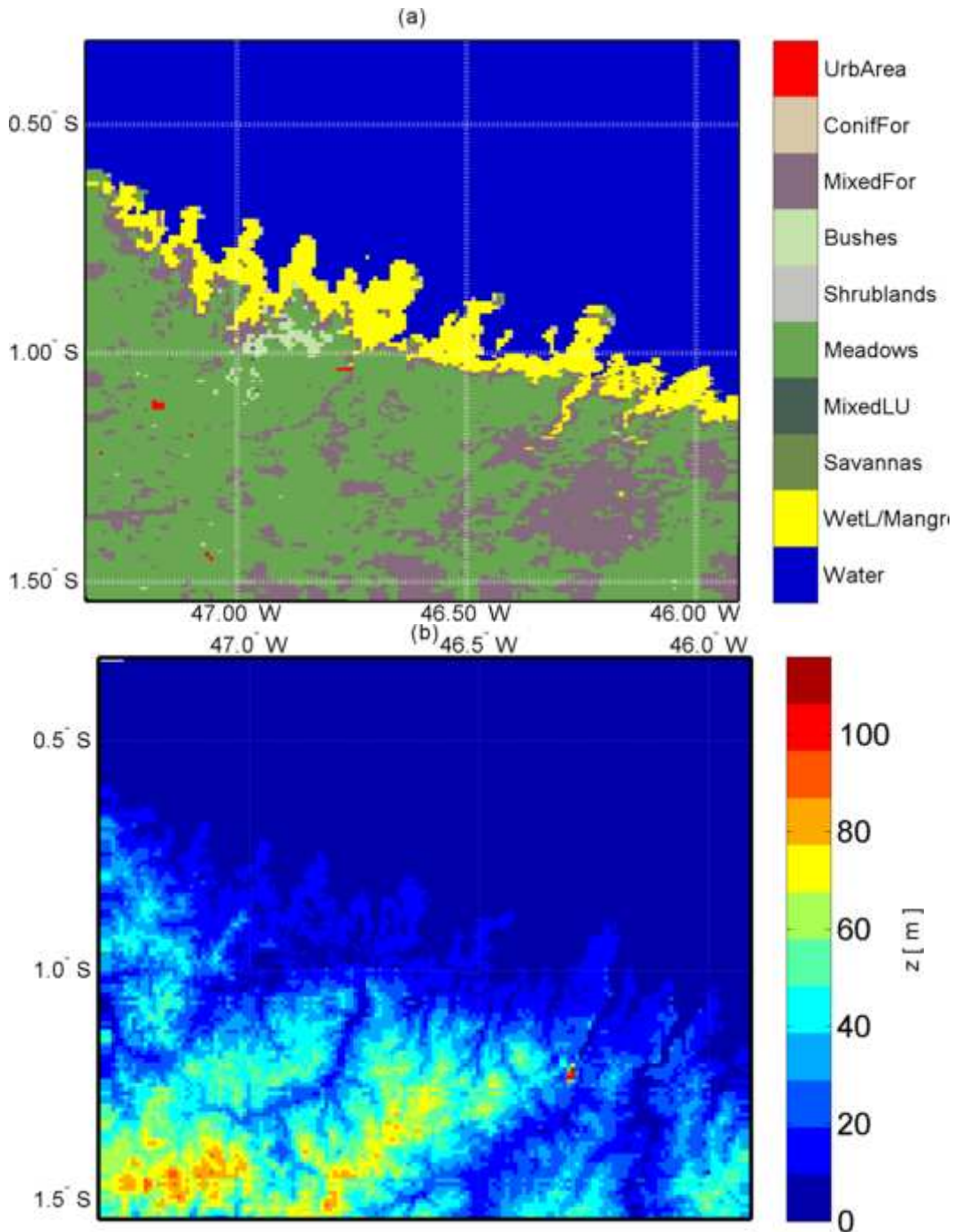


Figure 4.1 Different land-use classes (a) and orography (b) in the tropical Braganca region.

The MBAR forecast meteorological data of horizontal winds, potential temperature and specific humidity are used in METRAS as forcing fields. The MBAR is a limited area, finite difference, hydrostatic, primitive equation high resolution regional model whose domain covers most of South America. MBAR was developed by Deutscher Wetterdienst (DWD) which is the German Meteorological Service and was implemented at the National Institute

of Meteorology (INMET). The model MBAR needs initial and boundary conditions from the global model. DWD developed an operational global numerical weather prediction model, named GME, based on an almost uniform icosahedral–hexagonal grid. The MBAR model initial state and lateral boundary values are adapted from the analysis of the global model GME. DWD provides the analyses and forecasts of GME on all 60 model levels and seven soil layers at a horizontal resolution of 30 km up to 78 to 120 hours at 3-hourly intervals, based on the initial states for 00 and 12 UTC (Majewski, 2010). The horizontal resolution of the MBAR model is 7 km. Hourly data of wind, temperature and specific humidity are used as initial and lateral forcing for the METRAS model. The METRAS model has been setup for a Brazil domain with 1 km horizontal resolution. The model domain consisted of 157 km by 174 km horizontal and 34 non-homogeneous vertical grid levels. In this simulation sea surface temperatures are used from the observations by using a mean derived from the year 2010 for the month of December. The global ocean sea surface temperature data (HadISST1.1) developed by Rayner et al. (2003) were used in the simulation.

Since the limited area model domain is laterally limited, boundary values are required to integrate the model. The boundary conditions used in the METRAS model are as follows. For the lower boundary conditions of wind ( $u$ ,  $v$ ,  $w$ ), fixed values (i.e. zero) were prescribed. Large-scale values are prescribed at the upper boundary using absorbing layers below. The lateral boundary conditions for the boundary normal wind components are calculated as far as possible from the prognostic equations, for the boundary parallel wind components a gradient zero is assumed. Close to the lateral and upper boundaries a nudging term is added to the equations to ensure that wind, temperature and humidity can be nudged towards the forcing values of the coarser model (in this case MBAR).

The values of temperature and humidity are calculated from the energy budget equation at the lower model boundary. Zero gradients are used at the upper and lateral boundary for temperature and humidity. In the case of cloud water content, zero gradients were used at the lower and upper boundary. Large-scale values were prescribed as inflow points at the lateral boundary for cloud water content. For rain water content the flux at the boundary is set equal to the flux in the model at the lower boundary. The upper boundary conditions of rainwater content are zero gradients. At the lateral boundary, large-scale values are prescribed for rainwater content.

For the passive tracers at the lower boundary the flux at the boundary is calculated from deposition velocity. This is set to zero in the present case studies (see eq.4.1). At the upper

and lateral boundaries, zero gradients are used for the passive tracers. The boundary conditions are the same for all six tracers.

### 4.3 Adaptation of METRAS land-use classes to the tropical region of Braganca

In the METRAS model used here, 10 different land-use classes are distinguished. These classes were up to now adopted for the European region (Schlünzen et al., 1996) and widely used there. However, not all these land-use classes are represented in the Braganca region and other classes occur (Figure 4.1 a). In order to adopt this model, several sensitivity studies were conducted by tuning the physical parameters that are characteristic for each of the 10 different land-use classes, such as Albedo  $A_0$ , thermal diffusivity  $k_s$ , thermal conductivity  $\nu_s$ , soil water availability  $\alpha_q$  (starting value), saturation value for water content  $W_k$  and roughness length  $z_0$ . Table 4.2 gives the physical parameters obtained by sensitivity studies for the tropical Braganca region.

*Table 4.2 Surface characteristics adopted for the tropical Braganca region in the METRAS model.  $A_0$  denotes albedo,  $k_s [10^{-6} m^2 s^{-1}]$  and,  $\nu_s [J(Ksm)^{-1}]$  thermal diffusivity and conductivity of the soil,  $\alpha_q$  soil water availability (starting value),  $W_k [m]$  the saturation value for water in the ground,  $z_0 [m]$  the roughness length and  $h_\theta [m]$  is a resulting depth for the diurnal temperature wave.*

METRAS-changed	Class	$A_0$	$k_s$	$\nu_s$	$\alpha_q$	$W_k$	$z_0$	$h_\theta$
Water	0	$f(Z(t))$	0.15	100.0	0.98	100.0	$f(u_*)$	0.11
Wetland with mangroves	1	0.16	0.74	2.20	0.98	0.322	0.003	0.25
Savannas	2	0.20	0.57	1.05	0.90	0.026	0.0012	0.22
Mixed	3	0.20	0.52	1.33	0.90	0.138	0.04	0.21
Meadows	4	0.16	0.52	1.33	0.90	0.015	0.02	0.21
Shrubs	5	0.15	0.24	0.30	0.90	0.02	0.05	0.14
Bushes	6	0.20	0.52	1.33	0.90	0.081	0.10	0.21
Mixed forest	7	0.12	0.12	0.5	0.90	0.121	0.45	0.26
Coniferous forest	8	0.11	0.80	2.16	0.90	0.161	0.60	0.26
Urban area	9	0.15	1.4	2.93	0.90	0.05	0.70	0.45

The surface characteristics are used to calculate the surface temperature, which is calculated from the energy budget equation in the model METRAS. The surface energy budget equation is used in the model METRAS as follows:

$$(1 - \alpha)(I + D) + L \downarrow - L \uparrow + Q_H + Q_E + Q_S + Q_F = 0 \quad (4.2)$$

Here  $(1 - \alpha)(I + D)$  characterizes the direct and diffusive short wave radiation budget. The incoming and outgoing long wave radiative fluxes  $L$  are also calculated with respect to the radiation budget in the atmosphere. The terms  $Q_H$  and  $Q_E$  are the sensible and latent heat fluxes. They are calculated dependent on the friction velocity  $u_*$  and scaling values for temperature  $\theta_*$  and humidity  $q_*$ . These last three parameters depend on the roughness length  $z_0$ .  $Q_S$  is the heat exchange with the ground, which depends on the thermal characteristics of the ground. The last term  $Q_F$  is the anthropogenic heat emission, which is not considered in this study.

Following Tiedke and Geleyn (1975) and Deardorff (1978), eq. (4.1) is solved using the force-restore method, which results in the below form:

$$\frac{\partial \bar{T}_s}{\partial t} = \frac{2\sqrt{\pi k_s}}{v_s \cdot h_\theta} \left\{ \mu I_\infty \cos(Z(t)) - \hat{\varepsilon} \sigma \bar{T}_s^4 + c_p \rho_0 \theta_* u_* + l_{21} \rho_0 q_* u_* - \sqrt{\pi v_s} \frac{\bar{T}_s - \bar{T}(-h_\theta)}{h_\theta} \right\} \quad (4.3)$$

The values used for different land-use classes of the tropical Braganca are given in the Table 4.2. The values for the northern Europe land-use classes are given in the scientific documentation of the Multi Scale Model System M-SYS by Schlünzen et al. (2012).

The following sections discuss more in detail the energy fluxes calculated from the model and observed data for different land-use classes. The model METRAS was integrated per land-use class for one case with standard parameters named METRAS-standard. The second one is with changed parameters for the Braganca region named METRAS-changed. In order to understand the energy budget of the different land-use classes in the model, the surface type is defined as homogeneous in space which means total grid represents 100% of the same land-use class.

With the values in the Table 4.2 it can not be expected that model results agree completely with measurements, since the homogeneity is not found in reality. However, it is sufficient to check whether the range of the model calculated fluxes and their relative magnitudes are correct or not. For this, the METRAS model has been integrated for 20 days for all the land-

use classes. However, model calculated fluxes are shown here only for dates with measurements data available.

The most cited and available data were chosen at the time of model adaptation in this study. However, currently new data may or may not be available for these land-use classes. Hence, the newly available data were not considered in this study. It is noted that first priority was given to finding tropical measurements of different land-use class. All land-use classes did not have tropical measurements. Hence, homogeneous land-use data were created in order to run the model for the corresponding experimental location.

### **4.3.1 Adaptation of land-use class water**

Water covers 36% in the model domain. In this land-use class, no changes were made in the model METRAS surface characteristics. Hence, the METRAS-standard land-use class fluxes and changed land-use class fluxes are identical.

The METRAS water surface was initialized with a 23°C temperature, 80% humidity and a 3 m s<sup>-1</sup> wind speed, and the model was integrated from 13 July, 2010. The initialized water surface temperature represents the climatological value of the water temperature over the tropical Atlantic Ocean for July. Figure 4.2 shows the diurnal cycle of surface fluxes and temperature simulated by the model for 22 July, 2010. The Figure gives nearly constant sensible, latent and ground heat fluxes. It is common to see constant fluxes over the water surface, because the surface type is relatively homogeneous in space and time. Hence, SST is kept constant in the METRAS model integration.

The model METRAS can not changes the surface water temperature in the model integration. Hence, constant surface water temperature can be seen (Fig. 4.2 (b)). It is noted that a slight decrease in the 2 m and 10 m temperature occurs during the day. This is due to the vertical mixing of the atmosphere which mixes cooler Air to lower levels with increasing integration time.

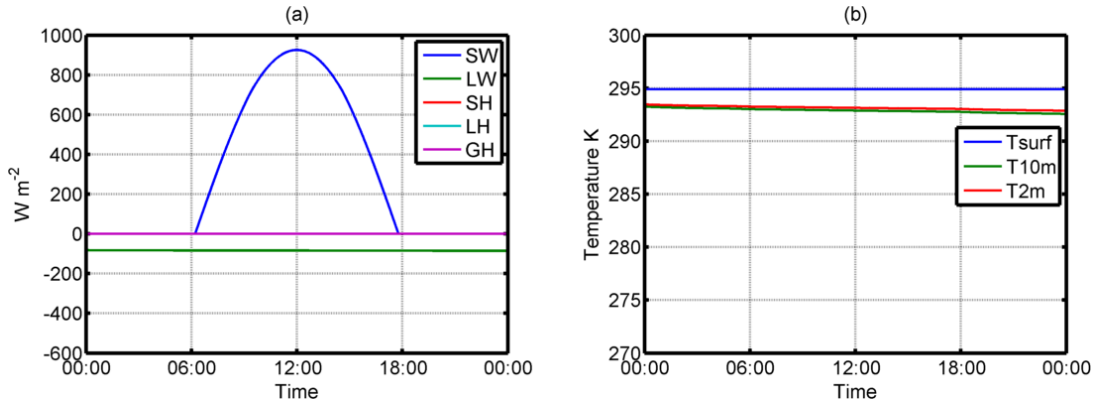


Figure 4.2: Diurnal cycle for water (a) contribution of surface fluxes to the surface energy budget as calculated by METRAS (shortwave radiation (SW), long wave radiation (LW), sensible heat flux (SH), latent heat flux (LH), ground heat flux (GH) in  $W m^{-2}$ ), and (b) surface temperature ( $T_{surf}$ ), temperature at 10 m above surface ( $T_{10m}$ ) and temperature at 2 m above surface ( $T_{2m}$ ).

### 4.3.2 Adaptation of land-use class mudflats to wetland with mangroves

The land-use class mangroves is newly introduced in the model METRAS. The only differences in the mudflats land-use class (METRAS-standard) and wetland with mangroves (METRAS-changed) are albedo and roughness length changes in the model. The wetland with mangroves land-use class consists in 6% in the model domain.

To check the validity of the newly found parameters for this class, the surface energy fluxes were validated for this class against the observed fluxes over an wetland ecosystem. This is not optimal, but there are no energy budget measurement studies for a mangrove region that could be used. Hence, this study used the wetland ecosystem surface energy fluxes. Energy exchange is among the most important processes in wetland ecosystems, because it affects variables such as temperature, water transport, plant growth and productivity (Dennison and Berry, 1989).

Burba et al. (1999) observed energy fluxes at Ballards Marsh ( $42^{\circ} 30' N$ ,  $100^{\circ} 25' W$ ) located in the Sand hills region of north central Nebraska, USA. In their study, they measured net radiation, incoming and outgoing radiation 1 m above the canopy. The observed air temperature and wind speed at 2 m above the canopy were  $30^{\circ} C$  and  $4 m s^{-1}$ , respectively, on 18 July, 1994. The canopy height was varying about 3 m to 1.5 m at the observational cite.

The METRAS model was initialized with a large-scale pressure of 1013.25 hPa, a temperature of  $30^{\circ} C$  and  $4 m s^{-1}$  wind speed, 80% relative humidity for the observational site

Ballards Marsh. The model has been integrated from 16 July, 1994. Figure.4.3 shows the diurnal cycle on day 2 of the model integration of all surface energy budget fluxes for the METRAS-standard surface class (Figure 4.3b), METRAS-changed (Figure 4.3a) against measured fluxes (Figure 4.3c) for wetlands

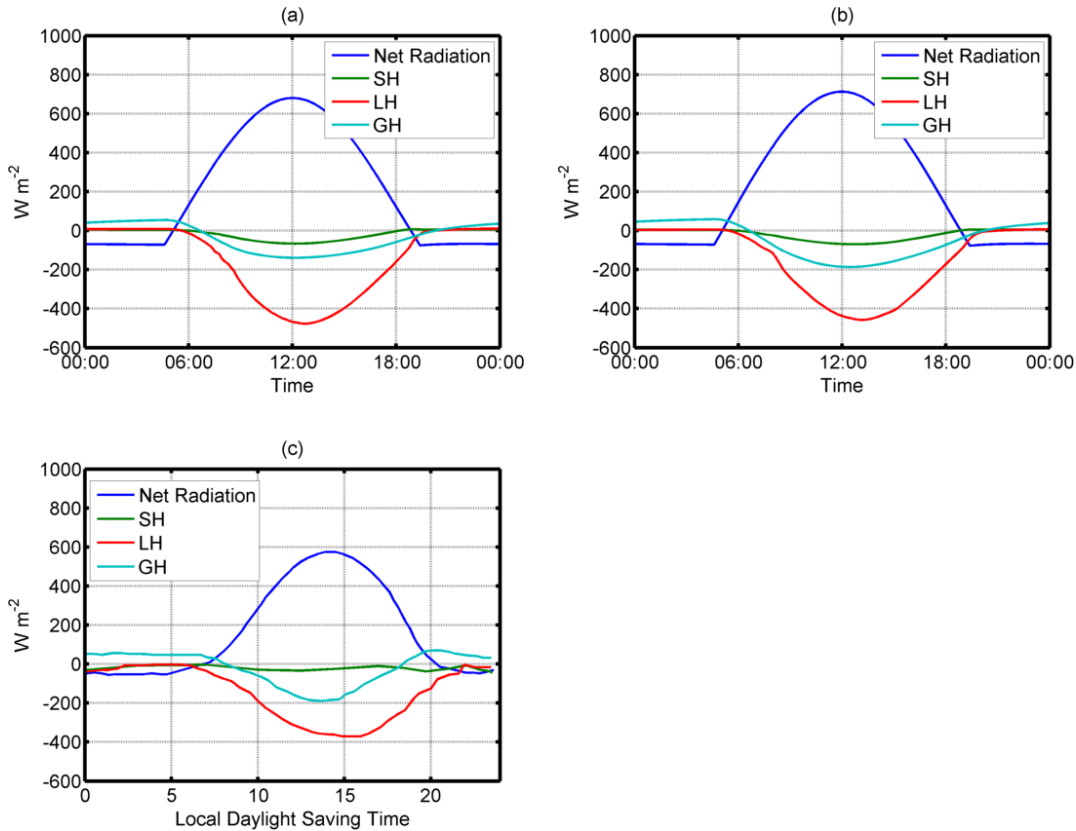


Figure 4.3 Diurnal cycle for wetland with mangroves. Contribution of surface fluxes of different surface energy fluxes of model (a) METRAS-changed (b) METRAS-standard and (c) measured. Sensible heat flux (SH), latent heat flux (LH), ground heat flux (GH) in  $W m^{-2}$ .

The net radiation fluxes simulated by the model in the two cases are higher than the observed data. The magnitudes of the observed sensible heat flux (SH) increases from  $0 W m^{-2}$  to  $40 W m^{-2}$  between 7:00 – 10:30 and then slightly decreased (to  $20 W m^{-2}$ ). Night time observed values of the sensible heat flux ranged from  $-40 W m^{-2}$  to  $-30 W m^{-2}$ . METRAS-changed and METRAS-standard calculated sensible heat fluxes are  $-11 W m^{-2}$  at 7:00,  $-55 W m^{-2}$  at 10:00 and then thereafter decreased to  $-20$  at 17:00. The off set in the observed and model energy fluxes are due to the local day light saving in the measurements (UTC-5).

Diurnal variation of measured latent heat flux (LH) ranged up to  $-300 W m^{-2}$  to  $-380 W m^{-2}$  during day. Peak magnitude of the latent heat flux LH occurred about one to two hours after

the peak in net radiation. This is likely due to enhanced evapotranspiration in the afternoon resulting from observed high air temperature. However, the model calculated fluxes are stronger than the measured values (between  $-241 \text{ W m}^{-2}$  to  $-476 \text{ W m}^{-2}$ ). These values are not completely out of range. For example, Lafleur (1990) measured latent heat flux ranging from  $-210 \text{ W m}^{-2}$  to  $-400 \text{ W m}^{-2}$  for sedge-dominated wetlands in Canada. Smid (1975) reported larger magnitudes of midday latent heat flux varying from  $-400 \text{ W m}^{-2}$  to  $-500 \text{ W m}^{-2}$ . The model was not initialized for the Lafleur or the Simd study, but it is considered that the model fluxes are comparable with observations.

The diurnal pattern of the observed ground heat flux (GH) generally follows that of net radiation. This can also be seen in the model results. The flux magnitudes of the model simulated are more or less close to the observed data.

Figure.4.4 shows the diurnal variation of model temperature compared with measured data. The air temperature at the site ranges from 291 K to 305 K. The model temperature ranges from 299 K to 305 K. The temperature is slightly higher for the METRAS-changed land-use class than the METRAS-standard. Although the model does not reach observed minimum temperatures, there is a good agreement with the magnitude of maximum temperature. The temperatures are damped in the model due to more latent heat flux (more evaporation) in the model. Both the models do show the diurnal cycle. Very small difference is noted in the two model temperatures at 2 m.

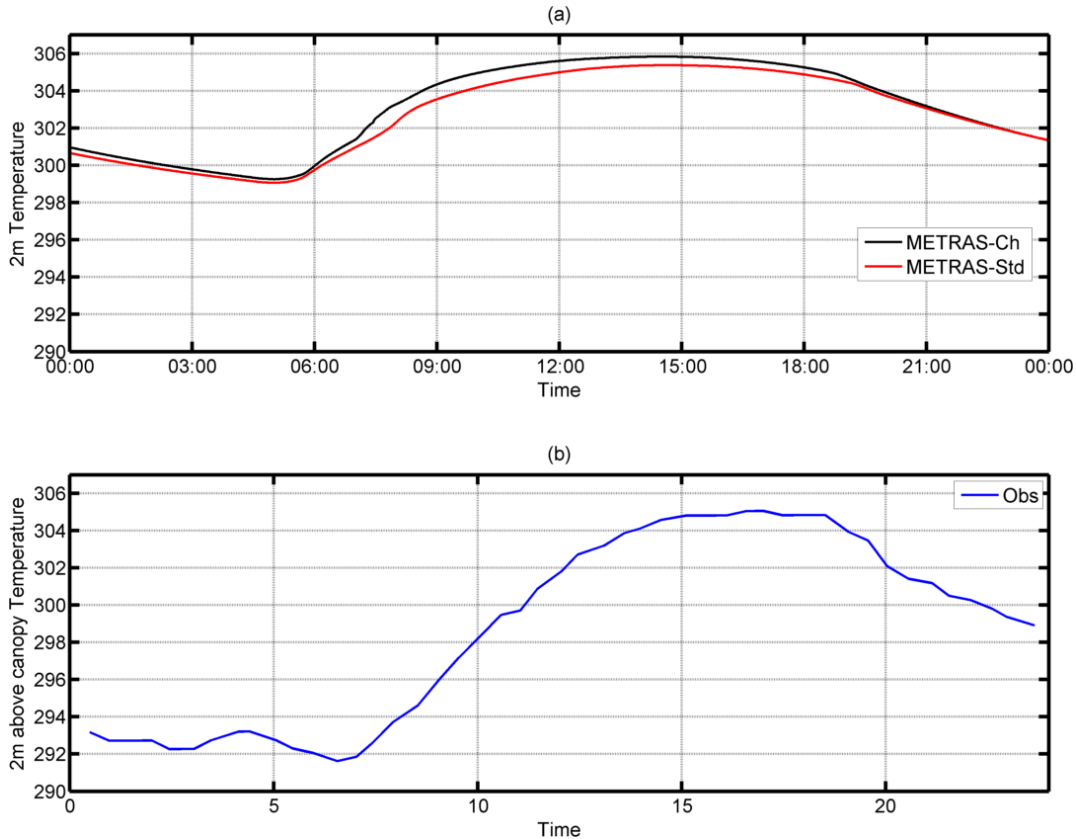


Figure 4.4 Comparison of diurnal variation of (a) model results and (b) measured temperature at the observational site.

The model calculated energy fluxes are within the range of measurements. The adopted parameters and standard parameters gave very small difference in the fluxes. But, with the new parameters the latent heat flux is slightly higher, which can be considered as characteristic for the tropical mangroves. Hence, the adopted new parameters are good for the tropical humid region.

### 4.3.3 Adaptation of land-use class savannas

The land-use class savanna is present in 0.1% of the model domain in the tropical Braganca. This is a new land-use class adopted in the model METRAS. Hence, the METRAS-standard fluxes are not calculated. Tropical savannas including those of central Brazil (Cerrado) serve as an important regulator of energy and mass exchange with the atmosphere (Miranda et al., 1997). Tropical savannas cover about one - eighth of the global land surface (Scholes and Archer, 1997) and are characterized by high plant species diversity.

Giambelluca et al. (2009) measured energy fluxes at the Cerrado region. Their field measurements were conducted at two sites within the Brazilian Institute for Geography and Statistics (IBGE) ecological reserve. The field experimental station was located approximately 33 km south of the centre of Brasilia ( $15^{\circ} 56'S$ ,  $47^{\circ} 53'W$ ) at approximately 1100 m in elevation. The annual range of monthly mean air temperature is very small, with a minimum of  $20.1^{\circ}C$  in June and a maximum of  $23.5^{\circ}C$  in October. Observational instruments such as the net radiometer were mounted above the canopy at 13.43 m. The canopy height is about 8 - 10 m in the experimental site.

The model was initialized with a  $20^{\circ}C$  temperature,  $3\text{ m s}^{-1}$  wind speed and 80% humidity for the same latitude and longitude as the observational site for 1 July 2001. Figure 4.5 shows a comparison of model calculated diurnal variation of surface fluxes with observed mean patterns of net radiation and latent heat flux for July 2001. Model data are taken on 3 July 2001 for comparison. The measured net radiation maximum in the month of July was  $558\text{ W m}^{-2}$ . Model calculated maximum net radiation is  $500\text{ W m}^{-2}$  in the noon. The net radiation calculated from the model is comparable in size with the measured data. In Figure 4.5 b, the maximum net radiation is observed at about 16<sup>th</sup> number of data point (i.e. about 12 LST) in the experimental site. A diurnal cycle of latent heat flux is observed in the model. There were no observational data of sensible heat fluxes in the canopy. Calculated Bowen ratio values are in the range between greater than zero to less than one for July in the canopy at the experimental site. Model calculated Bowen ratios are within the range of these measurements.

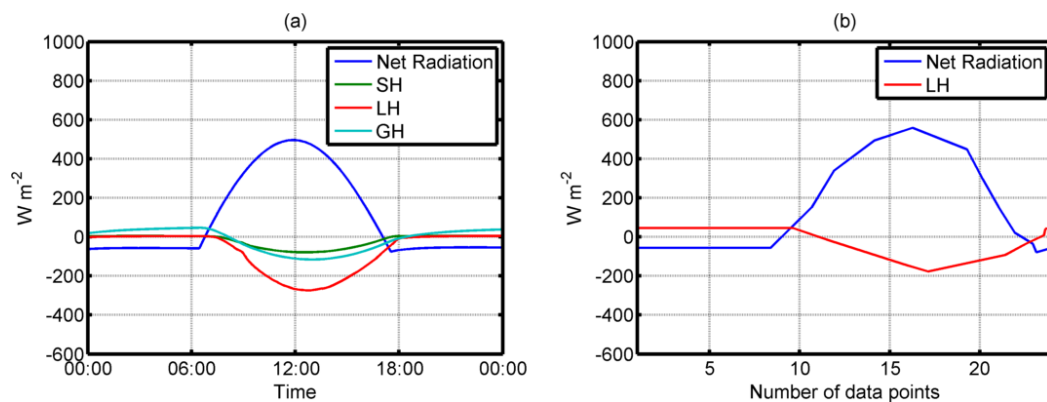


Figure 4.5 Different surface energy fluxes calculated by (a) METRAS-changed and (b) observed mean diurnal cycle of energy flux for July month at the experimental site.

Figure 4.6 shows the model calculated and measured temperature for the same site. Measured daily average temperature data were downloaded from the IBGE website. Measured

temperatures show a narrow diurnal variation of temperature over the savanna regions for July 2001. There are no hourly observed data available at the experimental site. The daily average data are shown in Figure 4.6 b, for July 2001. The model simulated maximum temperature is about 296 K for 3<sup>rd</sup> July 2001 which is slightly lower than the maximum measured daily mean (297 K).

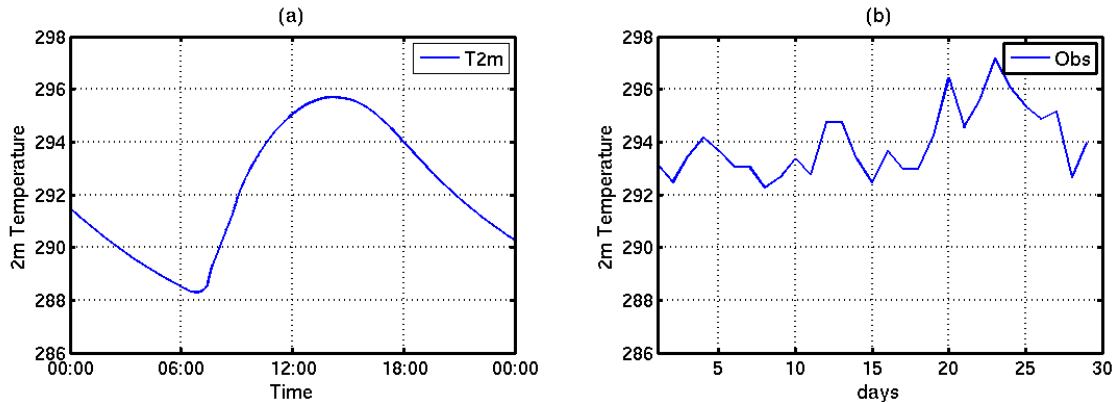


Figure 4.6 Comparison of (a) model temperature for one day, with (b) measured daily average temperatures for July 2001.

The adopted surface characteristics can not very well be evaluated due to a lack of all surface energy fluxes in the observed data. However, the model results are in a reliable range and may not affect the results of this study very much, due to a very small area in the domain covered with savannas. Hence, one can use these adopted savannas land-use class surface characteristic parameters.

#### 4.3.4 Adaptation of mixed land-use class

The mixed land-use class covers 0.2% of the model domain. Hemakumara et al. (2003) measured fluxes over a mixed vegetation area at Horana, a field site located about 40 km southeast of Colombo, Sri Lanka. The field site was typical of the Sri Lanka wet zone with mixed land cover composed of both perennial and non-perennial vegetation. These data were used to compare with, because only this study was available for the tropical region.

METRAS was initialized for 28 December 1999 initialized with 3 ms<sup>-1</sup> wind speed, 80% relative humidity and 26°C large-scale real temperature at the experimental site location. Soil water availability ( $\alpha_q$ ) only changed in the model METRAS-changed from 0.2 in METRAS-standard to 0.9 in METRAS-changed. Diurnal cycles of the fluxes are shown in Figure 4.7. The maximum net radiation measured was 700 Wm<sup>-2</sup>. Model simulated net radiation is

slightly lower than the measured data. Higher net radiation in the measurements is partly due to the somewhat higher altitude (about 200 m) of the field site. The sensible heat flux (SH) simulated from the model METRAS-changed is similar to measurements.

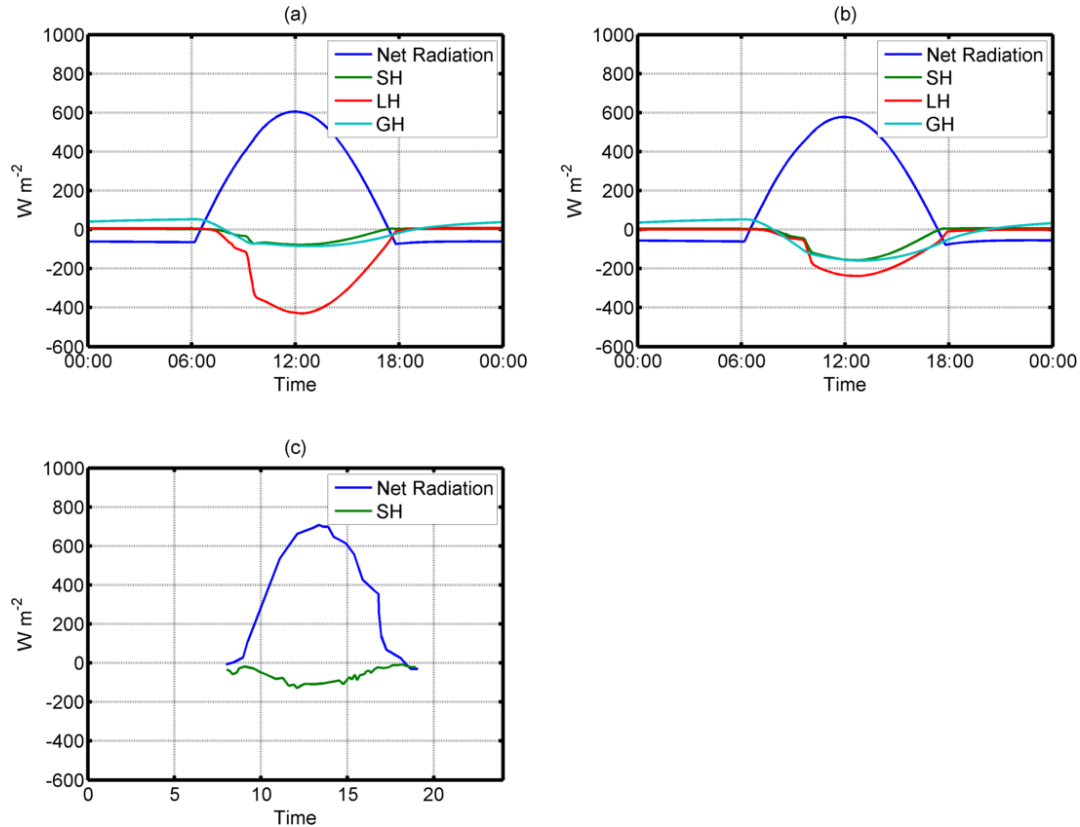


Figure 4.7 Variation of diurnal fluxes of models (a) METRAS-changed, (b) METRAS-standard and (c) measured data on 1 January 2000.

The adopted surface characteristics again cannot be well evaluated due to lack of all surface energy fluxes in the observed data. However, the available results look promising and, again, the model results may not be affected in this study very much by this land-use due to their very small area in the domain. Hence, one can use these adopted mixed land-use class surface characteristic parameters.

### 4.3.5 Adaptation of land-use class meadows

Meadows land-use class covered 41% in the model domain. In this land-use class observed data are adopted from Kurc and Small (2004). Data were collected from the McKenzie Flats area of the Sevilleta National Wildlife Refuge (SNWR), central New Mexico, U.S.A. Measurements were conducted at grassland (meadows) and a shrub land which are separated by 2 km. The temperature and wind speed data from the measurement site were not available.

The measurements were taken at both the sites at 3.5 m above the canopy. At both sites soil variables were measured at 5 cm depth. The observed data represent an average diurnal cycle of the energy fluxes for the season 1 June - 15 September for three years (2000-2002).

Albedo, soil water availability and roughness length are changed in the model METRAS-changed compared to the METRAS-standard. Both model versions were initialized with the temperature 24°C, 80% humidity and with wind speed of 5 ms<sup>-1</sup> for June 2000. The temperature, wind speeds and albedo were taken from observed data. The model results are presented for 3<sup>rd</sup> June 2000.

Figure 4.8 shows the model METRAS simulated energy fluxes compared with measured data at the site location. The shortwave radiation simulated by the model METRAS-changed is close to the observed radiation. The long wave radiation simulated by the model in both cases is smaller than observed. The ground heat flux magnitude is in the reasonable range with measured data in both the cases. The authors calculated sensible and latent heat fluxes using the Bowen ratio method (Shuttleworth, 1993; Moncrieff et al., 2000). The authors noted that at sunrise and sunset, the sensible and latent heat fluxes were opposite in sign and nearly equal. This gives a Bowen ratio close to -1. Similarly, we calculated Bowen ratio values at sunrise (5:50 am) and sunset (20:17 pm) are -1.8, -2.2, respectively, for the model METRAS-changed and -2.3, -8.5, respectively, for the model METRAS-standard.

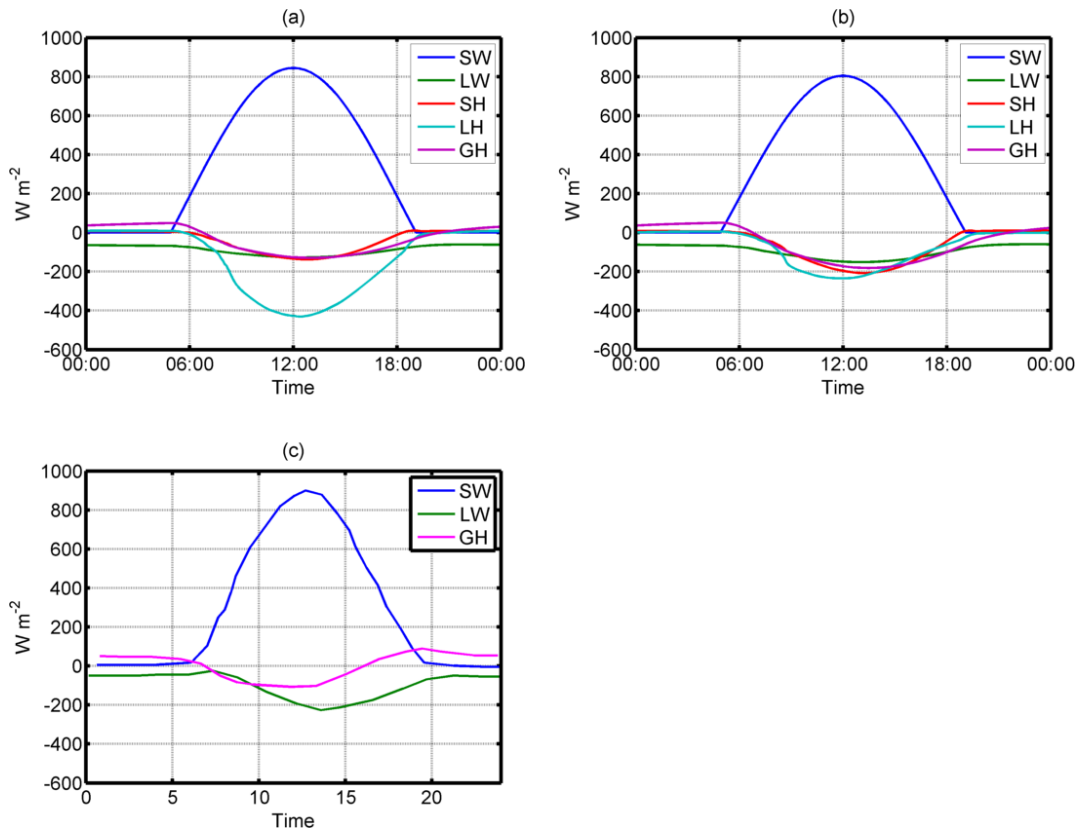


Figure 4.8 Simulated METRAS-changed (a), METRAS-standard (b) and measured (c) energy fluxes for the meadows land-use class.

The adopted surface characteristics gave a higher confidence into the Bowen ratio values and the net radiation values compared with measured data. Hence, one can use these adopted meadows land-use class surface characteristic parameters for the tropical humid region.

### 4.3.6 Adaptation of land-use class heath to shrubs

Small portion 0.04% of the model domain contains shrubs. The meteorological data collected for this land-use class are the same as for the meadows land-use class study. Hence, the model is initialized with the same meteorological data as used in the meadows class but with wind speed ( $3 \text{ ms}^{-1}$ ).

In this land-use class soil water availability and saturation value for water content are increased for the shrubs land-use class in the model METRAS-changed in order to represent humid tropical region.

Figure 4.9 shows the comparison of energy fluxes between measured data and model simulation. The shortwave radiation calculated from the model is slightly lower compared with observed data. The shortwave radiation peaked at noon at  $856 \text{ W m}^{-2}$  for METRAS-changed,  $853 \text{ W m}^{-2}$  for METRAS-standard and  $873 \text{ W m}^{-2}$  for the measurement site respectively. However, the net radiation calculated from the models is slightly lower than the observed data. Variation of ground heat flux between the measurements and METRAS-standard were seen. Slightly negative ground heat flux is seen in the METRAS-changed simulation.

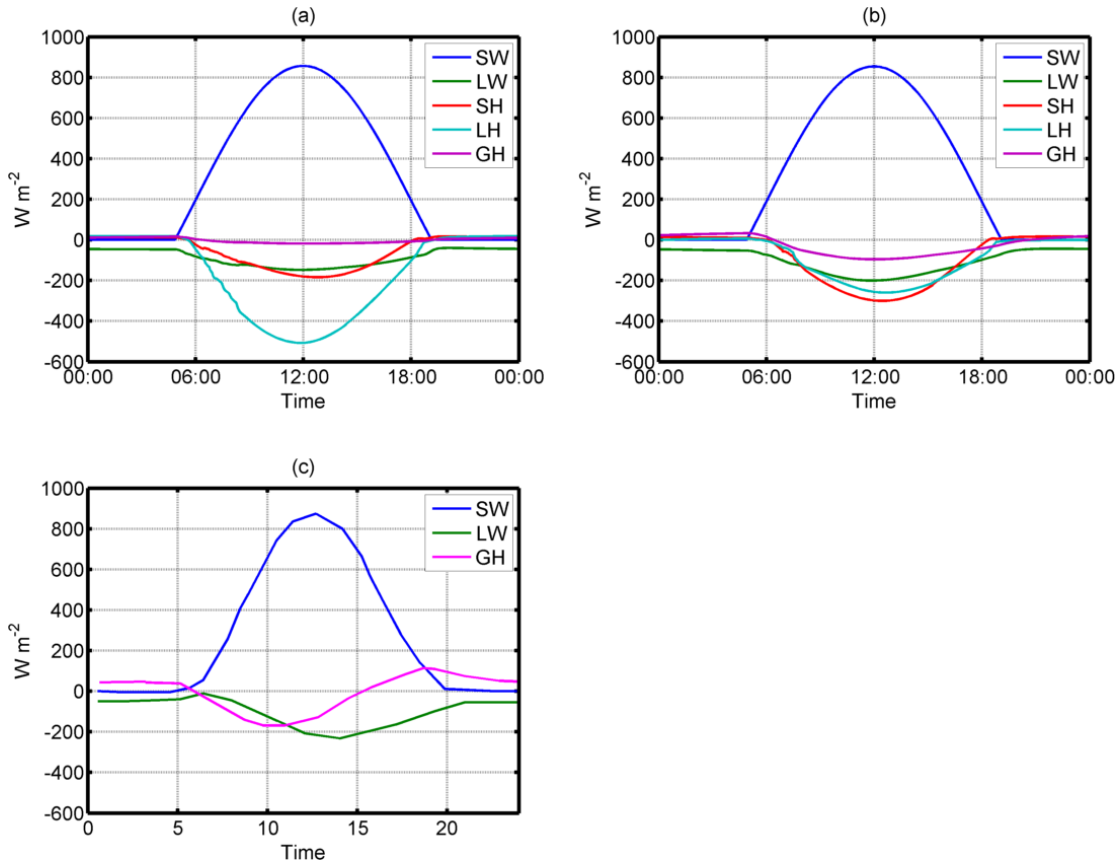


Figure 4.9 Simulated (a) METRAS-changed, METRAS-standard (b) and measured (c) energy fluxes for shrub land-use class at the experimental site.

The adopted surface characteristics again cannot well be evaluated due to a lack of all surface energy fluxes in the observed data. However, the selected model parameters may not affect much this study due to a very small area in the domain covered by shrubs land-use class. Hence, one can use these adopted shrubs land-use class surface characteristic parameters.

### **4.3.7 Adaptation of land-use class bushes**

This land-use class contains 1% in the model domain. Mauder et al. (2007) measured energy fluxes at NIMEX-1 site. The site was located at the Obafemi Awolowo University, Ile-Ife, Nigeria ( $7^{\circ} 33' \text{N}$ ,  $4^{\circ} 33' \text{E}$ ). The ground heat flux is measured at 0.02 m depth. The measurement heights of net radiation, sensible heat flux, latent heat flux, and temperature were 1.92 m, 2.48 m, 2.43 m, and 4.88 m, respectively.

The soil water availability is increased from 0.3 to 0.9 in the model METRAS-changed compared to METRAS-standard due to high soil water availability in the tropics. The remaining surface parameters of this land-use class are unchanged in the model run. The model METRAS was initialized with  $30^{\circ}\text{C}$  temperature, 80% humidity and  $3 \text{ m s}^{-1}$  wind speed on 29<sup>th</sup> February, 2004. The temperature and wind speed values are taken from the measurement site.

Figure 4.10 shows the model energy fluxes and observed data for March 6, 2004. The model has simulated higher short wave and net radiation in both the cases. The incoming shortwave radiation is too high because clouds are neglected and then with too much radiation all fluxes are higher in the model results than in the observations. The Bowen ratios calculated from the measurement data range between 0.3 and 0.5. Model calculated Bowen ratios are in range of 0.4 to 0.5 and 0.3 to 0.2 from METRAS-standard and METRAS-changed, respectively. The model simulated sensible and latent heat fluxes are comparable with the measurement data. The model METRAS-changed simulated higher latent heat flux than the METRAS-standard.

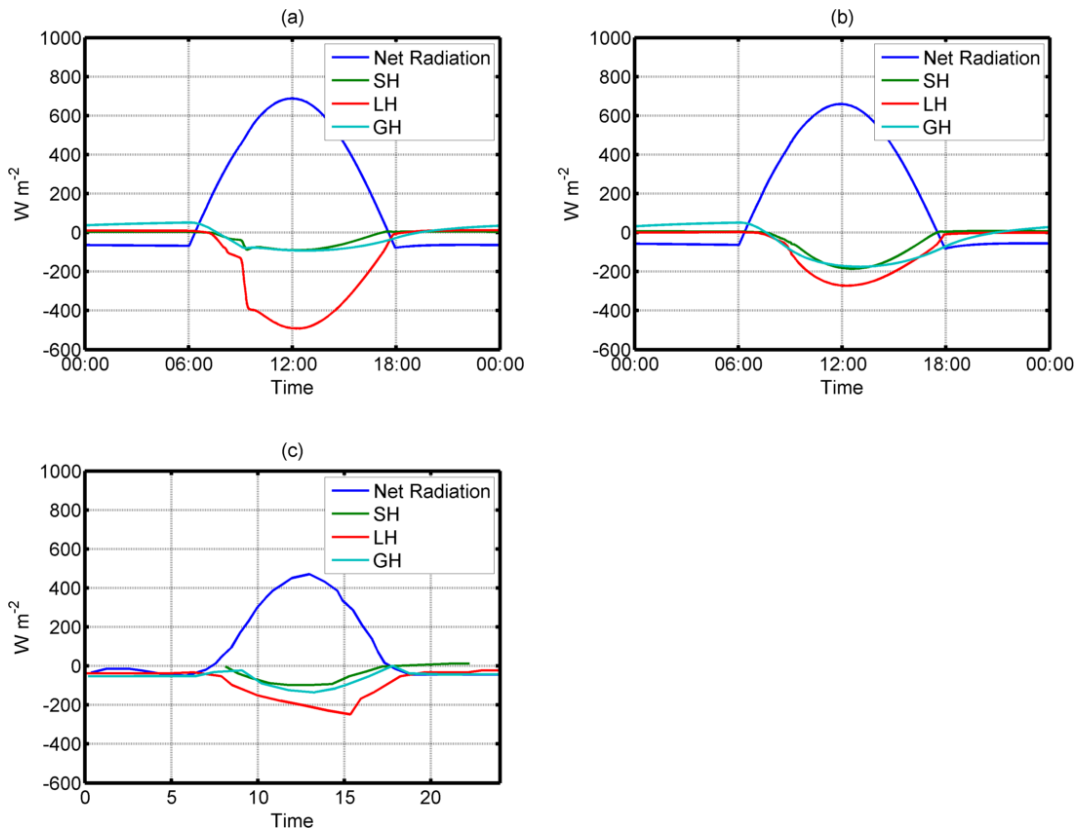


Figure 4.10 Comparison of simulated model METRAS-changed (a), METRAS-standard (b) and measured (c) energy fluxes for 6<sup>th</sup> March 2004.

The adopted surface characteristics gave sufficient confidence in model Bowen ratio values, but rather too high net radiation values compared with measured data. However, the selected model parameters may not affect much this study due to its small area (1%) in the domain. Hence, one can use these adopted bushes land-use class surface characteristic parameters for the tropical humid region.

#### 4.3.8 Adaptation of land-use class mixed forests

Mixed forest contains 17% in the model domain. McCaughey (1985) studied the energy budget over mixed forest during the summer of 1981 at the Petawawa National Forestry Institute, Chalk River, Ontario, Canada (45° 58'N, 77° 25' W). Instruments such as radiometers were mounted at 21 m. Based on observed meteorological conditions at this site, the model has been initialized with a temperature of 23°C, 82% humidity, 3 m s<sup>-1</sup> wind speed for 16 August 1981. Albedo, soil water availability, roughness length, thermal diffusivity and

conductivity parameters were changed in the model METRAS-changed compared to METRAS-standard.

Figure 4.11 shows the radiation and energy balance of model and measured data for August 18<sup>th</sup>. In the model METRAS-standard and METRAS-changed values are peaked at noon with maximum values of  $639 \text{ Wm}^{-2}$  and  $602 \text{ Wm}^{-2}$  respectively; the measured net radiation at the observational site in the noon peaked with the maximum value of  $600 \text{ Wm}^{-2}$ . The model METRAS-changed estimate of net radiation is close to the measurement data. The calculated mean hourly Bowen ratios from 08:00 to 16:00 LT varied from 0.2 to 1.0 in the measured data. Bowen ratios varied from 0.63 to 0.17 and 1 to 1.4 in the model METRAS-standard and METRAS-changed cases, respectively. Jarvis et al. (1976) suggested that it is important to establish the expected range of Bowen ratio values for forests. They found that, irrespective of species, for most forests the daytime Bowen ratios calculated as the mean hourly value from 08:00 to 16:00 LT varies from 0.1 to 1.5 for dry canopy conditions and from -0.7 to +0.4 for wet canopy conditions. Model calculated Bowen ratios are comparable with measured data.

Figure 4.12 shows the comparison of diurnal variation of surface temperature from the measurements and model simulations. The measured surface temperature shows large diurnal variation at the site. The model METRAS-changed also shows similarly large variation in the surface temperature. The model METRAS-standard shows a maximum temperature about 4 K smaller than that of observations and METRAS-changed.

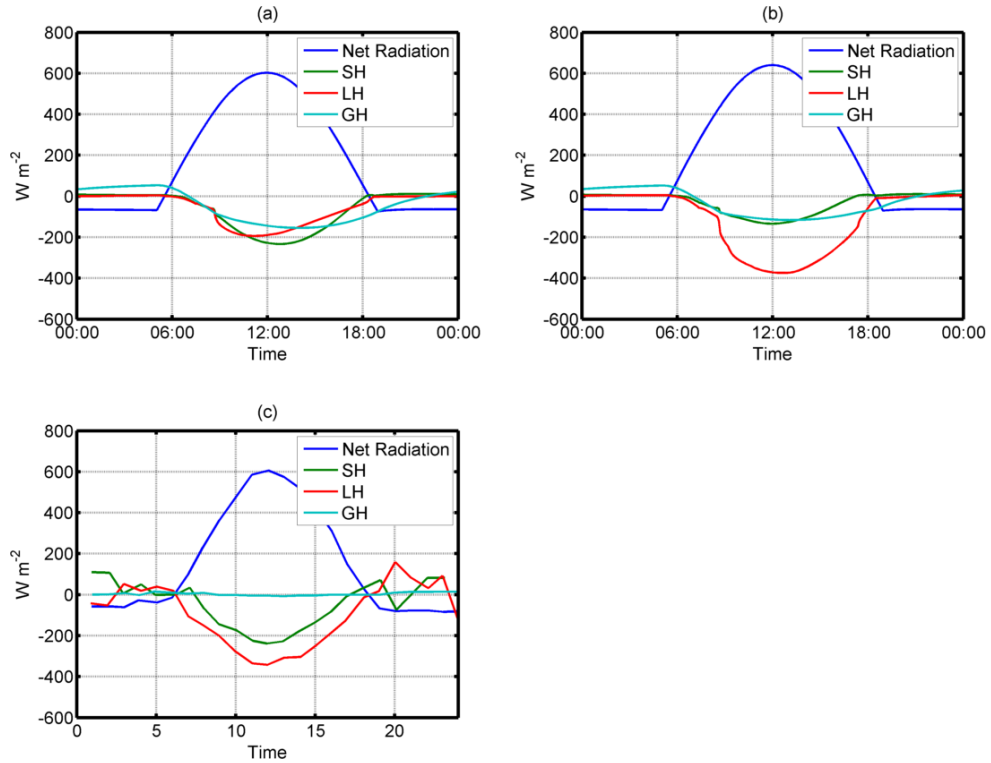


Figure 4.11 Comparison of simulated models (a) METRAS-changed, METRAS-standard (b) and measured (c) energy fluxes over the forest region on 18 August 1981.

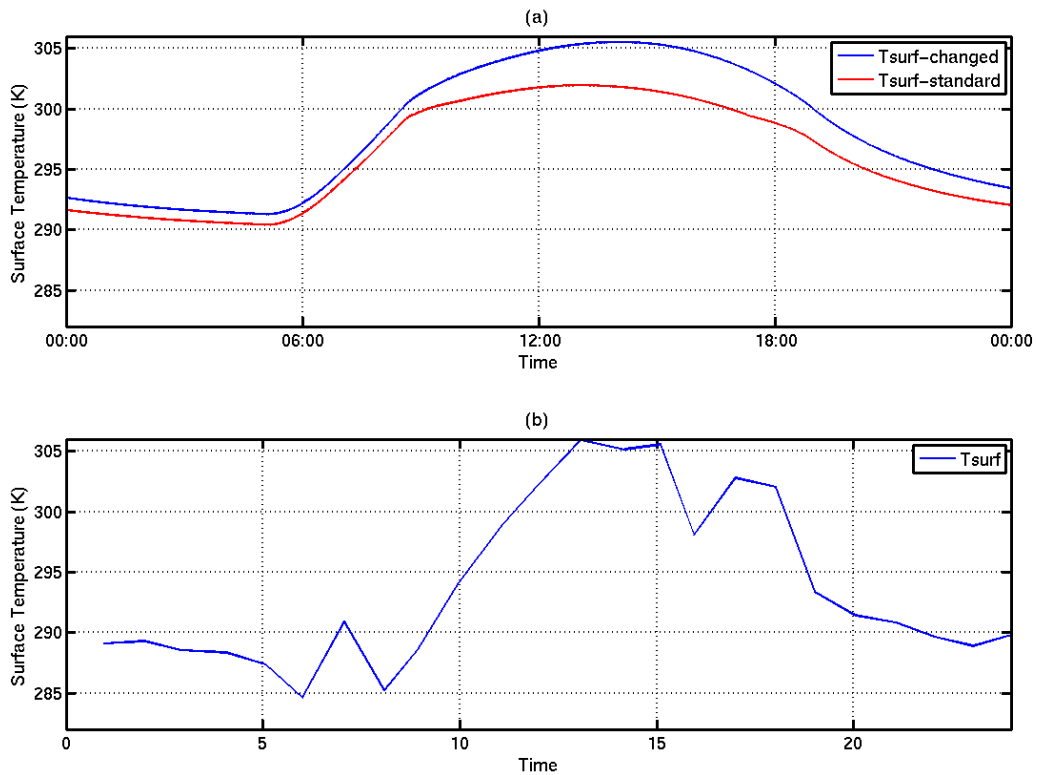


Figure 4.12 Diurnal cycles of surface temperature (a) models, (b) measured data on 18<sup>th</sup> August 1981.

The adopted surface characteristics gave model results that agreed sufficiently well with measured data for temperatures, the Bowen ratio values and the net radiation. Hence, one can use these adopted mixed forest land-use class surface characteristics parameters for the tropical humid region.

### 4.3.9 Adaptation of land-use class coniferous forest

Very small portion 0.2% of the model domain covered coniferous forest. Data from Abreu Sa et al. (1988) were used to compare the model results for the coniferous land-use class. The model was initialized for the experimental site with a 31°C temperature, 3 ms<sup>-1</sup> wind speed and 82 % humidity for 15 August, 1981. Albedo, soil water availability and roughness length are tuned in the model METRAS-changed to better represent tropical coniferous forests. These parameters are changed to reduce the peaks in model calculated energy fluxes (Fig. 4.13).

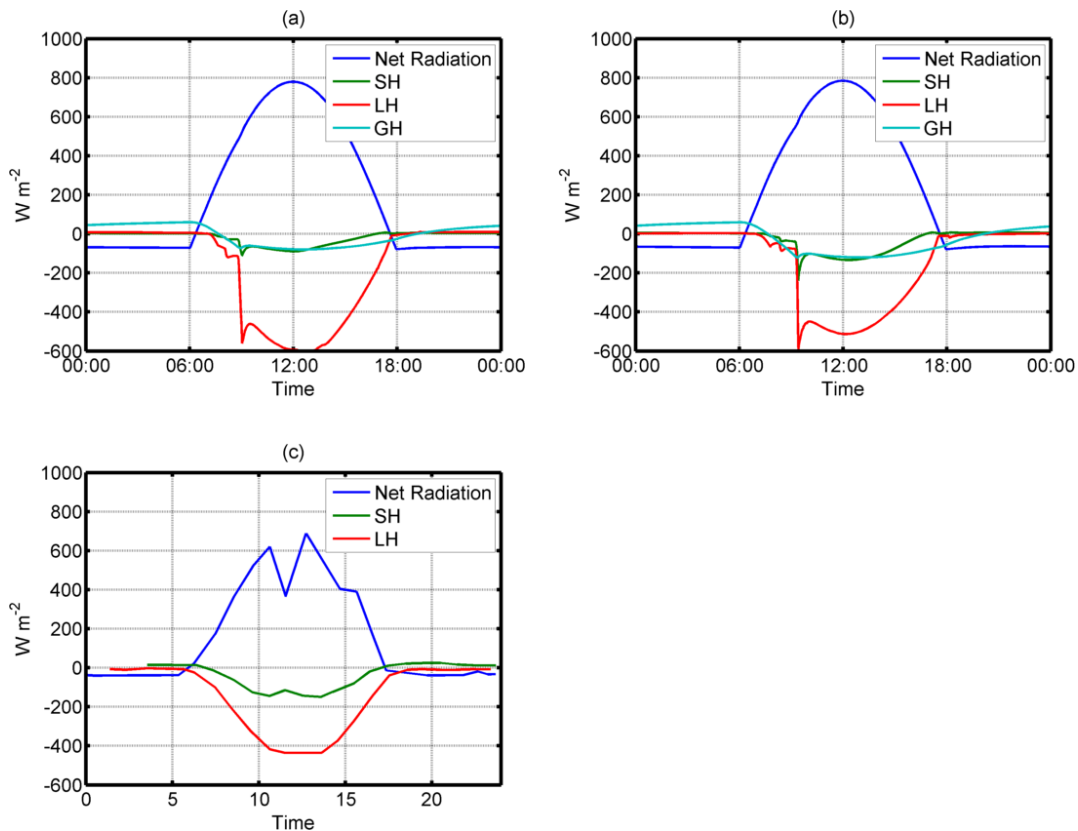


Figure 4.13 Diurnal variations of the energy balance components of models simulated (a) METRAS-changed, (b) METRAS-standard and (c) measured data on 21<sup>st</sup> August 1984.

The used measurements were conducted in the tropical evergreen forests of the Amazonas basin, Brazil. The measurements were made using a 45 m scaffolding tower at a site ( $2^{\circ} 57' S$ ;  $59^{\circ} 57' W$ ), situated in the Duke Reserve Forest (DRF), 26 km from Torquato Tapajos Highway, Manaus, Amazonas, Brazil. Figure 4.13 shows the model simulated and observed energy fluxes for the Amazon forest region at the experimental site. The measured net radiation was  $700 \text{ Wm}^{-2}$  at the noon at the site. Both the models reached about  $770 \text{ W m}^{-2}$ . Sensible and latent heat fluxes simulated by the model were comparable with measured data. The peak in the latent heat seen at 9 am suggests that more evaporation occurred in the model than observations. Figure 4.13 shows that the latent heat flux is larger than the sensible heat flux, i.e., Bowen ratio is less than one, which means that the heat input to the atmosphere is mainly in the latent form. This will increase the humidity of the lower atmosphere; therefore, weather is likely to be relatively cool and moist in the forest region.

The adopted surface characteristics gave not much confidence due to the peaks in the energy fluxes simulated in the model. However, the model results may not be affected in this study very much, due to very small area in the domain that is considered in the three-dimensional model investigations. Hence, one can use these adopted coniferous forest land-use class surface characteristic parameters

#### **4.3.10 Adaptation of urban land-use class**

A very small portion (0.1%) in the domain of the study region contains of urban areas. In both model studies the model has been initialized with a  $27^{\circ} \text{ C}$  temperature,  $3 \text{ ms}^{-1}$  wind speed and 80% humidity for the Braganca region. These input data were taken from the INMET weather station located in the Braganca. The only difference between METRAS-standard and METRAS-changed case is the soil water availability;  $\alpha_q$  changed from 0.05 to 0.90 and all other surface characteristics remain the same. Figure 4.14 shows the model simulated energy balance. The shortwave radiation simulated from the models METRAS-changed and METRAS-standard matches well with the observed data. It should be noted that the measured data were in UTC time, thus recalculated to local time measured short wave radiation peaked at about 15 UTC and 12 LST (local sun time). The Bowen ratio calculated at the noon is 2.3 in the model METRAS-standard, 0.23 in METRAS-changed.

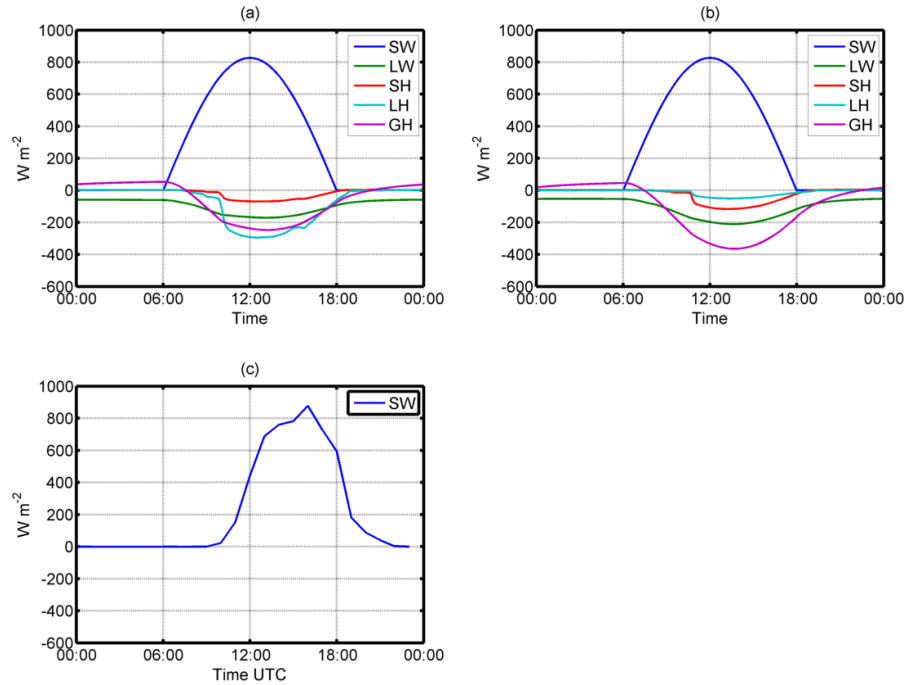


Figure 4.14 Surface fluxes calculated from (a) METRAS-changed (b) METRAS-standard and (c) INMET weather station (Time in UTC) for an urban area on 2 August 2010

Figure 4.15 shows the diurnal cycle of 2 m temperature simulated and observed over the Braganca region. Observed INMET data has an about 8°C variation of temperature during the daytime, with a peaked at 14 UTC (about 13 LST). The METRAS-standard urban case shows 7°C with a peak at about 14 LST. METRAS-changed shows a 5°C temperature variation during the day with a maximum at about 13:00 LST. Both METRAS models are able to reproduce diurnal variations of temperature consistent with the measured data. The METRAS-changed simulated lower temperature than the standard and observations.

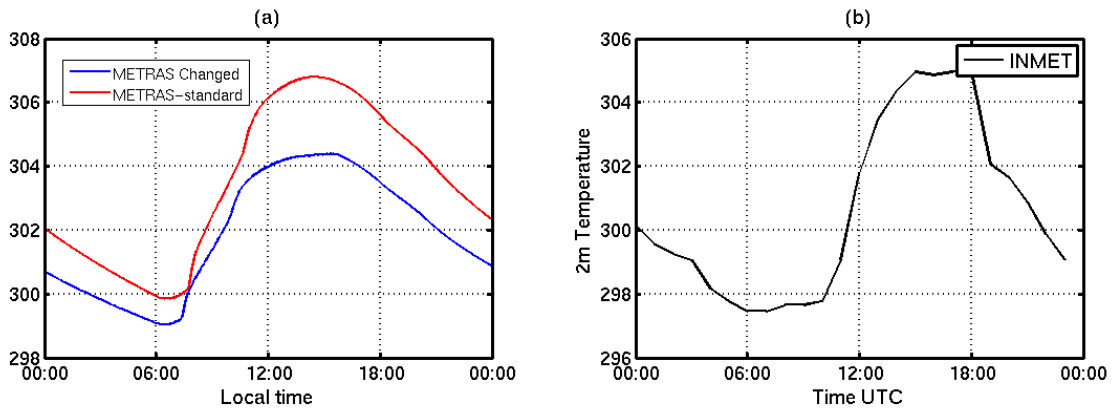


Figure 4.15 Simulated (a) model METRAS and (b) observed urban temperature (Time in UTC) on 2 August 2010 at Braganca.

The adopted surface characteristics again cannot be well evaluated due to lack of all surface energy fluxes in the observed data. However, the available results look promising and, again, the model results may not be affected in this study very much by this land-use due to their very small area (0.1%) in the domain. Hence, one can use these adopted land-use class surface characteristic parameters for the tropical urban area.

#### 4.4 Meteorology results from METRAS over the tropical Braganca region

The surface characteristic's parameters were adjusted and tested for different land-use classes for the tropical humid regions. The surface characteristic's parameters were summarized in the Table 4.2. These input values are used now in the model simulation over the Braganca region in the 3-dimensional study.

The model METRAS has been run for about 6 days and 8 hours. The model was run from 20:00 BRT, 15 December 2010, to 21 December 2010 (Table 4.3). The METRAS simulations were performed both with large-scale forcing of MBAR data and without any large-scale forcing in the model domain.

In the case without forcing, the model 1D-METRAS was initialized for 1.04522° S, 46.78270° W. The initial water temperature and large-scale temperatures were chosen to be 300 K. The model was initialized with a relative humidity of 75% at the surface, linearly decreasing with height. A geostrophic wind of 2 m s<sup>-1</sup> is used for the model initialization. The large-scale potential temperature gradient is set to 0.0035 K m<sup>-1</sup>.

In the case of with forcing, the model 1D-METRAS was initialized with large-scale profiles obtained from the MBAR model using the ECMWF pre-processor utility. The ECMWF pre-processor is used for interpolating the ECMWF data into the METRAS grid. The ECMWF pre-processor has been adjusted for the MBAR data to interpolate to the model METRAS grid. The details of the model options used in this study are given in the Table 4.3.

*Table 4.3 Details of METRAS model setup.*

Model Type	Non-hydrostatic model
Domain of integration	0.3194°S - 1.541°S; 45.9085°W - 47.329°W
Vertical levels	34 non homogeneous
Horizontal resolution	1 km

Cloud microphysics	Kessler Scheme
Grid	Arakawa-C
Number of passive tracers	6
Model starting time	15 December 2010, 20.00 local time
Filter for wind components	3 points

#### 4.4.1 Qualitative analyses

In order to understand the role of meteorology on concentrations, a qualitative comparison of model simulated meteorological features was performed. The land and sea breeze circulation is important for the study of pollution transport in the forecast area. It is also an important meteorological phenomenon in controlling the weather in coastal regions. Due to high radiative heating and convection in the tropics, land and sea breeze circulation occur more frequently in the coastal region than the high latitudes.

Land and sea breeze circulations and time series simulation by the model will be discussed. Simulated surface winds are mostly easterly over the domain region in the model METRAS and MBAR at 10 m above the ground level. Figure 4.16 and 4.17 show the evolution of the simulated near-surface (10 m AGL) wind fields at 00:00 BRT, 05:00 BRT, 12:00 BRT and 17:00 BRT in the model METRAS with and without forcing and in the forcing data from model MBAR. Land and sea breeze circulation patterns are found on 17<sup>th</sup> December 2010.

Surface temperature and low level winds were seen to vary diurnally and spatially in the model METRAS. During the evening (about 18:00-20:00) the surface winds over the tropical Braganca coast region were easterly on 16<sup>th</sup> December. It gradually becomes south-easterly, indicating the onset of a land breeze at 00:00 BRT in the model METRAS (nudge) case (Figure 4.16a). There is a strong land breeze (south-easterly) on 17 December at 05 BRT (Figure 4.16b). The land and sea breeze circulation is mainly caused by the temperature difference between land and water body. The temperature difference is about 3°C. In the case of MBAR, surface winds are mostly easterly, with a slight change in wind direction seen over the coast at 06:00 BRT (not shown here). Figure 4.16f shows mostly easterly winds in the model MBAR at 05:00 BRT. The model MBAR produces a clear land breeze and sea breeze circulation during the simulation.

At noon (12:00 BRT) the surface winds at the coast turns to north-easterly, indicating the onset of a sea breeze in the model METRAS (Figure 4.17a, c and MBAR (Figure 4.17e). The strong sea breeze occurring at 17:00 BRT has higher wind speeds of about 5 m s<sup>-1</sup> in the

METRAS model with forcing and more than that in the model MBAR. The temperature difference between land and water is about 5° C in both models. The surface winds induced by sea breezes are easterly to north-easterly over the tropical Braganca region during the model simulation period.

Surface winds simulated by the model METRAS for the next days reveal the recurrence of land breezes with south-easterly winds in the morning from about 04:00 BRT to 06:00 BRT and sea breezes with north-easterly winds in the evening time between 15:00 BRT and 19:00 BRT. It should also be noted that MBAR and METRAS do not have the same physics options for the simulation. METRAS consistently shows land and sea breeze circulations and clear day-time and night-time temperature differences over the land and water surface during the simulation.

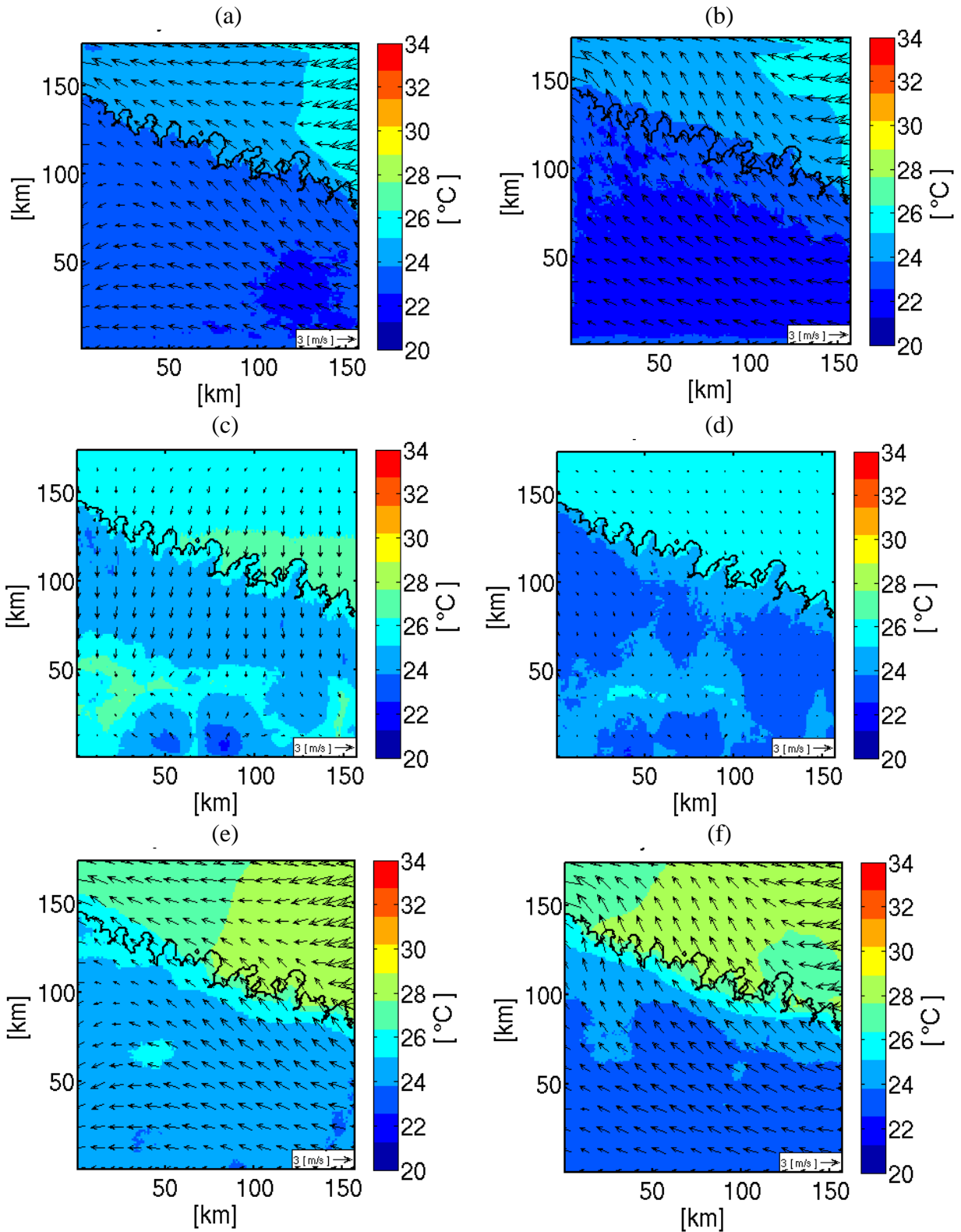


Figure 4.16 Simulated surface wind field at 10 m above the ground at (a, c, e) 00:00 BRT and (b, d, f) 05:00 BRT for (a, b) METRAS with forcing, (c, d) METRAS without forcing, (e, f) MBAR over the tropical Braganca region on 17 December 2010. Every 10<sup>th</sup> vector is shown.

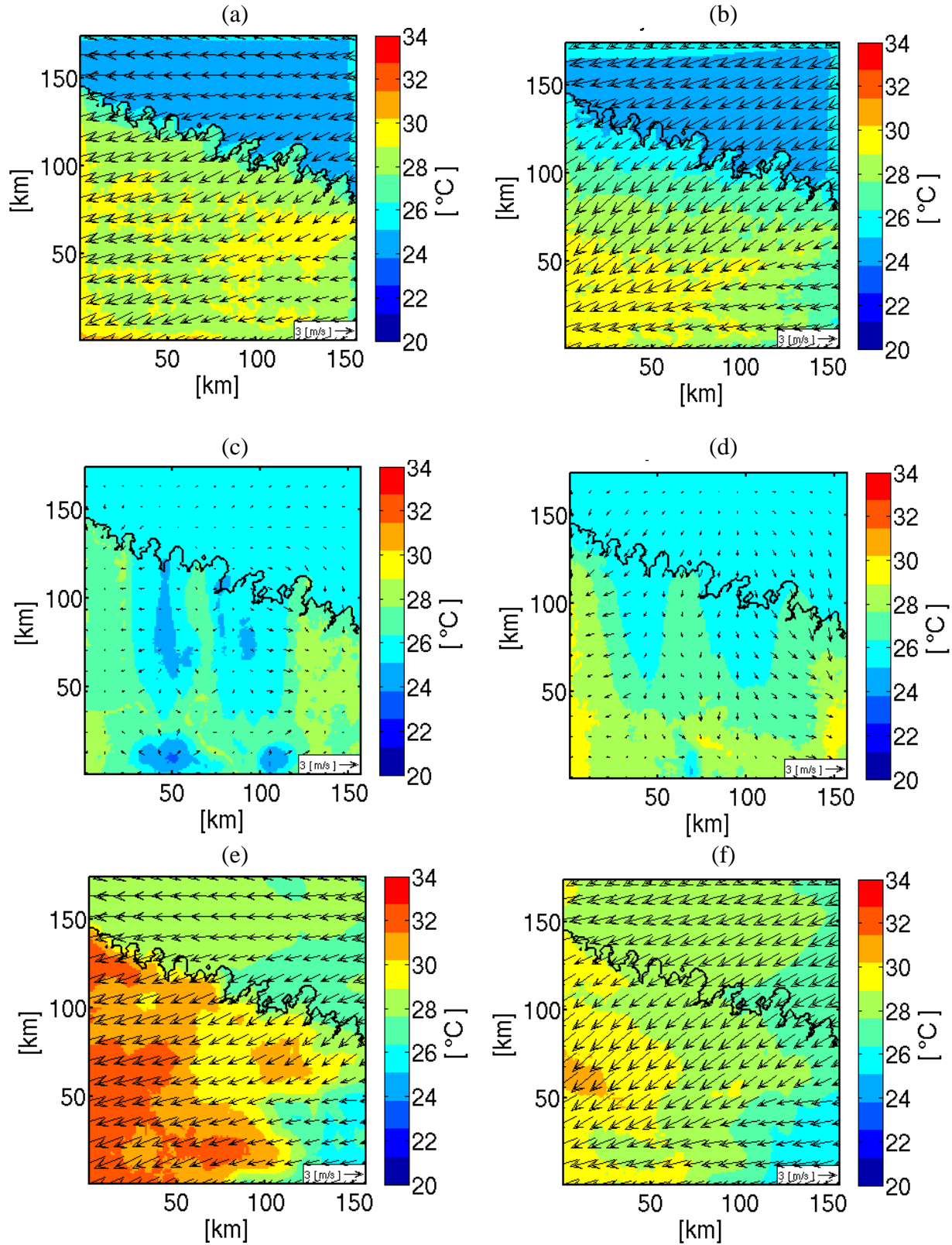


Figure 4.17 Simulated surface wind field at 10 m above the ground at (a, c, e) 12:00 BRT and (b, d, f) 17:00 BRT for (a, b) METRAS with forcing, (c, d) METRAS without forcing, (e, f) MBAR over the tropical Braganca region on 17 December 2010. Every 10<sup>th</sup> vector is shown.

In the case of METRAS without forcing (METRAS (unnudge)), surface winds are mostly from North with a temperature difference of 3°C between land and water. Very weak winds were simulated compared to MBAR and the forced (nudge) METRAS simulations. During the afternoon at the coast around 14:00 BRT, the southerly winds turn to northerly, indicating a delay in the onset of the sea breeze when compared with the forced (nudge) METRAS and the model MBAR. At 17:00 BRT surface winds are slightly higher due to the sea breeze influence over the coast region. More clouds were simulated in the model METRAS without forcing than in the model METRAS with forcing and MBAR. Furthermore, the model METRAS is able to produce land and sea breeze circulations over the domain region. However, the large-scale phenomena in the equatorial tropical region also influence the model results and need to be considered in the model domain. Thus, the model METRAS without forcing (unnudge) could not simulate constant trade winds. Therefore, forcing of meteorological parameters from the outer domain is needed. Hence, in this study, MBAR meteorological data was used for forcing METRAS.

Figure 4.18 shows vertical profiles simulated at the coast region in the morning (05:00 BRT) for the land breeze setup and in the evening (17:00 BRT) for the sea breeze situation in the model domain. The potential temperature profiles of the model METRAS match well with MBAR profiles. The profiles show increasing potential temperature and increasing wind speed with height at 05:00 BRT. It is also noted that stable atmospheric conditions in the morning and in the evening at the coast exist during the land sea breeze circulation.

The wind speed profiles in the model METRAS without forcing (unnudge), show lower values than the model MBAR and with the forced METRAS (nudge) profiles. METRAS (nudge) profiles match well with MBAR, but about 1 ms<sup>-1</sup> - 2 ms<sup>-1</sup> lower wind speeds were simulated at a height of 1 km to 2 km during the evening time. METRAS (nudge) also shows lower wind speeds than the MBAR model in the lower atmosphere up to 500 m, and above the profile well match the MBAR profile.

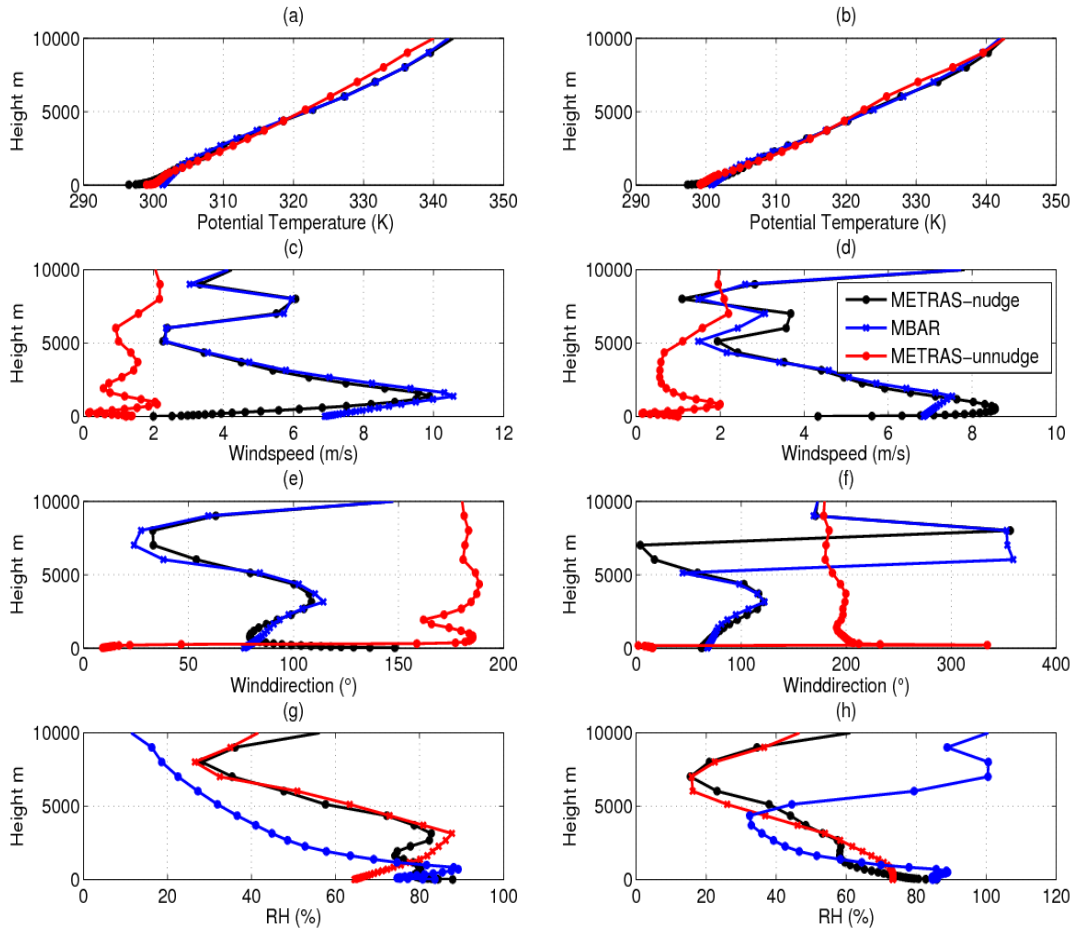


Figure 4.18 Comparison of vertical profiles of the model METRAS (nudge, unnudge) and MBAR, for simulated (a, b) potential temperature, (c, d) wind speed, (e, f) wind direction, (g, h) relative humidity at 05:00 BRT (a, c, e, g), and 17:00 BRT (b, d, f, h) for a grid point at a coastal location on 17 December 2010.

There is a convectively unstable atmosphere between 09:00 BRT – 16:00 BRT all days during the simulation. The METRAS simulation shows an unstable layer at a height about 150 m in the forced run and 300 – 500 m AGL in METRAS without forcing for this grid point near the coast. The wind direction profile in METRAS clearly shows a difference between morning and evening time. The relative humidity profiles show more humidity in METRAS than the MBAR model in the lower levels. Higher relative humidity is simulated in the upper atmosphere at 17:00 BRT by the model MBAR than the model METRAS without forcing (unnudge) and with forcing (nudge).

## 4.4.2 Quantitative comparison

Figure 4.19 shows the diurnal variations of surface layer data simulated by the models compared with measurements. The station name is Tracuateua located at  $1.083^{\circ}\text{S}$  and  $46.933^{\circ}\text{W}$ . The station location is marked as a green circle in Figure 4.21d. All model variables are at 10 m above the ground level. Temperature and humidity are measured at 2 m at the observational site. Wind was measured at 10 m. There are no continuous data available at the observation site. Hourly data were downloaded from the NOAA website (<http://www.ncdc.noaa.gov/cdo-web/>).

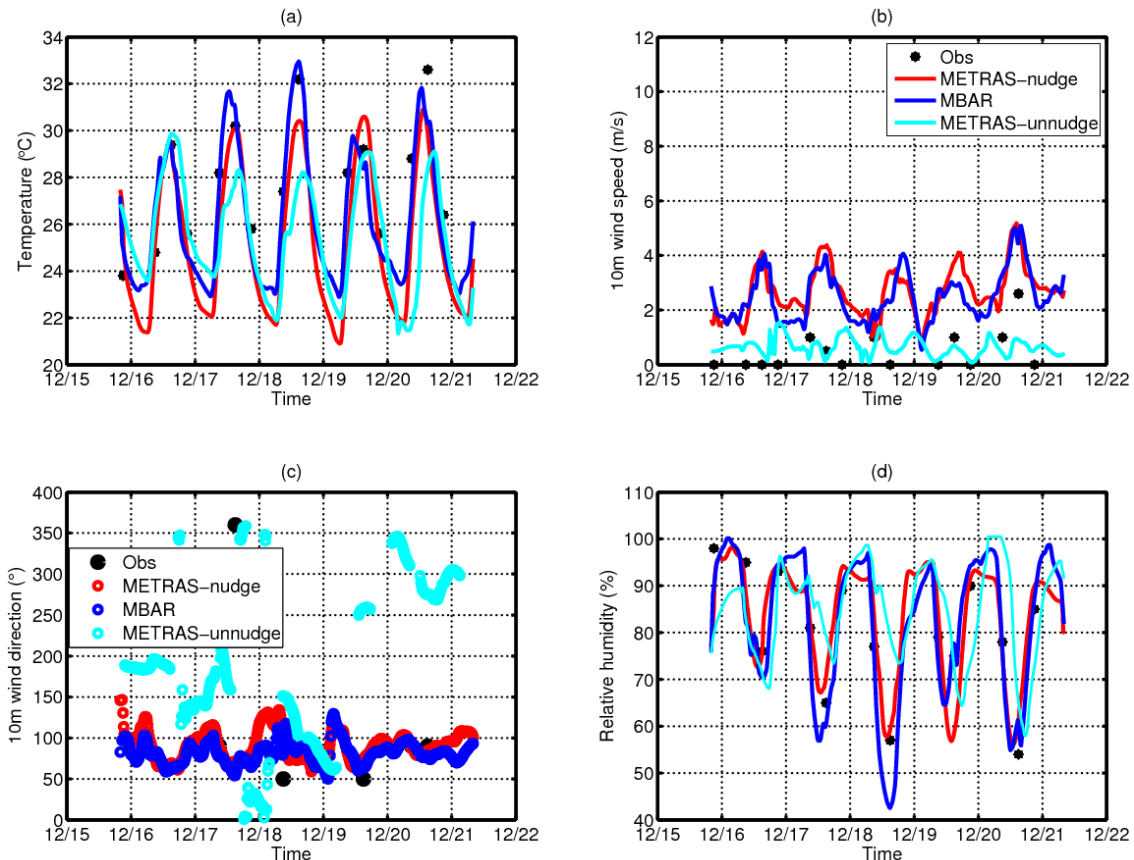


Figure 4.19 Diurnal variation of simulated and observed a) temperature, b) wind speed c) wind direction d) relative humidity during 16 – 21 December 2010 at Tracuateua station of latitude  $1.083^{\circ}\text{S}$   $46.933^{\circ}\text{W}$

The model METRAS (nudge) is able to produce similar temperatures for the first two days and underestimates maxima by about  $2^{\circ}\text{C}$  compared with measured data on December 18<sup>th</sup> and 20<sup>th</sup> 2010. MBAR temperature shows slightly higher temperature during the day on December 17<sup>th</sup> and 18<sup>th</sup> 2010. Both models show very similar maximum temperatures at December 19<sup>th</sup> and 20<sup>th</sup> 2010. Minimum temperatures are not available in the measurements,

thus it is unclear how low they were. The models reach values of 22°C to 24°C. The model METRAS (unnudge) shows underestimates the maximum temperatures. All the models do show diurnal variation in the temperature at this location during the simulation.

Wind speed predicted in the model METRAS (nudge) and MBAR shows higher values compared to observations (Figure 4.19b). The model METRAS (unnudge) shows wind speed comparable to observations and lower than the other models. This is due to the model initialization which contained weaker wind speeds and the neglectance of large-scale forcing. The simulated relative humidity in METRAS is close to the observations (Figure 4.19d). MBAR underestimates humidity when compared to observations and METRAS (nudge) on December 17<sup>th</sup> and 18<sup>th</sup> 2010. METRAS (unnudge) simulates too high humidities compared to observations and the other models. The wind direction simulated by the METRAS (nudge) and MBAR mostly varies between 50° (north-easterly) to 150° (south-easterly). It is common to observe these trade winds at the equator. The wind direction in METRAS (unnudge) deviated more from other simulations. All the models do show diurnal variation of temperature and humidity at the observational site.

Figure 4.20 shows the diurnal variation of surface meteorological variables, similar to Figure 4.19, but at another location: the automatic weather station at 1.04522°S, 46.7827°W (INMET). The measurement location is noted as magenta circle in Figure 4.21d. The diurnal variation of temperature is simulated very well by MBAR and matches the measured data at the measurement location. METRAS (nudge) and METRAS (unnudge) simulate temperatures that underestimate the temperatures from the observation and MBAR. This is due to the soil temperature and SST initialization in the model METRAS. One can speculate that the large-scale specified SST is less than the actual value because SST's are taken from monthly mean data. MBAR uses a different soil temperature data set (GME). In the case of METRAS (nudge) and METRAS (unnudge), the soil temperature is calculated from the large-scale temperature at 1000 m. A modification of initial soil temperature and SST would be needed to improve the model simulations further. However, there is no accurate soil temperature data available in the domain region.

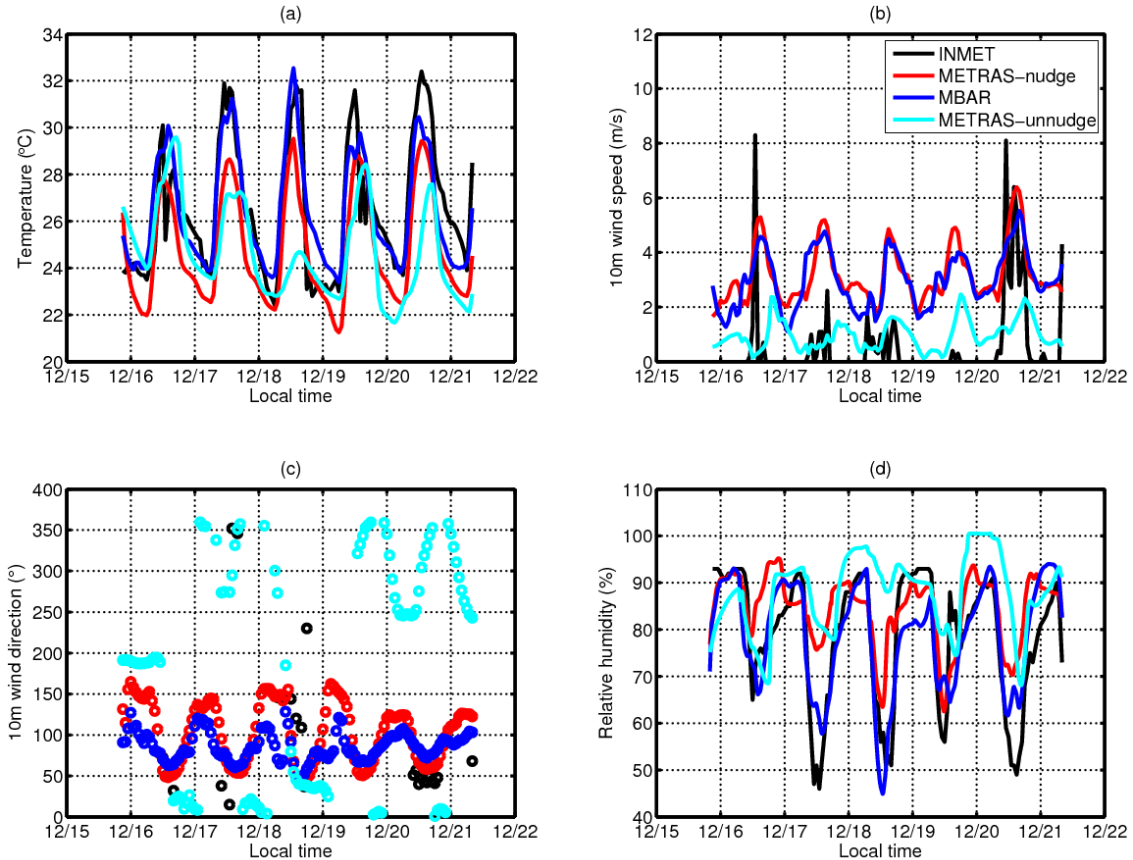


Figure 4.20 Diurnal variation of simulated and observed a) temperature, b) wind speed c) wind direction d) relative humidity during 16 – 21 December 2010 at the INMET station.

Wind speed in the model METRAS (nudge) follows the MBAR and again is found to be higher in both models compared to observations. It is also noted that strong winds were temporarily measured but not simulated on December 16<sup>th</sup> and 20<sup>th</sup> 2010. The smaller wind speeds of METRAS (unnudge) agrees better with observed data. Higher humidity was simulated in METRAS compared with MBAR and the observational site, especially when METRAS (unnudge) is used. Wind direction in the model METRAS (nudge) shows large differences between midnight and morning, which indicates the influence of land and sea breeze circulation. This is simulated better in the model METRAS, however, due to the low wind speeds only few reliable wind direction measurements remained in the data.

Figures 4.21 and 4.22 show the diurnal variation of the meteorological variables close to the surface at the coast and inland sites, where the experimental data were taken during the field campaign (Figure 4.21d). The models METRAS (nudge) and METRAS (unnudge) underestimate temperatures compared to MBAR and observations at both locations. The wind direction simulated by the model METRAS at the coast (Figure 4.21c) and inland

(Figure 4.22c) clearly show a diurnal cycle with south-easterly winds in the morning (land breeze) and north-easterly winds in the evening (sea breeze) at both locations. These two observational sites are near to the Braganca coast. MBAR shows mainly easterly to north-easterly winds at both the locations. Since very few measurements are available it cannot be concluded if MBAR or METRAS (nudge) is closer to reality. However, it can be stated that the wind directions simulated with METRAS (unnudge) are not realistic. The METRAS (nudge) simulated wind speed is in the range of the measurement (Figure 4.21b and Figure 4.22b) and closer than MBAR and METRAS (unnudge) at the coast.

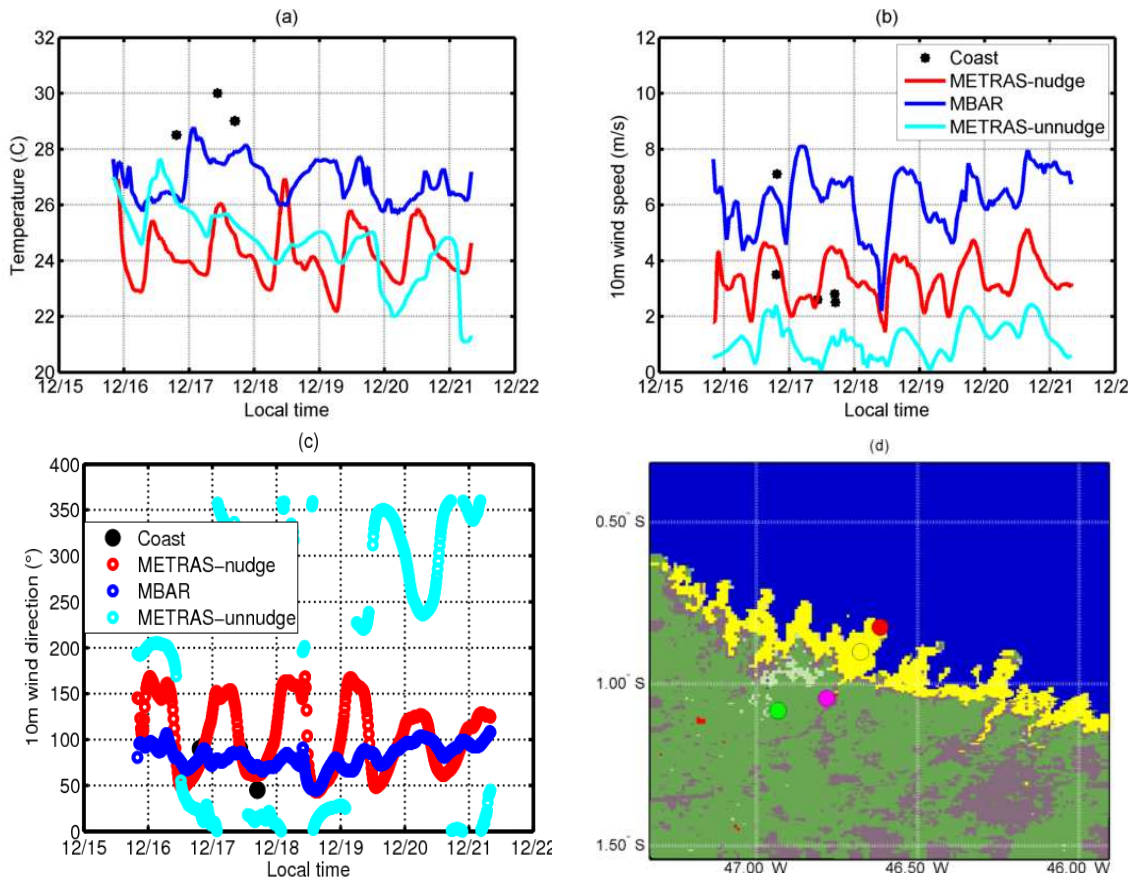


Figure 4.21 Diurnal variation of simulated and observed a) temperature, b) wind speed c) wind direction during 16 – 21 December 2010 at the coast, and (d) measurement locations (red circle: Coast, yellow circle: Inland, Magenta circle: INMET station and green circle: Tracuateua station)

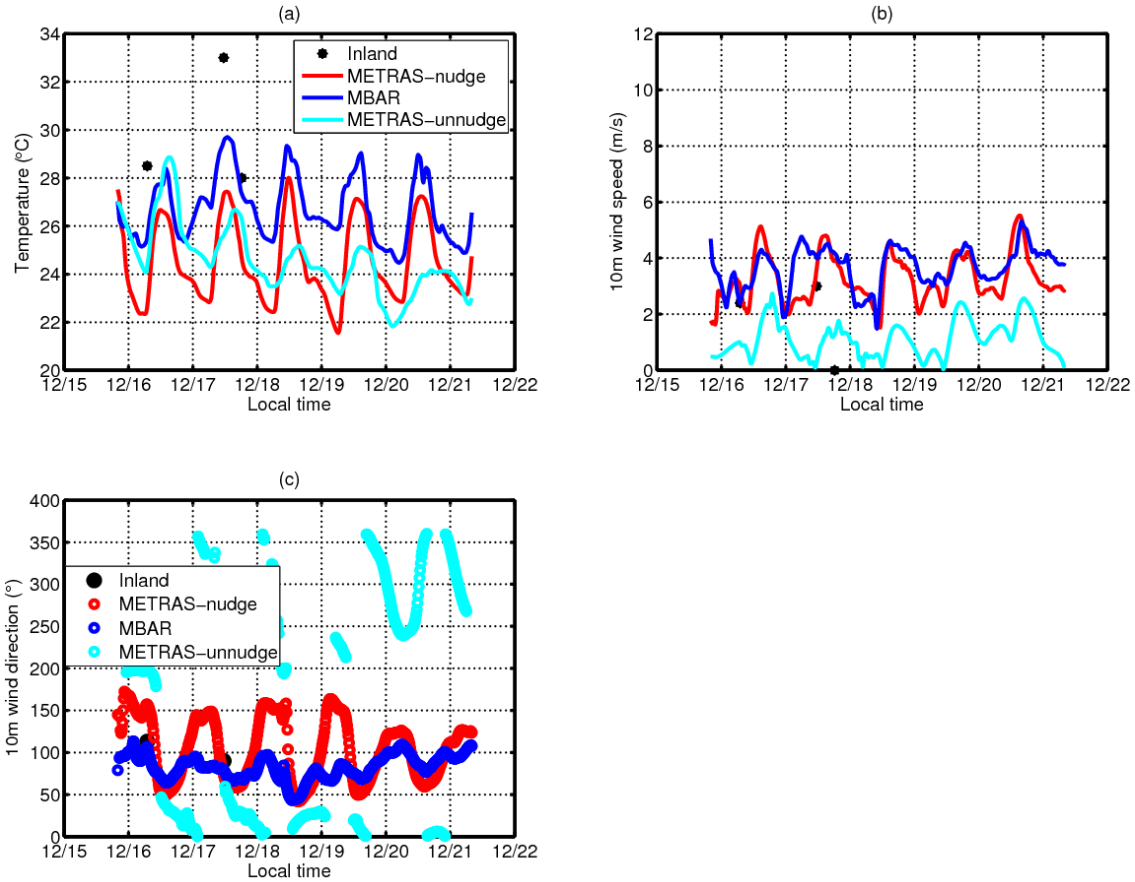


Figure 4.22 Diurnal variation of simulated and observed a) temperature, b) wind speed c) wind direction during 16 – 21 December 2010 at the inland.

## 4.5 Conclusions

This chapter mainly focuses on the adaptation of the model METRAS to the tropical Braganca region and the evaluation of the meteorology results. There were ten surface land-use classes available in the model METRAS, which were adopted for the tropical Braganca region. Per land-use class simulations were made in order to get a better representation of the surface energy balance in the model for the adjusted land-use classes. The surface characteristic parameters for ten land-use classes were obtained. With the limited available observational data of energy fluxes for the ten different land-use classes, the model METRAS is able to reproduce observed values as good as it can be expected from idealized case studies and keeping in mind that the data do not fully represent tropical regions. The surface characteristic parameters adopted in this study are only applicable for tropical high humidity regions. It would have been better, if measurements for the land-uses of the region investigated had been available. However, they are not there, but we would need high spatial and temporal measurements over the different land-use classes for a more accurate

representation of surface energy fluxes in the mesoscale models. Also further land-use classes could now be introduced into METRAS, which in the meantime is capable of simulating more than ten land-use classes. Nonetheless, this is the first study adapting METRAS for the South American region at the equator.

The model METRAS has been simulated for a three-dimensional model domain situated at the coast of Braganca for about 6 days in December, 2010, with adapted surface parameters. The model METRAS is able to simulate land and sea breeze circulation patterns over the tropical Braganca region. The strength of the sea breeze is about  $4 \text{ m s}^{-1}$ . METRAS model simulations reveal a consistent diurnal cycle in close-to-surface variables such as air temperature, wind and relative humidity. It is also noted that METRAS simulations forced with MBAR improved the results considerably in comparison to METRAS without forcing. It has been noted that the large-scale flow influences the meteorological situation in the model domain. Thus, METRAS is forced with MBAR meteorological fields. METRAS (nudge) simulates quite reliable humidity fields. However, METRAS simulates lower temperatures compared with the model MBAR and the measured data near to the coast. This could be due to the smaller SST in the model simulation. A modification of soil temperature and SST initialization would be necessary to improve the simulations. The model METRAS can simulate essential characteristics of the coastal atmospheric phenomena (such as the land-sea breeze circulation) and equatorial trade winds (north-easterly and south-easterly). Thus, the model METRAS could be used for pollution dispersion application studies in the tropical Braganca region.

## **5. Role of meteorology and emission functions for concentration values**

This chapter presents the detailed information on the passive tracer (i.e. no chemical reactions involved) concentrations simulated with the model METRAS over the tropical Braganca region. The model METRAS has been run with a constant emission function and a time dependent emission function, which depends on humidity. These emission functions were adopted from pollen measurement data. The methyl halide emission from the mangrove forest is unknown, therefore this study cannot have a relation with constant emission functions and a time dependent emission function for methyl halides.

### **5.1 Introduction**

Most of the mangrove forests in South America are found on the Atlantic and Pacific coasts in the bays and estuaries. Mangrove forests occupy slightly less than 2 million hectares in South America (FAO, 2005). Brazil has the third largest mangrove area in the world. The global mangrove surface area covers about  $2 \times 10^5 \text{ km}^2$  (Duarte et al., 2005). The mangrove forest area has been substantially reduced worldwide since the 1980's due to land competition for aquaculture, agriculture, infrastructure and tourism (FAO, 2005). Current estimate of the global total area of mangroves using recently available Global Land Survey (GLS) and the Landsat archives is about  $1.4 \times 10^5 \text{ km}^2$  (Giri et al., 2011). This global total surface area of mangroves will be used for the up-scaling of methyl halide emissions that are derived from the present model and measurement study.

A quantification of methyl halide emissions from mangroves is relevant for the tropospheric ozone since they are relevant for its destruction. However, its major relevance is given for climate studies since methyl halides have long life times (e.g. 1 year for  $\text{CH}_3\text{Cl}$  and 0.5 year for  $\text{CH}_2\text{Cl}_2$  (WMO, 2010)). This long life time is enough for them to be transported and mixed into the stratosphere, making an impact on the atmospheric chemistry in the regional and global scale. Therefore, it is important to determine the methyl halide emissions from mangroves. Quantified methyl halide emissions from mangroves can be used in climate models to understand the impact of mangrove forest on the global atmospheric chemistry. Furthermore, since a change of area covered by mangroves can be expected due to sea level rise and global warming, it will be expected that the amount of mangroves on the globe will also change in future and thereby affect emissions of methyl halides into the atmosphere.

To quantify emissions model studies are performed that are normalized with measured data (Chapter 3) to achieve a reliable value for the emissions. However, measurements are rare and the commonly used method of a Lagrange approach is strictly valid only for homogeneous and stationary conditions. In order to understand the role of meteorology on measured concentrations, two experiments were conducted with the mesoscale atmospheric model METRAS. In one experiment METRAS was run without forcing, and in the other with forcing from MBAR data. In both experiments 6 different passive tracers were considered. The meteorology experiments results of both were already discussed in Section 4.4.

Another uncertainty to the determination of emissions from concentrations is the form of the emission function. If emissions were merely constant with time, the measured concentrations might differ from those that were measured, such as with a time dependent emission function. However, the actual behavior of the plants is more-or-less unknown. Therefore, both meteorological studies were performed for two types of emissions, a constant one and a time dependent one. The case studies performed are summarized in Table 4.1.

The main objective of this chapter is to address the following questions:

1. Is a Lagrangian approach possible for measurements?
2. What is the role of meteorology on concentrations?
3. Can emission functions (also time dependent) be determined from observed data?

## **5.2 Emissions in the model domain and emission functions used**

Oceans and mangroves contribute to the emission of methyl halides to the atmosphere. These two sources are included as passive tracers in the model METRAS domain. Two emission functions are used, a constant emission function and a time dependent emission function where emission depends on humidity. The humidity-dependent emission function relation was originally obtained for pollen emissions and determined for the area of Lübeck by Schueler and Schlünzen (2006). Both emission functions might not describe the real situation, but they are used to study the possible impact of emission function form on concentrations. These emissions are to be scaled to achieve methyl halide emissions using observational data.

The concentration (eq. (4.1)) is linearly dependent on emissions, if no nonlinear chemical reactions take place. For pollen dispersion this is not the case, therefore, the ratios between

concentrations difference to emissions are constant. Hence, the whole eq. (4.1) in the section 4.1 can be normalized with the emissions, resulting in the following relation:

$$\frac{\Delta C}{\Delta E} = \text{Constant} \quad (5.1)$$

The relation should not only hold for model results but also for measured data, thus for emissions based on the measured data one receives:

$$\frac{\Delta C_{Measured}}{\Delta E_{Measured}} = \frac{\Delta C_{Model}}{\Delta E_{Model}} \quad (5.2)$$

In the eq. (5.2)  $\Delta C_{Measured}$  and  $\Delta C_{Model}$  are the measured and modeled concentration gradients of methyl halides during the observational time interval, respectively.  $\Delta E_{Model}$  is the model emission of the source region in the simulation during the observational time interval. Therefore, the measurement based emission (named  $\Delta E_{Measured}$  here) can be calculated as follows:

$$\Delta E_{Measured} = \frac{\Delta C_{Measured} \Delta E_{Model}}{\Delta C_{Model}} \quad (5.3)$$

The  $\Delta C_{Measured}$  is calculated as the concentration difference between upwind and downwind at the measurement sites.  $\Delta C_{Model}$  is the model simulated concentration difference between upwind and downwind at the measurement sites.  $\Delta E_{Model}$  is used for the corresponding measurement time interval for quantifying the methyl halide emissions.

In order to understand the impact of emission functions on concentration, the model concentrations were scaled such that the total emission (for the whole integration) for the time dependent emission function and constant emission function should be same. Based on this assumption scaling factors were calculated (eq. 5.4 – 5.7) and these scaling factors were then used to scale the simulated concentrations. Hence, one can compare, after normalization, the model simulated concentrations with different emission functions.

The following equations show the scaling factor between the time dependent emission functions and constant emission function concentrations for the mangrove area. For nudged meteorology case:

$$\frac{E(\text{Time dependent, nudge})}{E(\text{Constant, nudge})} = D_{En} \cong 90 \quad (5.4)$$

Here  $D_{En}$  (90) is the normalization coefficient of time dependent and constant emission functions for the nudged meteorology case over the mangrove region.

For the unnudged meteorology case:

$$\frac{E(\text{Time dependent, unnudge})}{E(\text{Constant, unnudge})} = D_{E_{un}} \cong 97 \quad (5.5)$$

Here  $D_{E_{un}}$  is the normalization coefficient of time dependent and constant emission functions for the unnudged meteorology case over the mangrove region.

In the case of an emission source region over water, the scaled factor is as follows. For nudged meteorology case:

$$\frac{E(\text{Time dependent, nudge})}{E(\text{Constant, nudge})} = D_{E_{wn}} \cong 74 \quad (5.6)$$

Here  $D_{E_{wn}}$  is the normalization coefficient of time dependent and constant emission functions for the nudged meteorology case over water.

For unnudge meteorology case:

$$\frac{E(\text{Time dependent, unnudge})}{E(\text{Constant, unnudge})} = D_{E_{wun}} \cong 133 \quad (5.7)$$

Here  $D_{E_{wun}}$  is the normalization coefficient of time dependent and constant emission functions for the unnudged meteorology case over water.

To recalculate the same total emission of time dependent and constant emission functions, the normalization factors D are used to divide the concentrations of time dependent emission functions. Still, the model concentrations are not comparable with measured data. Therefore, the relation between modeled and measured concentration gradients (e.q. (5.8)) is used to come up with realistic concentrations from model results.

$$\frac{\Delta C_{Model}}{\Delta C_{Measured}} = R_T \quad (5.8)$$

The equation (5.8) is calculated after applying eqs. (5.4 to 5.7) in order to get a concentration factor for real source contribution.

In the case of the water source region we did not measure the ocean contribution of concentrations during the observation period. Here one could assume that the same mangrove measured locations measure contributions from the ocean source region as well. Hence, the model METRAS simulated concentrations from the water source were scaled using the observed concentration data as done for the mangroves' emission. Table 5.1 shows the

relation of the methyl halides' modeled concentrations and observed concentrations for constant and time dependent emission functions for different source regions.

Table 5.1  $R_T$  (particles per pptv) values for the different sources. Meaning of T3 to T6 is given in Table 4.1.

<b>Tracer Compound</b>	<b>T3</b>	<b>T4</b>	<b>T5</b>	<b>T6</b>	<b>Forcing</b>
CH <sub>3</sub> Cl	2.6095x10 <sup>8</sup>	2.9819x10 <sup>8</sup>	3.9263x10 <sup>8</sup>	6.1897x10 <sup>8</sup>	Nudged
CH <sub>2</sub> Cl	1.0907x10 <sup>9</sup>	1.2464x10 <sup>9</sup>	1.6411x10 <sup>9</sup>	2.5872x10 <sup>9</sup>	Nudged
CH <sub>3</sub> Cl	2.0402x10 <sup>8</sup>	3.4756x10 <sup>8</sup>	1.4471x10 <sup>9</sup>	1.9087x10 <sup>9</sup>	Unnudged
CH <sub>2</sub> Cl <sub>2</sub>	8.5274x10 <sup>8</sup>	1.4527x10 <sup>9</sup>	6.0487x10 <sup>9</sup>	7.9778x10 <sup>9</sup>	Unnudged

Chapter 4 suggests that the model meteorological conditions are better in the nudged simulation. The unnudged meteorology case is not considered as the real atmospheric conditions. Hence, the concentrations are scaled using the nudged meteorology case values from the Table 5.1 for the unnudged meteorology case as well.

The emissions simulated in METRAS for the different source regions and emission functions are shown in the Figure 5.1. Originally the model emission functions are in number of pollen emitted per square meter area per second. These units are converted for methyl halide compounds in  $\text{g m}^{-2} \text{s}^{-1}$  for all source regions. For the mangrove source region, the time dependent emission functions of CH<sub>3</sub>Cl (Fig. 5.1a) and CH<sub>2</sub>Cl<sub>2</sub> (Fig. 5.1b), do show diurnal variation for METRAS (nudge) and METRAS (unnudge) meteorology case (denoted n or un). The constant emission functions are the same for the nudged meteorology case and unnudged meteorology case study. Higher emissions were simulated in the time dependent nudged meteorology case for mangroves and water (Figure 5.1c, d) except for the 16<sup>th</sup> December 2010. It can also be seen that emissions are higher during the daytime than the night-time.

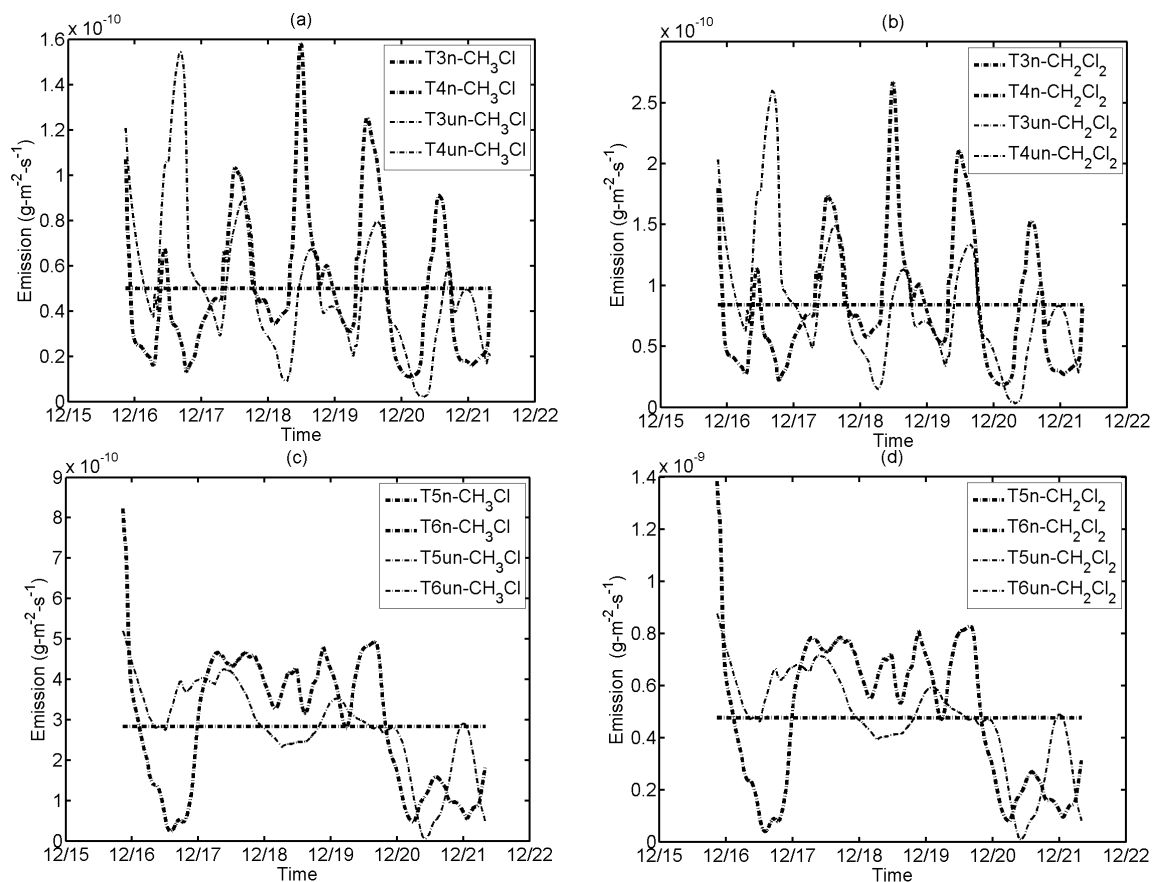


Figure 5.1 Emission of methyl halides for (a, b) mangrove forest source region and for (c, d) water source region, T3n and T5n: constant emission function for nudge case; T4n and T6n time dependent emission function for nudge case (Adapted from pollen study).

## 5.3 Determination of the different impacts on concentrations

### 5.3.1 Impact of meteorology on concentrations of methyl halides in a coastal mangrove region

This study used the Lagrangian approach for the measurements as discussed in Chapter 3. Wind direction showed mostly north-easterly winds during the observation time. Figure 5.2 gives the measured concentrations and model simulated meteorological conditions for the sampling time. Model simulated winds are mostly north-easterly (Figure 5.2b) before and after the sampling time. The winds were changed at night-time only. Thus the selected upwind and downwind locations were the most suitable for the air sample collections. Hence, the Lagrangian approach is applicable for the air sample collections if the winds are constant with time.

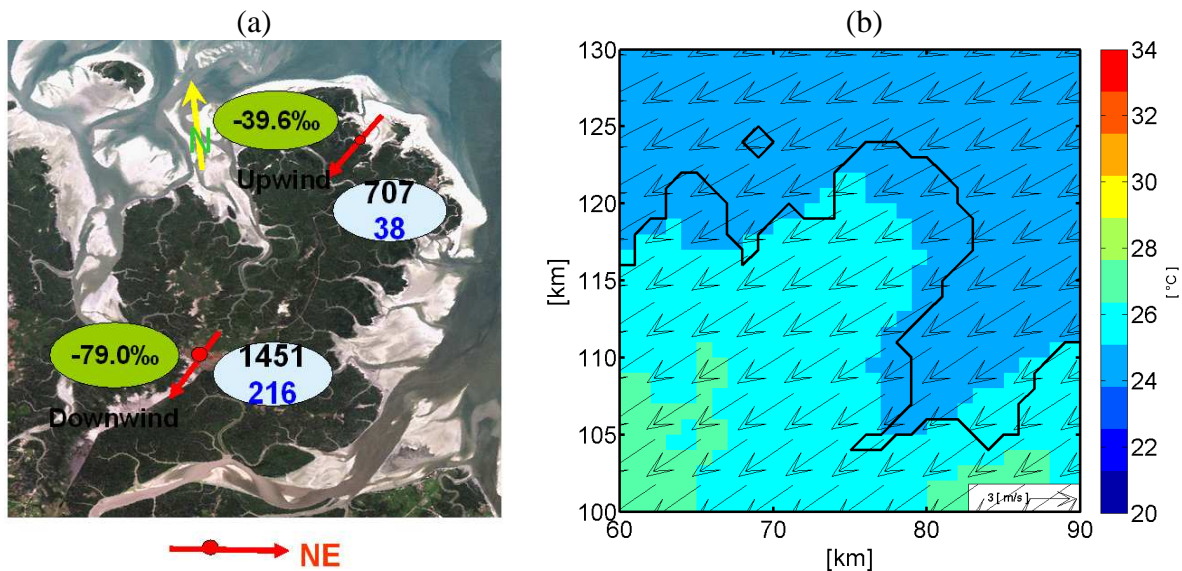


Figure 5.2 (a) Measured methyl chloride concentrations, stable carbon isotope ratios (black) and methylene chloride (blue) concentrations (pptv), (b), meteorological conditions simulated with METRAS (section of the model domain) for 17.12.2010 in the forest region, every 3<sup>rd</sup> vector is shown.

The concentrations are mainly dependent on the meteorological factors such as diffusion, horizontal advective transport and vertical winds in the atmospheric boundary layer, but also on the emission. The distinction between meteorological factors and emission functions is quite difficult to be determined from concentrations. Therefore, dispersion of passive tracers is studied using the mesoscale METRAS model with two different experiments. One is METRAS with forcing (nudge) and the other METRAS without forcing (unnudge). Furthermore, for both cases, different emission functions are considered. Figure 5.3 shows the concentration transport during day (Figure 5.3a, b) and night (Figure 5.3c, d) time for the nudged and unnudged meteorology case for mangrove emission.

The scaled concentrations of  $\text{CH}_3\text{Cl}$  (pptv) and  $\text{CH}_2\text{Cl}_2$  (pptv) are shown in Figures 5.3 and 5.4. The METRAS (nudge) concentrations are in the measurement data range. For example, the topical plants estimated source strength is within the range of about 1000 pptv to 3500 pptv (Yokouchi et al., 2002). The concentrations are transported by the model simulated flow. The concentrations are higher during the night; this can be seen in both of the case studies. It is also noted that higher concentrations in METRAS (unnudge) are simulated than in METRAS (nudge). This difference in concentration is due to the different meteorology. Higher concentrations in METRAS (unnudge) are due to the normalization of concentration with the METRAS (nudge) results as well.

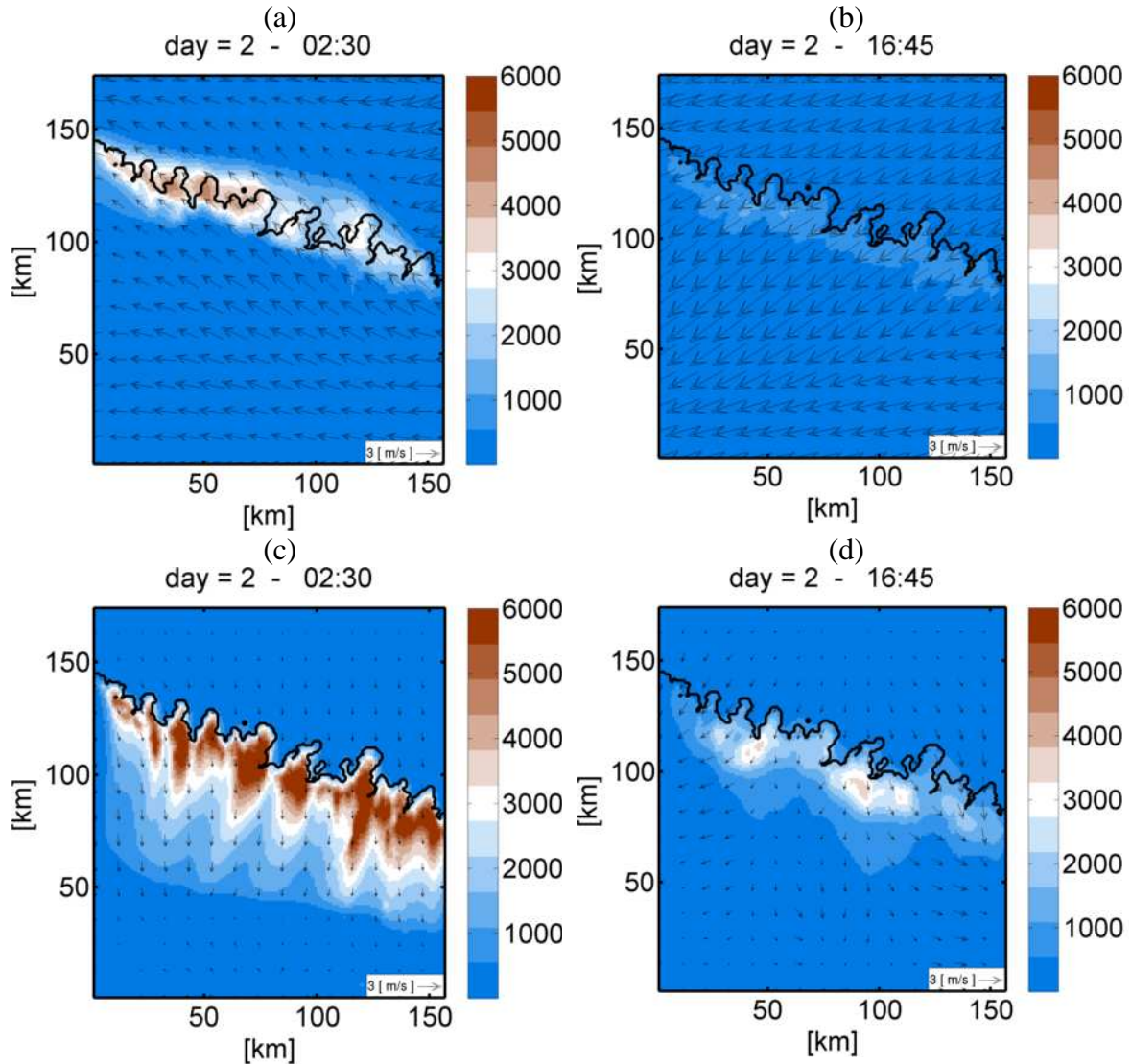


Figure 5.3  $\text{CH}_3\text{Cl}$  scaled concentrations and wind pattern at 20 m above the ground for (a), (b) nudge case and (c), (d) unnudge case at (a, c) night and (b, d) day for 17.12.2010 with constant emission functions for mangrove emissions. Every 10<sup>th</sup> vector is shown.

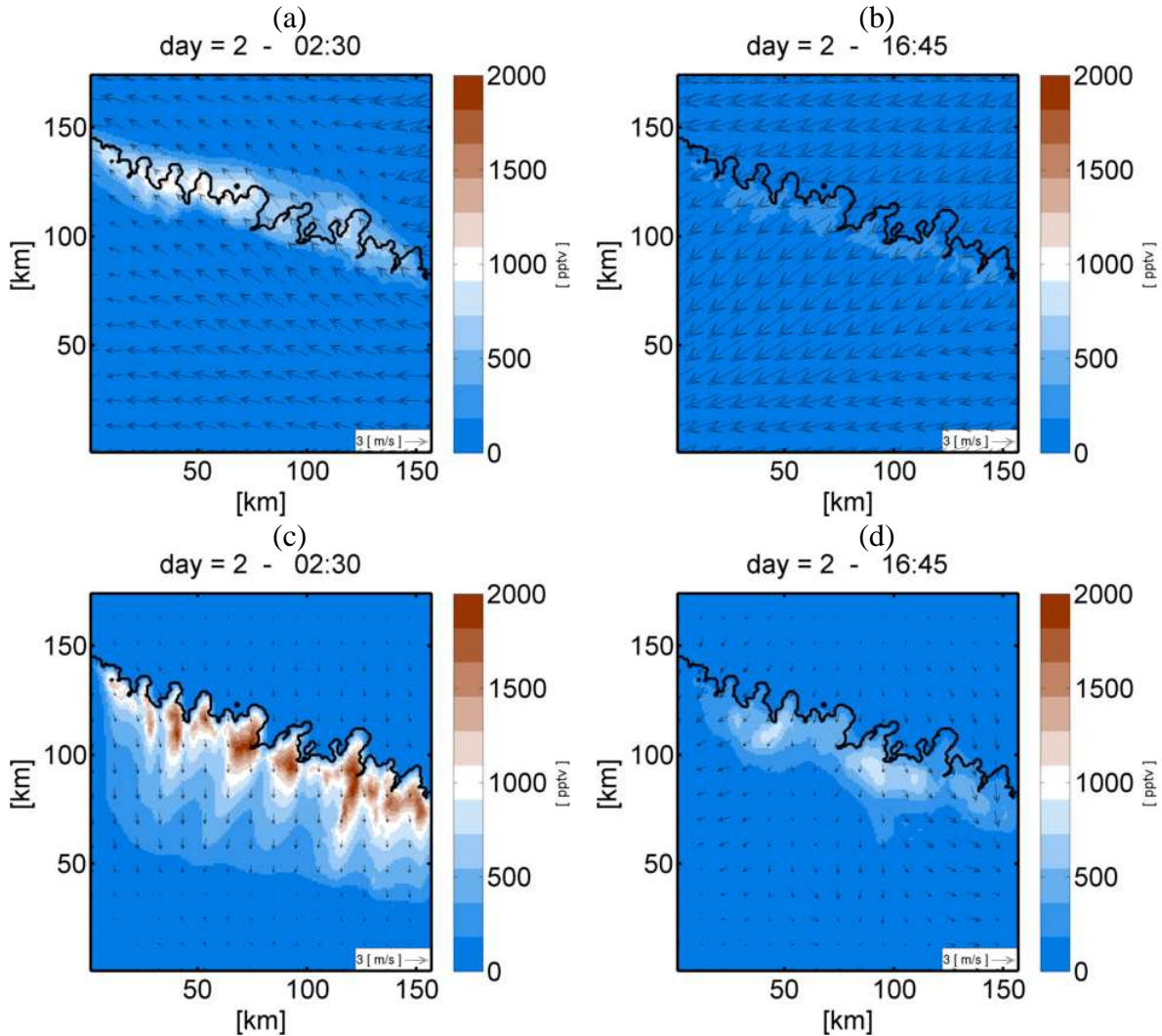


Figure 5.4  $\text{CH}_2\text{Cl}_2$  scaled concentrations and wind pattern at 20 m above the ground for (a), (b) nudge case and (c), (d) unnudge case at (a, c) night, and (b, d) day for 17.12.2010 with constant emission functions for mangrove emissions. Every 10<sup>th</sup> vector is shown.

Figures 5.5, 5.6 show the concentration gradient of methyl halides in the mangrove forest region calculated from the model simulation. The gradient is calculated as concentration difference between downwind and upwind positions in the mangrove forest after scaling model concentrations using eq. (5.8), which is denoted as G in the Figures. This gradient is thus comparable to the measurement approach and will give the mangrove forest contribution of methyl halides.

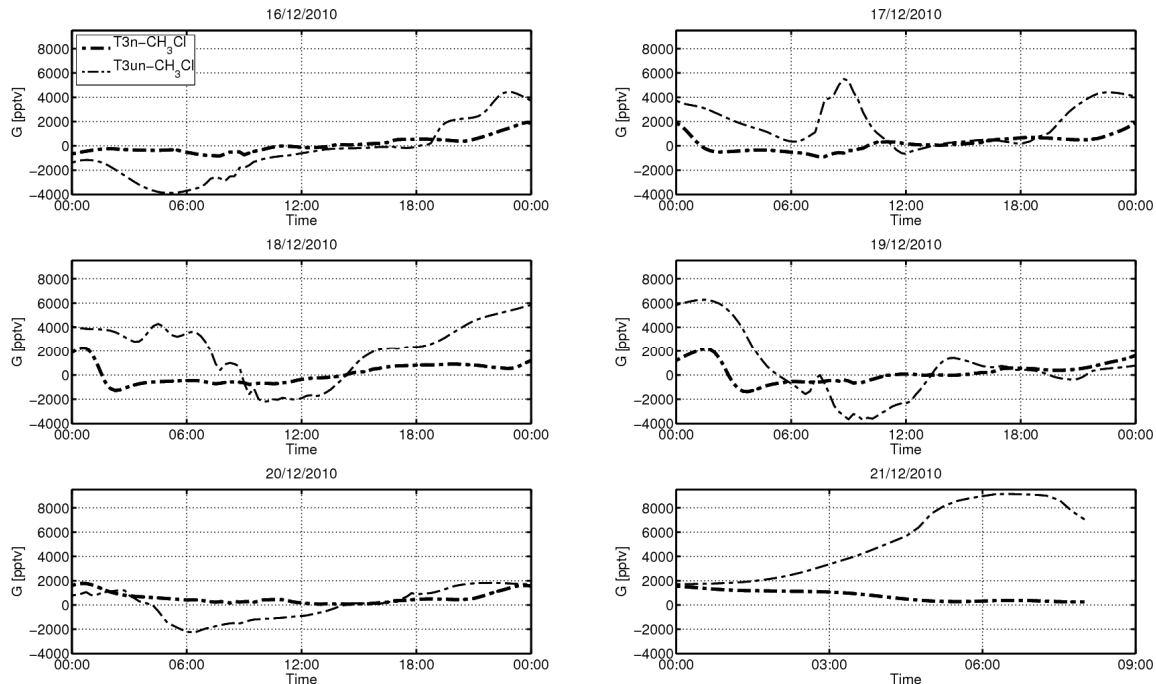


Figure 5.5 Mangrove contribution (Concentration Gradient) of  $\text{CH}_3\text{Cl}$  with constant emission functions for nudge (T3n), unnudge (T3un) for different days. Note that 21.12.2010 is not for 24 hours.

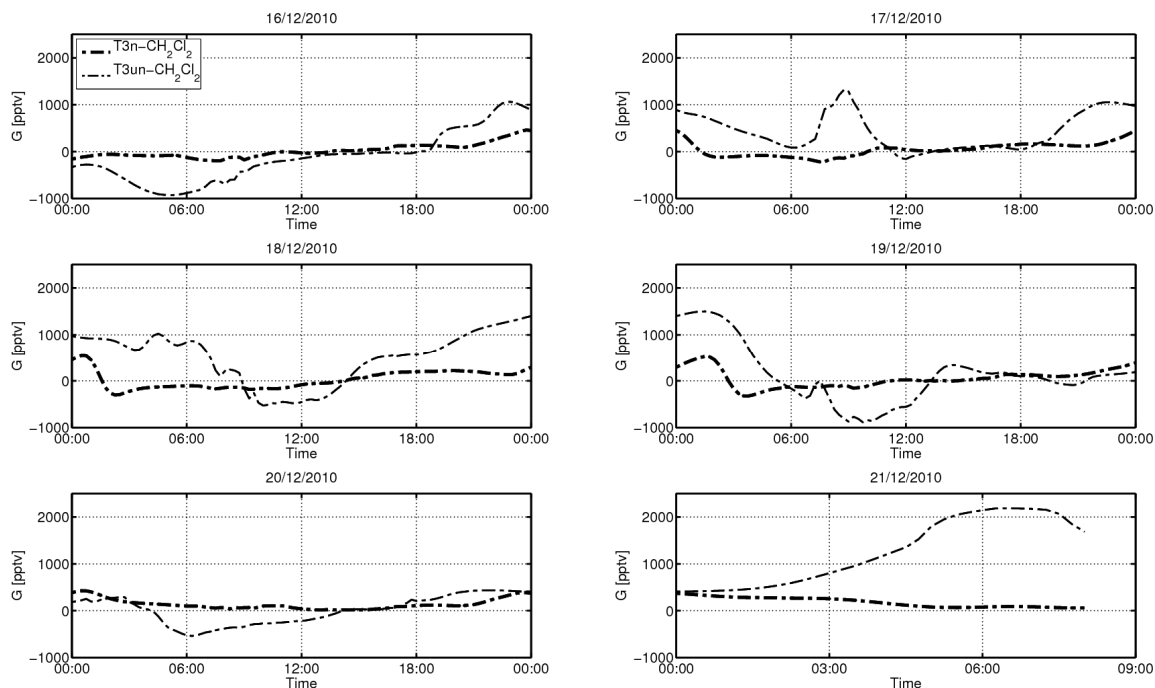


Figure 5.6 Mangrove contribution (Concentration Gradient) of  $\text{CH}_2\text{Cl}_2$  with constant emission functions for nudge (T3n), unnudge (T3un) for different days. Note that 21.12.2010 is not for 24 hours.

The diurnal cycle of methyl halide gradients calculated from METRAS (nudge) and METRAS (unnudge) model simulations are studied to understand the meteorology impact on the concentrations. The diurnal cycle of the methyl halide gradient varies similarly for both tracers but differs in magnitude (Figures 5.5, 5.6). The gradient of methyl halides varies little during the night-time in METRAS (nudge). In METRAS (unnudge), higher differences in the gradients are seen between the night-time and the daytime. A higher difference in the gradient of CH<sub>3</sub>Cl and CH<sub>2</sub>Cl<sub>2</sub> is noticed on 17<sup>th</sup>, 18<sup>th</sup>, 19<sup>th</sup>, and 21<sup>st</sup> December 2010 in METRAS (unnudge). These higher differences in the two different meteorology simulations suggest that meteorology is playing a role in the concentrations of the constant emission function at the coastal mangrove forest.

The ratio of the gradient of CH<sub>3</sub>Cl and CH<sub>2</sub>Cl<sub>2</sub> concentration for unnudged and nudged meteorology suggests that in METRAS (unnudge) gradients are about 10 times higher than METRAS (nudge) case except for 21<sup>st</sup> December. On 21<sup>st</sup> December about 30 times higher concentration gradients are found in METRAS (unnudge) for constant emission functions.

Observations were conducted on December 17<sup>th</sup> 2010 between 16:40 to 18.05 BRT in the forest region. The gradients of CH<sub>3</sub>Cl and CH<sub>2</sub>Cl<sub>2</sub> concentrations in both the cases are not varying during the sampling time and are very small. This implies that the observational time was not the best time to determine the emission function using measurements. To determine the constant emission function from measurements, we need to have observations of methyl halides continuously during the night and the daytime. Hence, it has been concluded that it is impossible to determine the constant emission functions using measured data in the coastal mangroves forest of Brazil based on only very few measurements.

In order to quantify the role of meteorology on concentrations, the model METRAS simulated concentrations were normalized using the equation (5.9) for the constant emission function:

$$\text{Normalized concentration differences} = \frac{T3un(z, x, y, t) - T3n(z, x, y, t)}{\max(T3un(z, x, y, t); T3n(z, x, y, t))} 100 \quad (5.9)$$

Here  $T3un(z, x, y, t)$  denotes the scaled concentration simulated by METRAS (unnudge) using a constant emission function. Similarly,  $T3n(z, x, y, t)$  is for METRAS (nudge).

Figure 5.7 shows the normalized concentration differences as derived from eq. (5.9) of methyl halides for 17.12.2010 (Figure 5.7a, c) at 02:30 and for 19.12.2010 (Figure 5.7b, d) at 4:30. The normalized concentration difference values are zero over the coast for a few hours

(about 9:00 to 12:00; not shown here) and, thereafter, increased notably on 20<sup>th</sup> December 2010 for CH<sub>3</sub>Cl and CH<sub>2</sub>Cl<sub>2</sub> (not shown here). The normalized concentration differences of CH<sub>3</sub>Cl, CH<sub>2</sub>Cl<sub>2</sub> are in the magnitude of about +50 percent to -50 percent of the maximum concentrations. Hence, the quantified role of meteorology in the methyl halide concentrations for constant emission function is about ±50 percent in the mangrove forest region.

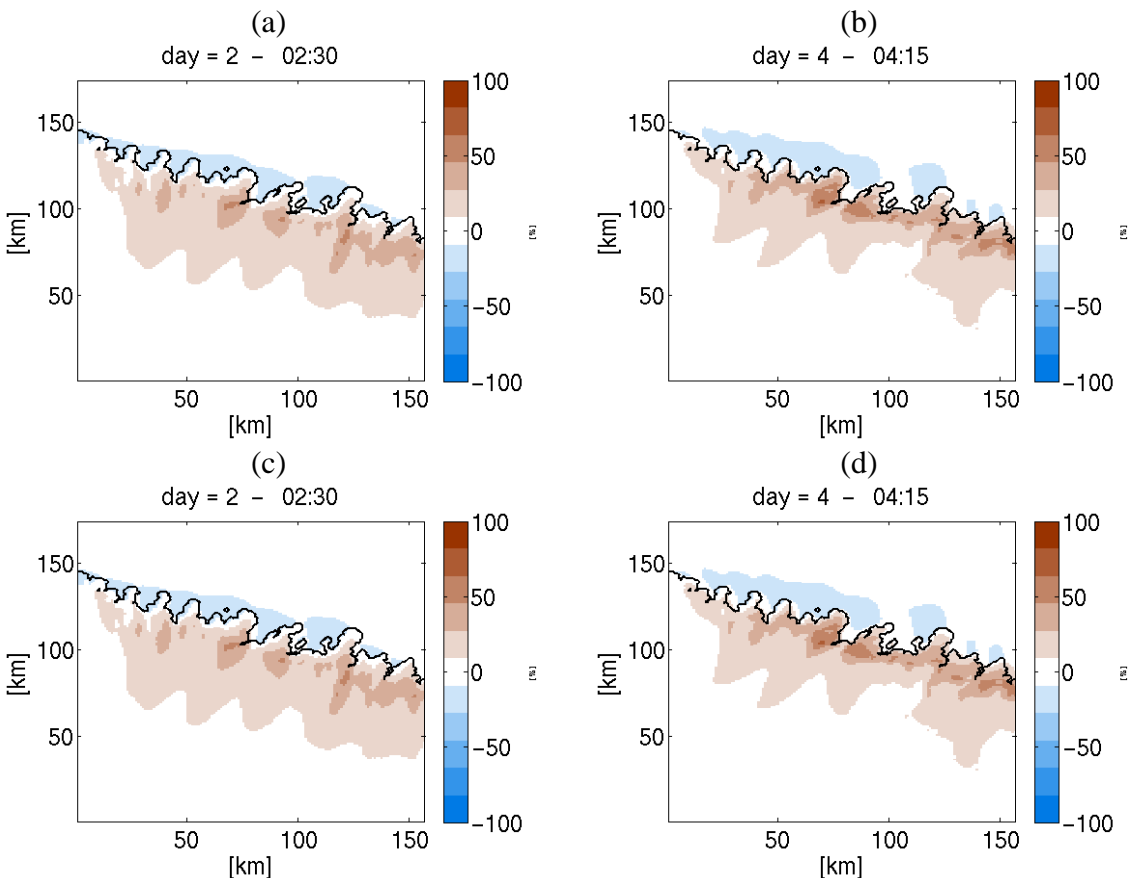


Figure 5.7 Normalized concentration differences based on eq. (5.9) for (a, c) 17.12.2010 and (b, d) 19.12.2010, for (a, b) CH<sub>3</sub>Cl and for (c, d) CH<sub>2</sub>Cl<sub>2</sub>.

### 5.3.2 Impact of time dependent emission functions on concentrations

The time dependent emission function simulation results is the focus of this section. The scaled CH<sub>3</sub>Cl and CH<sub>2</sub>Cl<sub>2</sub> concentrations are shown in the Figures 5.8 and 5.9 for the night-time and daytime. Like the concentrations resulting from the constant emission functions, concentrations simulated by the time dependent emission functions show similar patterns in METRAS (nudge) and METRAS (unnudge). Higher concentrations are seen for both tracers during the night due to stable stratification in the atmosphere. The stable stratification discourages vertical mixing of the tracers in the atmosphere. Hence, the higher

concentrations are noticed during the night-time. This stability impact is larger than the impacts of the increased emissions during the daytime (Figure 5.1).

The magnitude of  $\text{CH}_3\text{Cl}$  and  $\text{CH}_2\text{Cl}_2$  concentrations in METRAS (nudge) case is within the observed data range. However, the magnitudes in METRAS (nudge) also vary substantially during the night with a magnitude about 3000 pptv due to meteorology changes. In METRAS (unnudge) case the concentrations of  $\text{CH}_3\text{Cl}$  and  $\text{CH}_2\text{Cl}_2$  are mostly trapped in the coastal mangrove region due to lower wind speeds simulated in the model. Unlike METRAS (unnudge), the concentrations are more dispersed in METRAS (nudge) due to higher wind speeds in the coastal mangrove region.

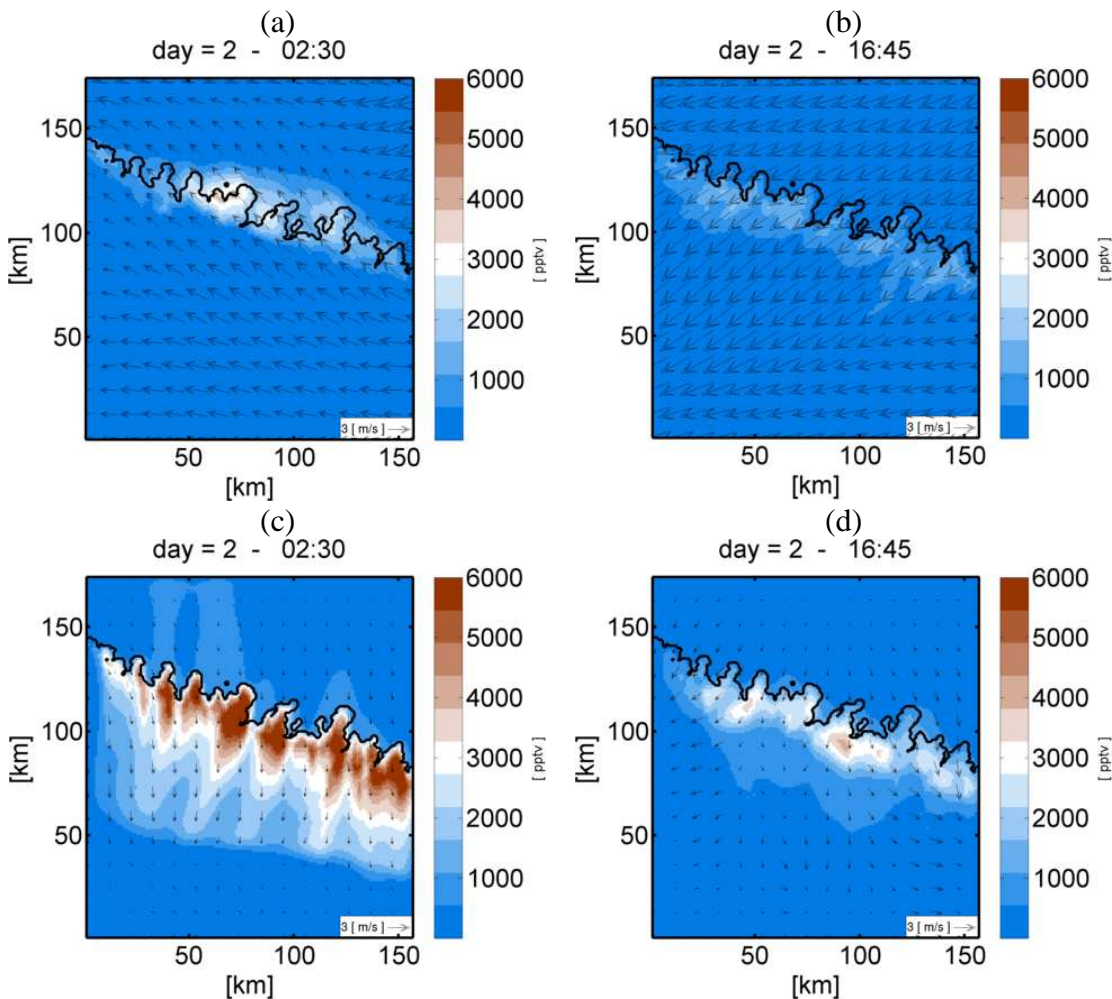


Figure 5.8  $\text{CH}_3\text{Cl}$  scaled concentrations and wind pattern at 20 m above the ground for (a), (b) nudge case and (c), (d) unnudge case at (a, c) night and (b, d) day for 17.12.2010 with time dependent emission functions for mangrove emissions. Every 10<sup>th</sup> vector is shown.

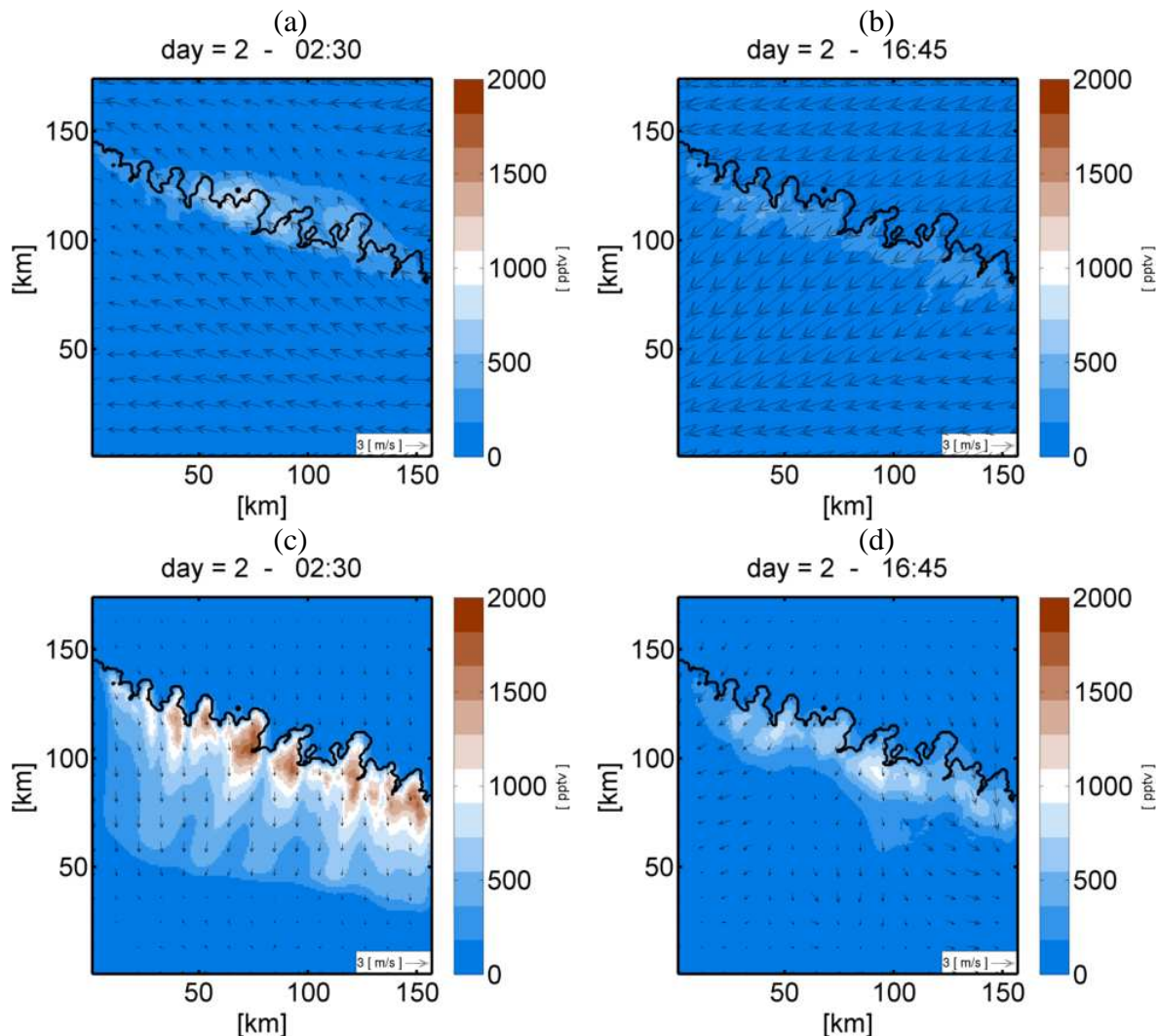


Figure 5.9  $\text{CH}_2\text{Cl}_2$  scaled concentrations and wind pattern at 20 m above the ground for (a), (b) nudge case and (c), (d) unnudge case at (a, c) night and (b, d) day for 17.1210 with time dependent emission functions for mangrove emissions. Every 10<sup>th</sup> vector is shown.

The diurnal cycle of concentration gradients of  $\text{CH}_3\text{Cl}$  and  $\text{CH}_2\text{Cl}_2$  are shown in Figures 5.10 and 5.11. The concentration gradients of methyl halides in METRAS (nudge) case are mostly constant during the day but slightly vary in the night. Unlike METRAS (nudge), the gradient of methyl halides differ highly between night and day on the 17<sup>th</sup>, 18<sup>th</sup>, 20<sup>th</sup> and 21<sup>st</sup> December in METRAS (unnudge). There is a higher magnitude of gradient on the 21<sup>st</sup> noted in METRAS (unnudge) due to larger meteorological changes after 5 days of simulation.

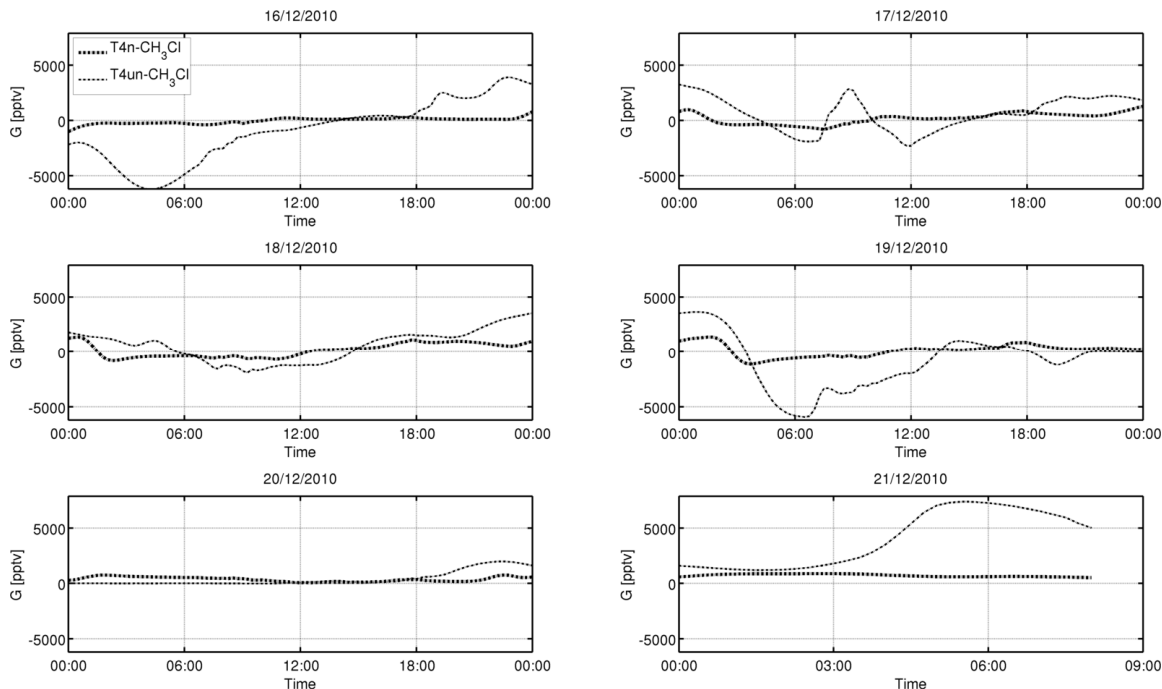


Figure 5.10 Mangrove contribution (Concentration Gradient) of  $\text{CH}_3\text{Cl}$  with time dependent emission function for nudge (T4n), unnudge (T4un) for different days. Note that 21.12.2010 is not for 24 hours.

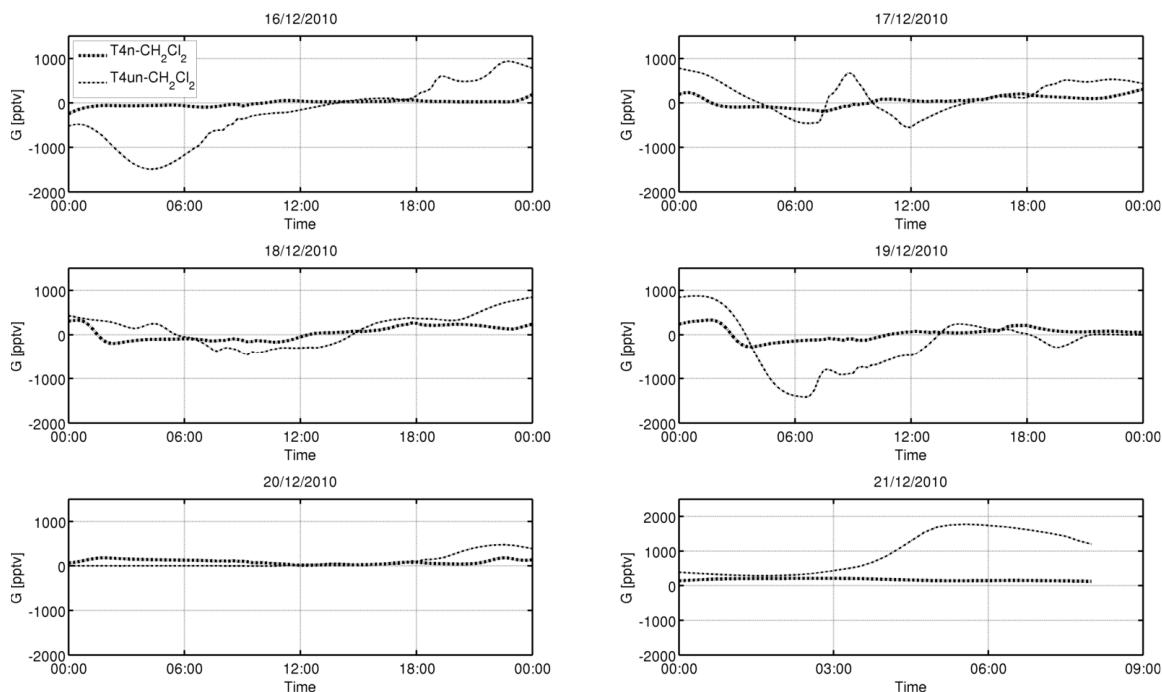


Figure 5.11 Mangrove contribution (Concentration Gradient) of  $\text{CH}_2\text{Cl}_2$  with time dependent emission function for nudge (T4n), unnudge (T4un) for different days. Note that 21.12.2010 is not for 24 hours.

A similar pattern of diurnal variation of methyl halide concentration gradients are found for the time dependent emission function and constant emission function in METRAS (nudge) and METRAS (unnudge). The only difference is the magnitude for both types of emission functions. This suggests that the type of emission functions likely does not have the largest impact on concentration. The ratios of methyl halide concentration gradients from METRAS (unnudge) to METRAS (nudge) are: about 20 times on the 16<sup>th</sup> December; -10 to 10 times on the 17<sup>th</sup> December; and slight variations are found on the 18<sup>th</sup> and 20<sup>th</sup> December, 2010.

Eq. (5.9) is also applied to the concentrations simulated using time dependent emission functions. Figure 5.12 shows the normalized  $\text{CH}_3\text{Cl}$  concentration differences (Figure 5.12a, b) and  $\text{CH}_2\text{Cl}_2$  concentration differences (Figure 5.12c, d) for different days. The normalized model-simulated concentration differences of methyl halides using time dependent emission functions are in the range of up to  $\pm 50$  percent. Mostly the normalized concentration difference calculated is +50 percent in the whole model simulations for  $\text{CH}_3\text{Cl}$  and  $\text{CH}_2\text{Cl}_2$  in the coastal mangrove region. Hence, meteorology plays the same role on the concentrations given different types of emission functions.

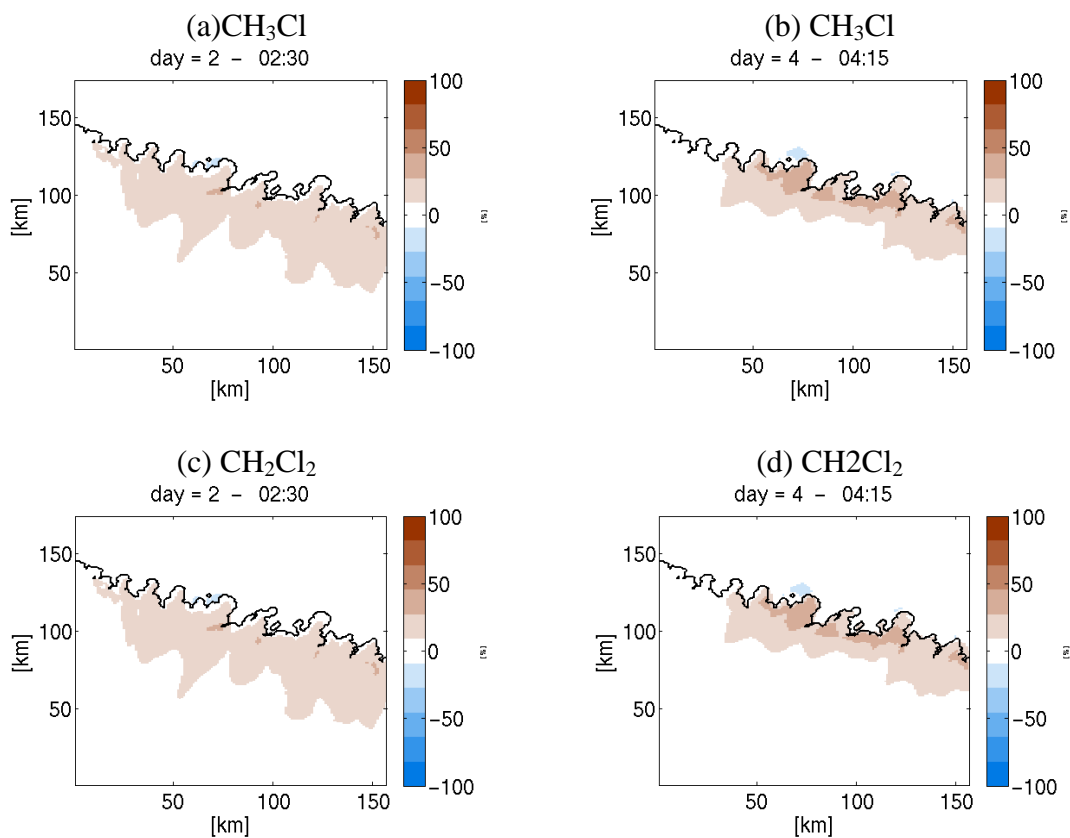


Figure 5.12 Normalized concentration differences based on eq. (5.9) for (a, c) 17.12.2010 and (b, d) 19.12.2010, for (a, b)  $\text{CH}_3\text{Cl}$  and for (c, d)  $\text{CH}_2\text{Cl}_2$ .

### 5.3.3 Frequency distributions to quantify impacts

This section presents the frequency distribution of differences in methyl halide concentrations simulated by the different model set-ups for the coastal mangrove region. To understand the role of both meteorology and time dependent emission functions, different combinations of frequency distributions were calculated. Such as one frequency distribution with different meteorology and constant emission functions. Another one with constant emission functions with different meteorology. Figure 5.13 shows the differences in distribution of  $\text{CH}_3\text{Cl}$  (Figure 5.13a, c) and  $\text{CH}_2\text{Cl}_2$  (Figure 5.13b, d). The x-axes denotes the concentration difference between METRAS (unnudge) and METRAS (nudge) cases in pptv. The y-axes represent the number of grid points in percent. The total number of grid points was calculated as the product of total number of grid points in the south-north-direction (176), in the west-east-direction (159) and time (526 output intervals) at the 10 m model level.

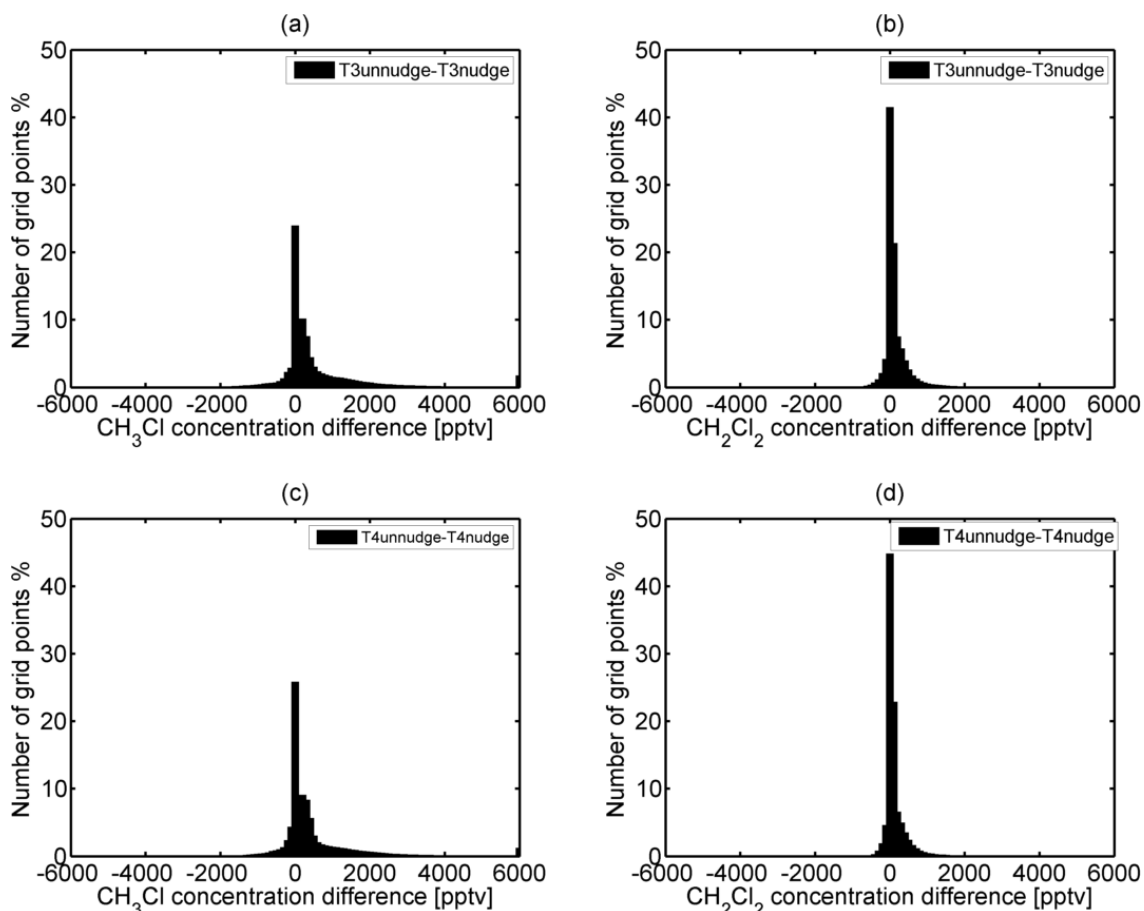


Figure 5.13 Frequency distribution of concentration differences unnudge minus nudge case for methyl halides for (a, b) constant emission functions and for (c, d) time dependent emission functions.

Frequency distributions of CH<sub>3</sub>Cl and CH<sub>2</sub>Cl<sub>2</sub> show the distribution is mostly positively skewed. More grid points show higher values in METRAS (unnudge), the concentrations are higher. The majority of grid points yield CH<sub>3</sub>Cl concentration difference estimates within ±2000 pptv for constant and time dependent emission functions. In the case of CH<sub>2</sub>Cl<sub>2</sub> the concentration difference is about ±1000 pptv. Thus, the frequency distribution plot suggests that the impact of meteorology on concentrations is high.

Similarly, the frequency distributions of the differences between concentration gradients of METRAS (nudge) and METRAS (unnudge) meteorology case were studied for the different emission functions. The frequency distribution of the differences in concentration gradients also reveals large differences due to meteorology changes (Figures not shown). The CH<sub>3</sub>Cl concentration gradient difference extends from about -4500 pptv to 5000 pptv for constant and time dependent emission functions at the coastal mangrove region. In the case of CH<sub>2</sub>Cl<sub>2</sub>, the differences in concentration gradients are smaller, varying between -500 pptv to 1000 pptv for both types of emission functions. The wide distributions in the concentration gradient difference also support that meteorology has a large impact on the concentrations measurable over the coastal mangrove region.

Table 5.2 shows the 1<sup>st</sup>, 5<sup>th</sup>, 50<sup>th</sup>, 95<sup>th</sup>, 99<sup>th</sup> percentiles of concentration differences (METRAS (unnudge) minus METRAS (nudge)) of methyl halides for constant emission function (T3CH<sub>3</sub>Cl, T3CH<sub>2</sub>Cl<sub>2</sub>) and for time dependent emission functions (T4CH<sub>3</sub>Cl, T4CH<sub>2</sub>Cl<sub>2</sub>). Higher values of the 99<sup>th</sup> percentile of the data suggest that larger differences in the concentrations occur due to meteorology changes.

*Table 5.2 Percentiles of concentration difference of unnudge and nudge for CH<sub>3</sub>Cl and CH<sub>2</sub>Cl<sub>2</sub> in pptv.*

<b>Percentiles</b>	<b>1</b>	<b>5</b>	<b>50</b>	<b>95</b>	<b>99</b>
T3CH <sub>3</sub> Cl	-1748	-598	204	3236	7528
T4CH <sub>3</sub> Cl	-1165	-413	179	2830	6423
T3CH <sub>2</sub> Cl <sub>2</sub>	-418	-143	48	774	1801
T4CH <sub>2</sub> Cl <sub>2</sub>	-278	-98	42	677	1536

The analyses performed before by comparing results with the same emissions but different meteorology is now repeated for using the same meteorology but different emission functions. Figure 5.14 shows the frequency distribution of methyl halides concentration difference of different emission function calculated with the same meteorology. The

frequency distribution figure shows that the largest percentage of grid points are in the 0 pptv concentration bin. Unlike in the different meteorology but same emission functions case (Figure 5.13), a small percentage of grid points show a concentrations difference of less than -400 pptv or more than 400 pptv in the constant meteorology but different emission functions case. This suggests that the type of emission function does not have more influence than the meteorology on the concentrations signals that are measurable in the coastal mangrove region.

The same frequency distribution is also calculated for the concentration gradient differences. The gradient Figures are not shown but reveal qualitatively the same results for methyl halides emissions of mangroves.

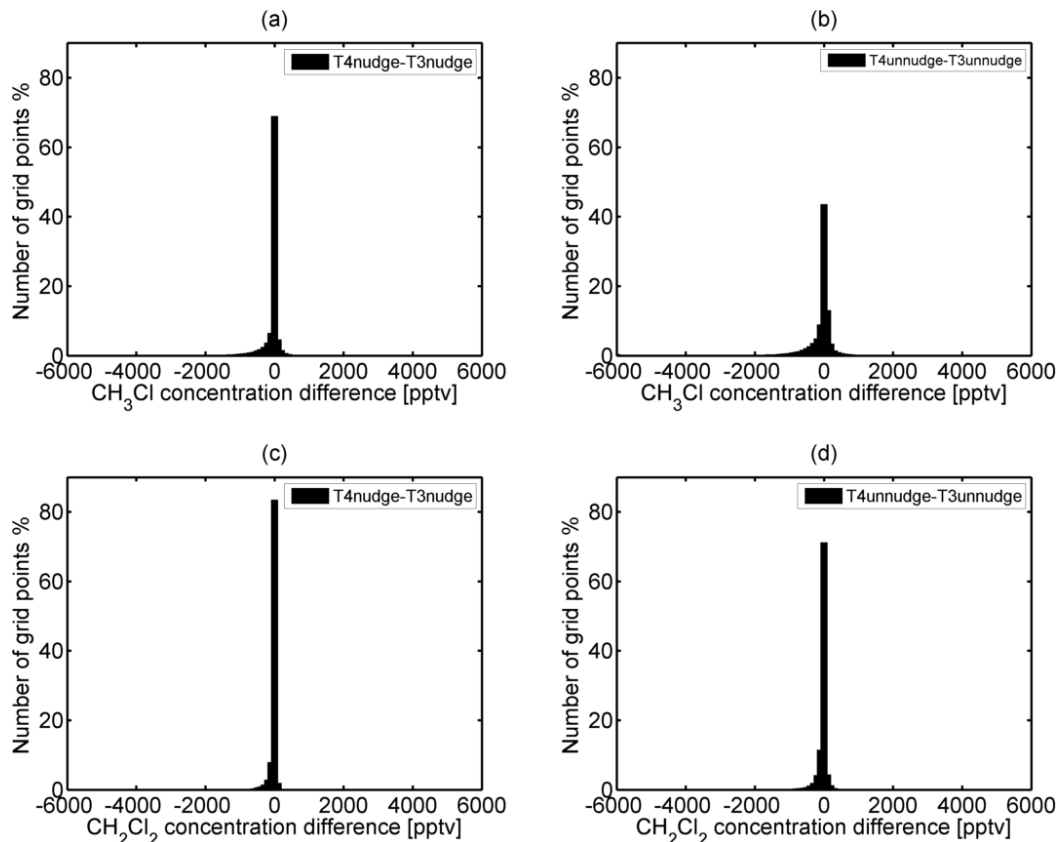


Figure 5.14 Frequency distribution of methyl halides concentration difference of different emission function with constant meteorology.

The percentiles of constant meteorology but different emission function concentration difference are shown in the Table 5.3. Table 5.3 supports the previous results of smaller difference in concentrations when the same meteorology is used. The 99<sup>th</sup> percentiles data of the Table 5.2 is higher than compared with data in the Table 5.3. Hence, it has been

concluded that meteorology has shown more influence on the concentration than the different emission functions in the coastal mangrove region.

*Table 5.3 Percentiles of concentration difference between different emission functions for CH<sub>3</sub>Cl and CH<sub>2</sub>Cl<sub>2</sub> in pptv.*

<b>Percentiles</b>	<b>1</b>	<b>5</b>	<b>50</b>	<b>95</b>	<b>99</b>
T4n-T3nCH <sub>3</sub> Cl	-2005	-788	-0.8	102	357
T4un-T3unCH <sub>3</sub> Cl	-4000	-1300	0	303	1112
T4n-T3nCH <sub>2</sub> Cl <sub>2</sub>	-479	-188	0	24	85
T4un-T3unCH <sub>2</sub> Cl <sub>2</sub>	-957	-311	0	72	266

## **5.4 Contribution of different emission sources to the coastal concentrations**

The observed concentrations in forest region are used to scale the concentration of water tracers as well. We assumed here that the observed methyl halide concentrations are from the ocean contribution in order to understand the relevance of methyl halide emission from the water source region.

Figures 5.15 and 5.16 show CH<sub>3</sub>Cl concentrations of constant and time dependent emission function simulations for 17.12.2010 in day and night-time transport. METRAS (nudge) case water concentrations (Figure 5.15 a, b and Figure 5.16 a, b) at the boundary show zero concentrations due to prescribed boundary condition number 15 used in the model simulation. The boundary condition 15 means that the large-scale values are prescribed at the inflow boundary. But there are no inflow concentrations from the large-scale values. Hence the concentrations at the boundary are zero in METRAS (nudge) case.

Figures 5.15, 5.16 show the large difference in the concentrations between METRAS (nudge) and METRAS (unnudge) case. They also show that the concentration transport and magnitude changed during night and daytime for both cases. The time dependent emission function concentrations (Figure 5.16) show little variation in the concentration compared with constant emission functions from the water source region. Higher concentrations are noted in the constant emission function than the time dependent emission function in both meteorology case simulations. Hence, the concentration patterns in the water region suggest that a large influence of meteorology is more relevant for the concentrations than the impact of emission. However, one should note here that the concentration pattern is also affected by

the boundary conditions chosen to simulate concentrations. As mentioned before, a zero concentration is assumed for inflow at the boundary which results in small values close to the eastern and northern model domain boundary in case of METRAS (nudge), while the gradients are small in METRAS (unnudge) (outflow at these boundaries with gradient zero boundary condition).

The  $\text{CH}_2\text{Cl}_2$  scaled concentrations also showed the same properties; only changes in the magnitude are noticed. Therefore, here the  $\text{CH}_2\text{Cl}_2$  concentration patterns are not shown.

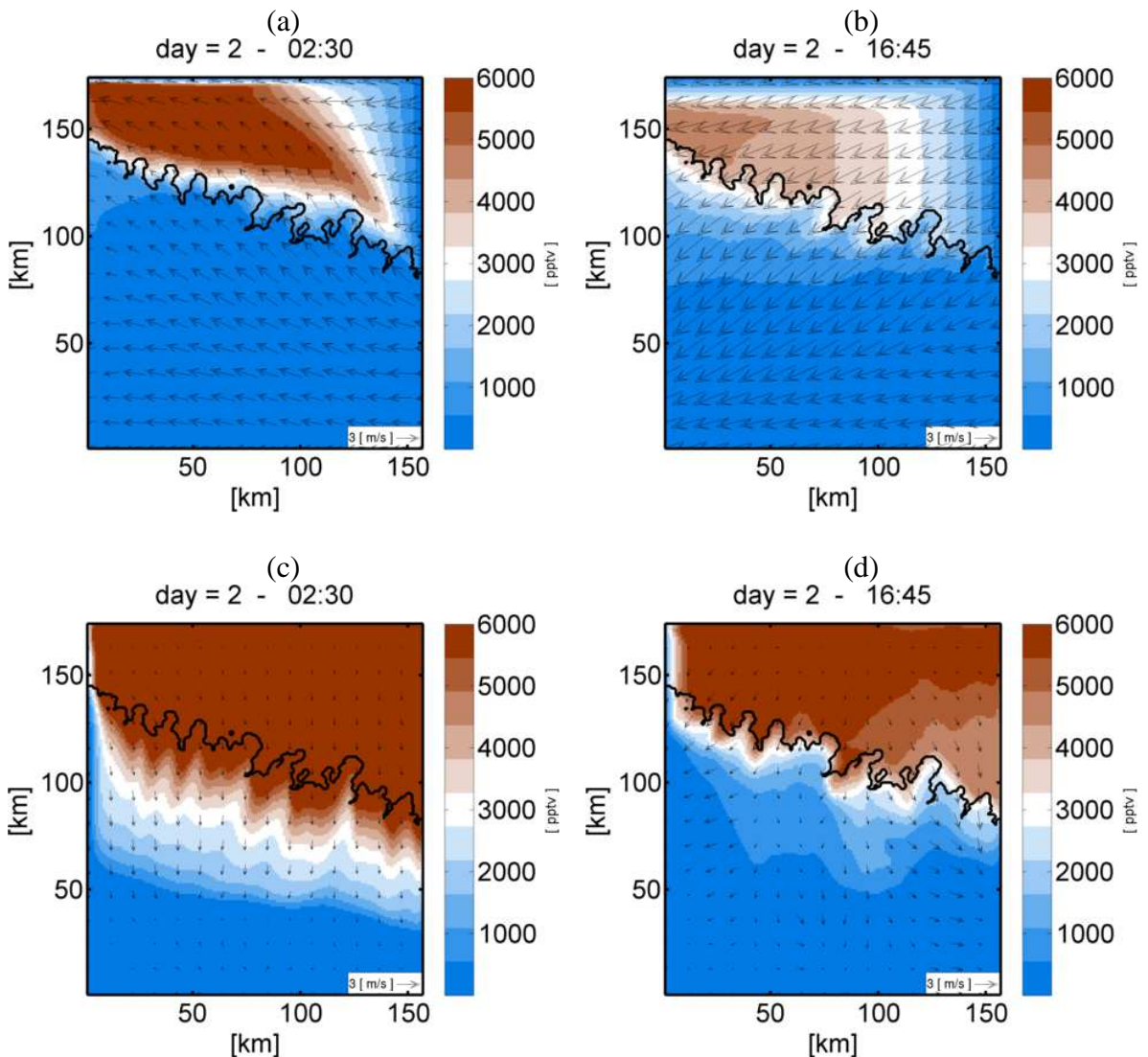


Figure 5.15  $\text{CH}_3\text{Cl}$  scaled concentrations and wind pattern at 20 m above the ground for (a), (b) nudge case and (c), (d) unnudge case at (a, c) night and (b, d) day for 17.12.2010 with constant emission functions for water emissions. Every  $10^{\text{th}}$  vector is shown.

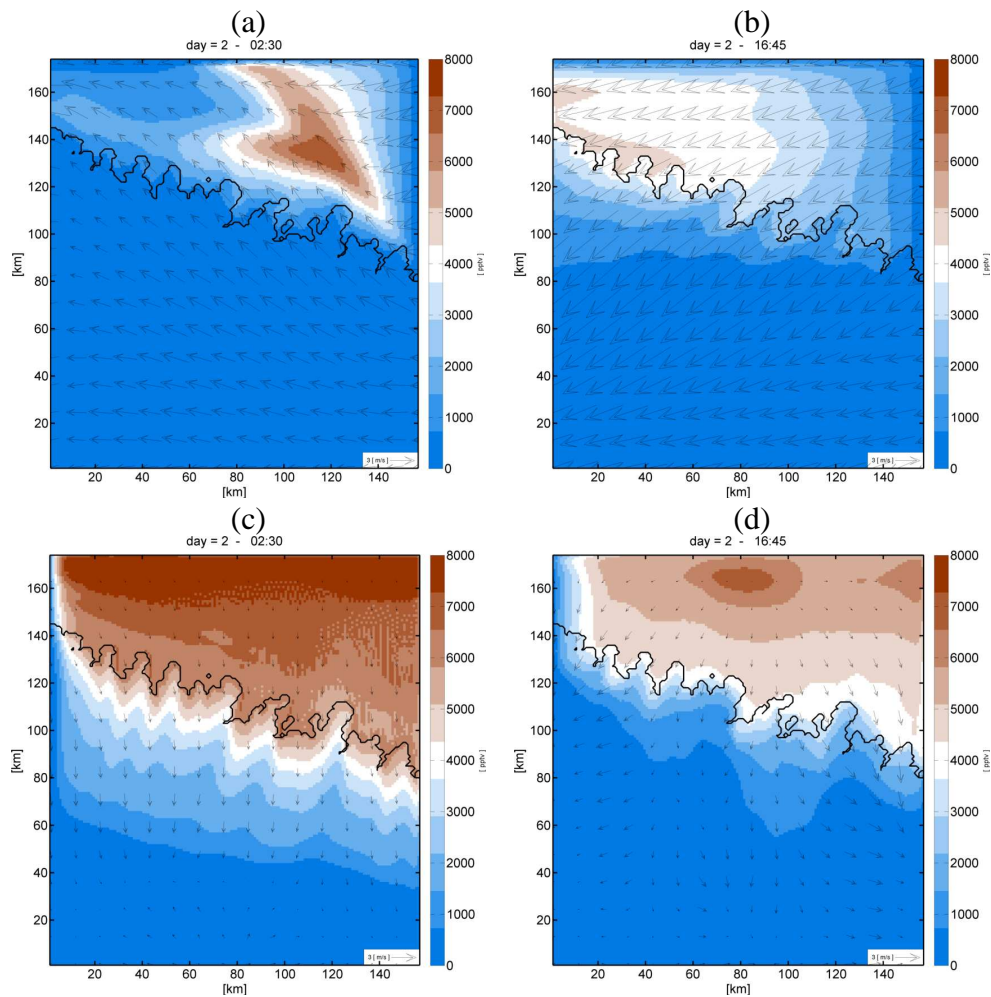


Figure 5.16  $\text{CH}_3\text{Cl}$  scaled concentrations and wind pattern at 20 m above the ground for (a), (b) nudge case and (c), (d) unnudge case at (a, c) night and (b, d) day for 17.12.2010 with time dependent emission functions for water emissions. Every 10<sup>th</sup> vector is shown.

Figures 5.17 and 5.18 show the  $\text{CH}_2\text{Cl}_2$  concentration gradient time series simulated by the model using a constant emission function (Figure 5.17) and time dependent emission function (Figure 5.18) in the water source region. The negative sign indicates that the upwind and downwind locations are not valid at the measurement site displayed in Figure 5.2a for the whole time series (i.e., the observed upwind would be downwind in the model).

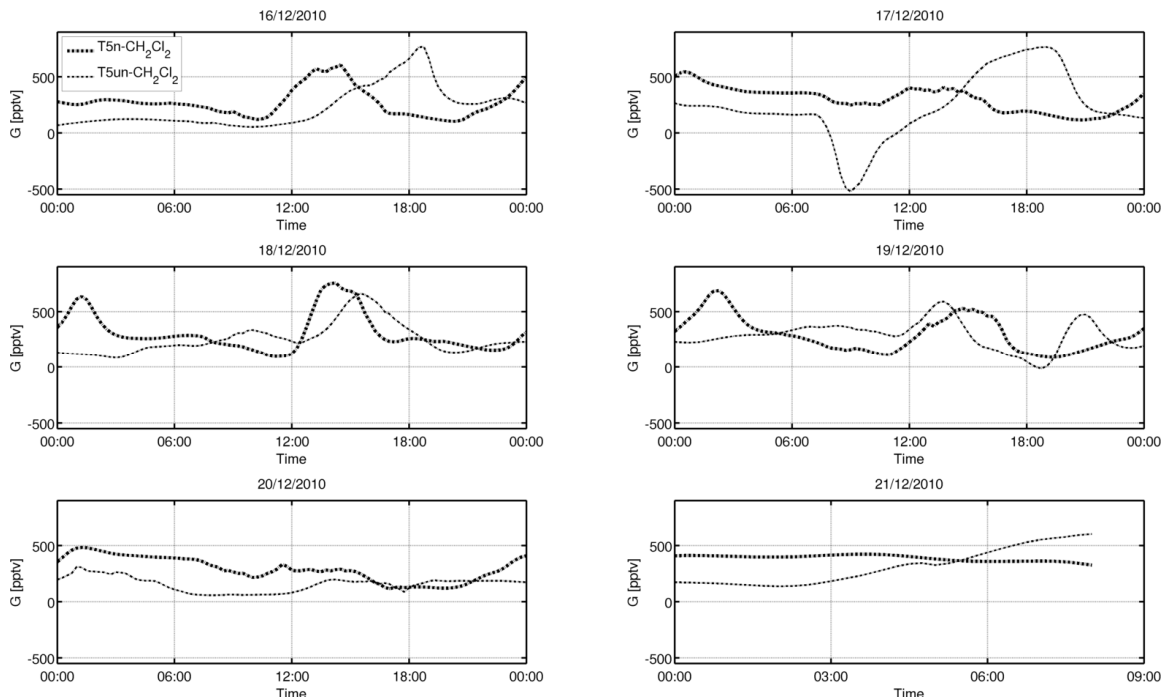


Figure 5.17 Water contribution (Concentration Gradient) of  $\text{CH}_2\text{Cl}_2$  with constant emission functions for nudge (T5n), unnudge (T5un) for different days. Note that 21.12.2010 is not for 24 hours.

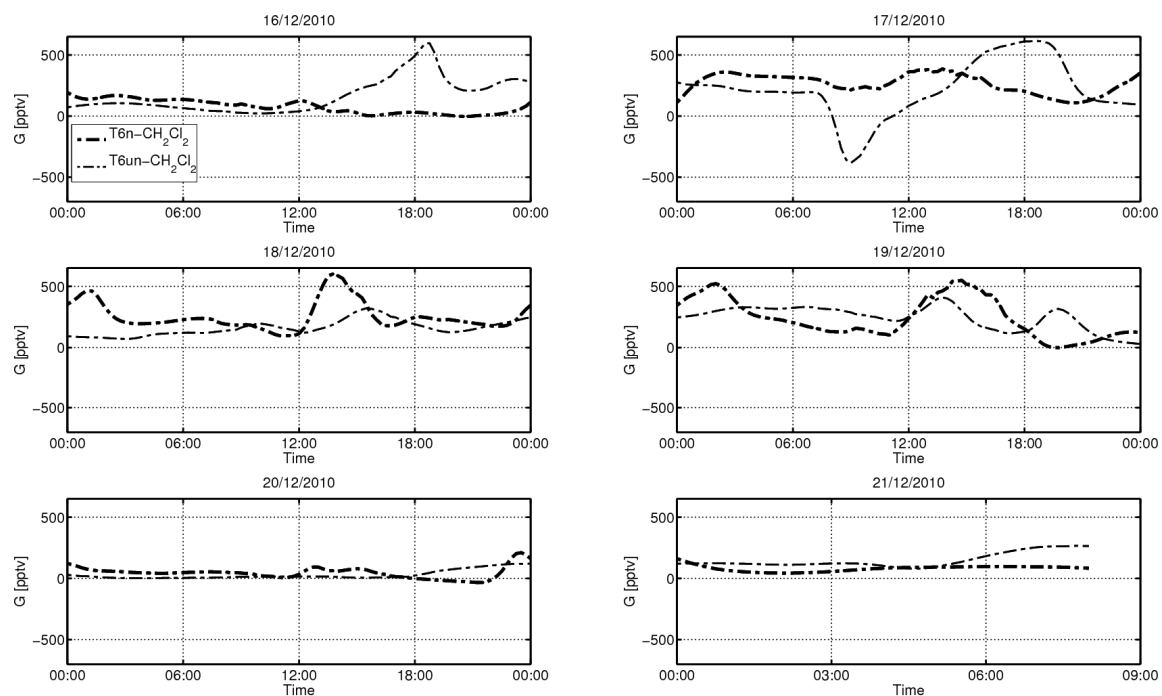


Figure 5.18 Water contribution (Concentration Gradient) of  $\text{CH}_2\text{Cl}_2$  with time dependent emission functions for nudge (T6n), unnudge (T6un) for different days. Note that 21.12.2010 is not for 24 hours.

The  $\text{CH}_3\text{Cl}$  and  $\text{CH}_2\text{Cl}_2$  concentration gradients give the water contribution of the methyl halides. The scaled  $\text{CH}_3\text{Cl}$  and  $\text{CH}_2\text{Cl}_2$  concentration gradients are overestimated because the measurements did not pick up the emissions resulting from water but from the mangroves. The diurnal cycle of concentration gradients of different emission functions show similar patterns in the whole model simulation. The concentration gradients do not vary much in the METRAS (nudge) and METRAS (unnudge) for both emission functions on December 20<sup>th</sup> and 21<sup>st</sup> 2010. Variations of the concentration gradients are seen in the daytime from December 16<sup>th</sup> to 19<sup>th</sup> 2010 for different emission functions in METRAS (nudge) and METRAS (unnudge) meteorology case. Unlike in the mangrove source region the concentration gradients varied at daytime much for the water source regions due to advection and meteorology impact.

The ratio of METRAS (unnudge) to METRAS (nudge) methyl halide concentration gradients using a constant emission function varies by a factor of about 1 to 3. In the case of time dependent emission functions, the concentration gradients ratio varies by a factor of about -2 to 2. These ratios indicate the concentration gradient changes due to meteorology. It has been noted that the ratios of concentration gradients are far less for the water source region than for the mangrove source region.

The normalized eq. (5.9) is also applied for the water source region. The  $\text{CH}_3\text{Cl}$  normalized concentration differences vary about  $\pm 50$  percent for the constant emission function (Figures 5.19 a, b). In the case of time dependent emission functions, the normalized concentrations vary slightly less than those of constant emission functions for the water source region. Normalized concentrations exceeding 50 percent are seen at the northern boundary due to zero inflow at the boundaries. Similar magnitudes are noted in the case of  $\text{CH}_2\text{Cl}_2$  normalized concentrations. Therefore, here the  $\text{CH}_2\text{Cl}_2$  normalized concentrations are not shown. Thus, it has been concluded that the role of meteorology in methyl halide concentration is about  $\pm 50$  percent for the water source region irrespective of type of emission functions used in the model.

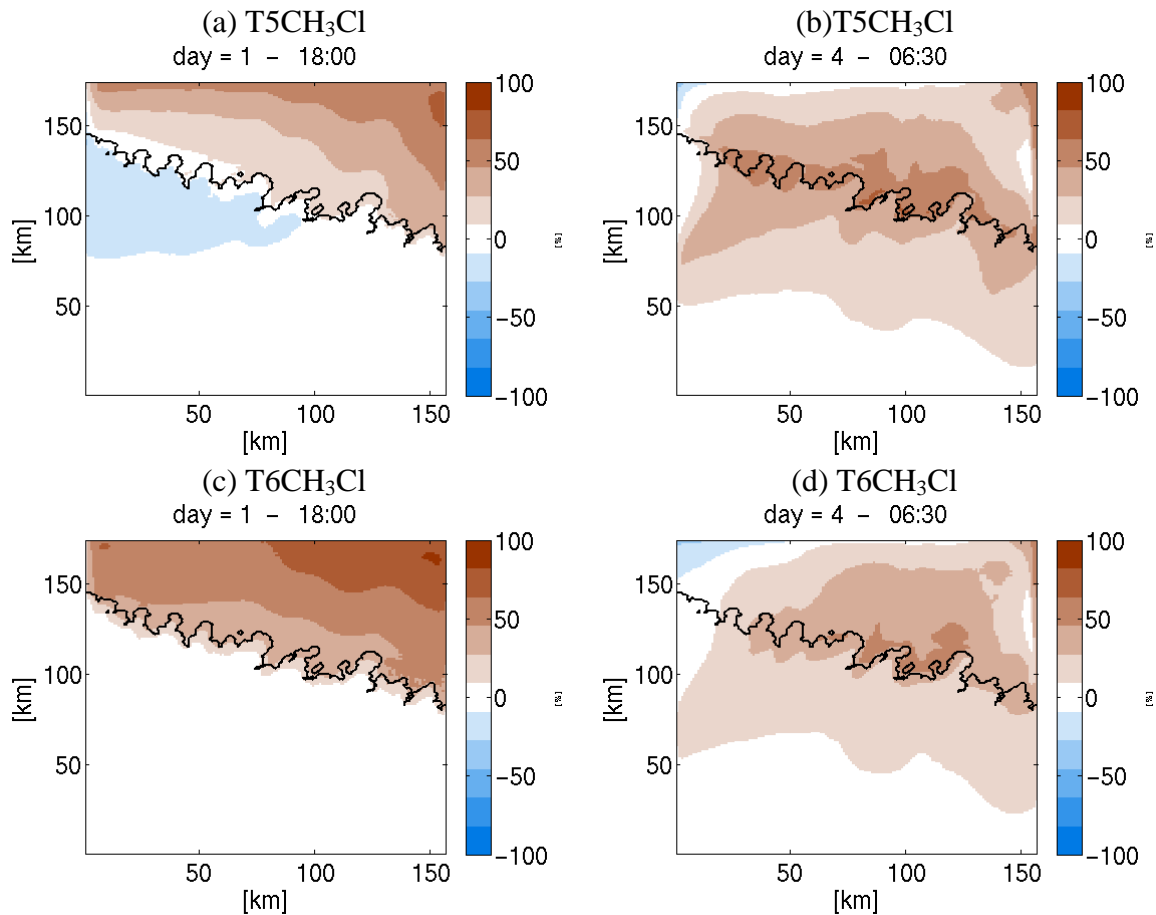


Figure 5.19 Normalized concentrations based on eq. (5.9) with (a, b) constant emission function and (c, d) time dependent emission function for (a, c) 16.12.2010 and (b, d) 19.12.2010, for  $\text{CH}_3\text{Cl}$ .

The frequency distribution of different meteorology and same emission functions concentration difference (pptv) in x-axis and percentage of frequency in y-axis is shown in Figure 5.20. The frequency distribution histogram suggests that the  $\text{CH}_3\text{Cl}$  concentration differences are negatively skewed. A high percentage of grid points are in the range of about 1000 pptv to -4000 pptv for  $\text{CH}_3\text{Cl}$ .

In the case of  $\text{CH}_2\text{Cl}_2$  about 70 percent of the grid points are in the range of -2000 pptv to 100 pptv in the water source region. Table 5.4 shows the percentiles calculated for concentration differences of different meteorology with the same emission functions. From the percentile calculation one can see the large difference in the concentrations for the 1<sup>st</sup> percentile and the 99<sup>th</sup> percentiles. Hence, meteorology has an impact on concentrations in the water source region as well.

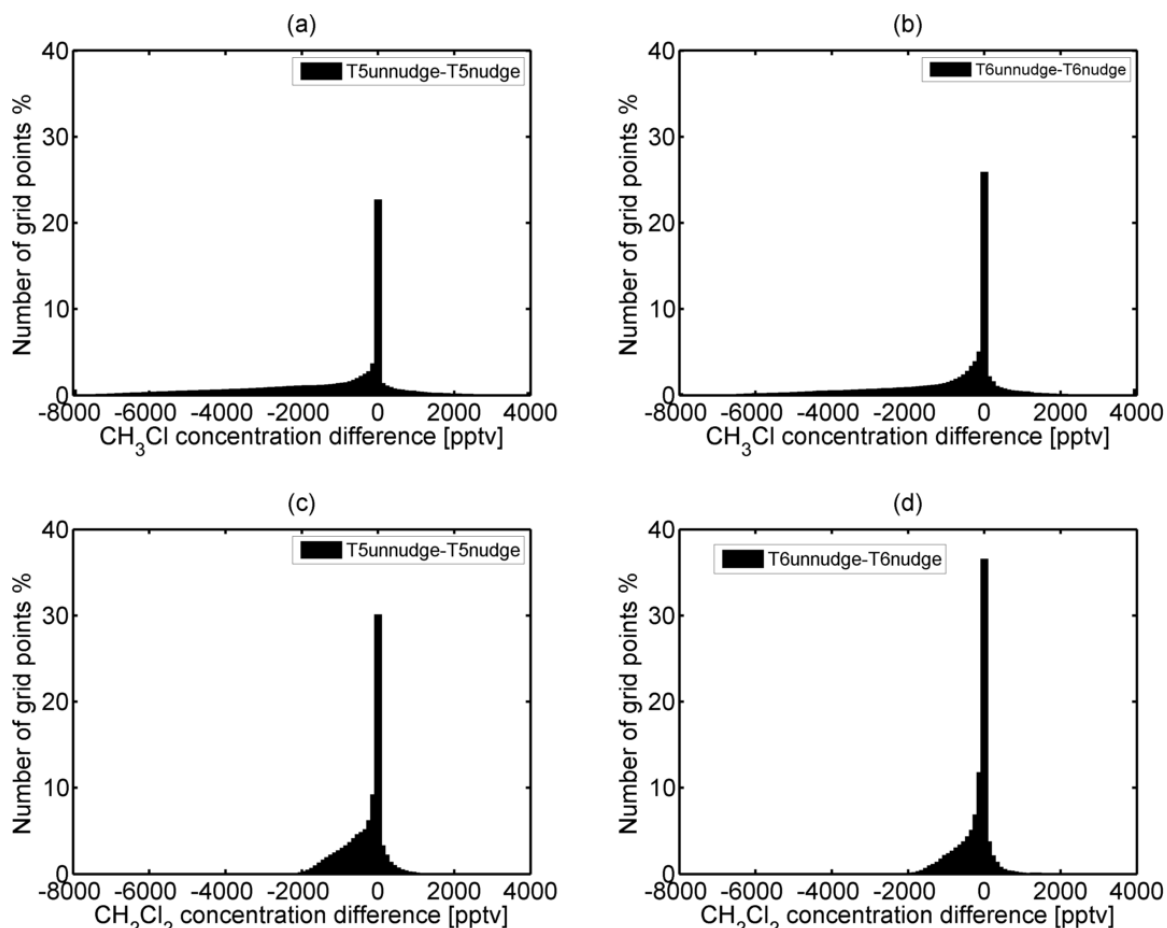


Figure 5.20 Frequency distribution of concentration differences unnudge minus nudge case for methyl halides for (a, b) constant emission functions and for (c, d) time dependent emission functions for water source region.

Table 5.4 Percentiles of concentration difference between the unnudge and nudge for  $\text{CH}_3\text{Cl}$  and  $\text{CH}_2\text{Cl}_2$  in pptv for the water source region.

Percentiles	1	5	50	95	99
T5 $\text{CH}_3\text{Cl}$	-7554	-5868	-646	1014	2969
T6 $\text{CH}_3\text{Cl}$	-6684	-4927	-284	984	3443
T5 $\text{CH}_2\text{Cl}_2$	-1807	-1403	-154	242	710
T6 $\text{CH}_2\text{Cl}_2$	-1599	-1178	-68	235	823

Figure 5.21 shows the frequency distribution of methyl halide concentration differences using different emission functions concentration with the same meteorology. In the case of nudged meteorology, the  $\text{CH}_3\text{Cl}$  and  $\text{CH}_2\text{Cl}_2$  concentration difference is zero in about 50 percent of the grid points. On the other hand, in the unnudged meteorology case, 60 percent of the grid points are positively skewed in the frequency spectra. This suggests that, unlike in

the mangrove source region, the type of emission function also plays a role in the concentration for the water source region.

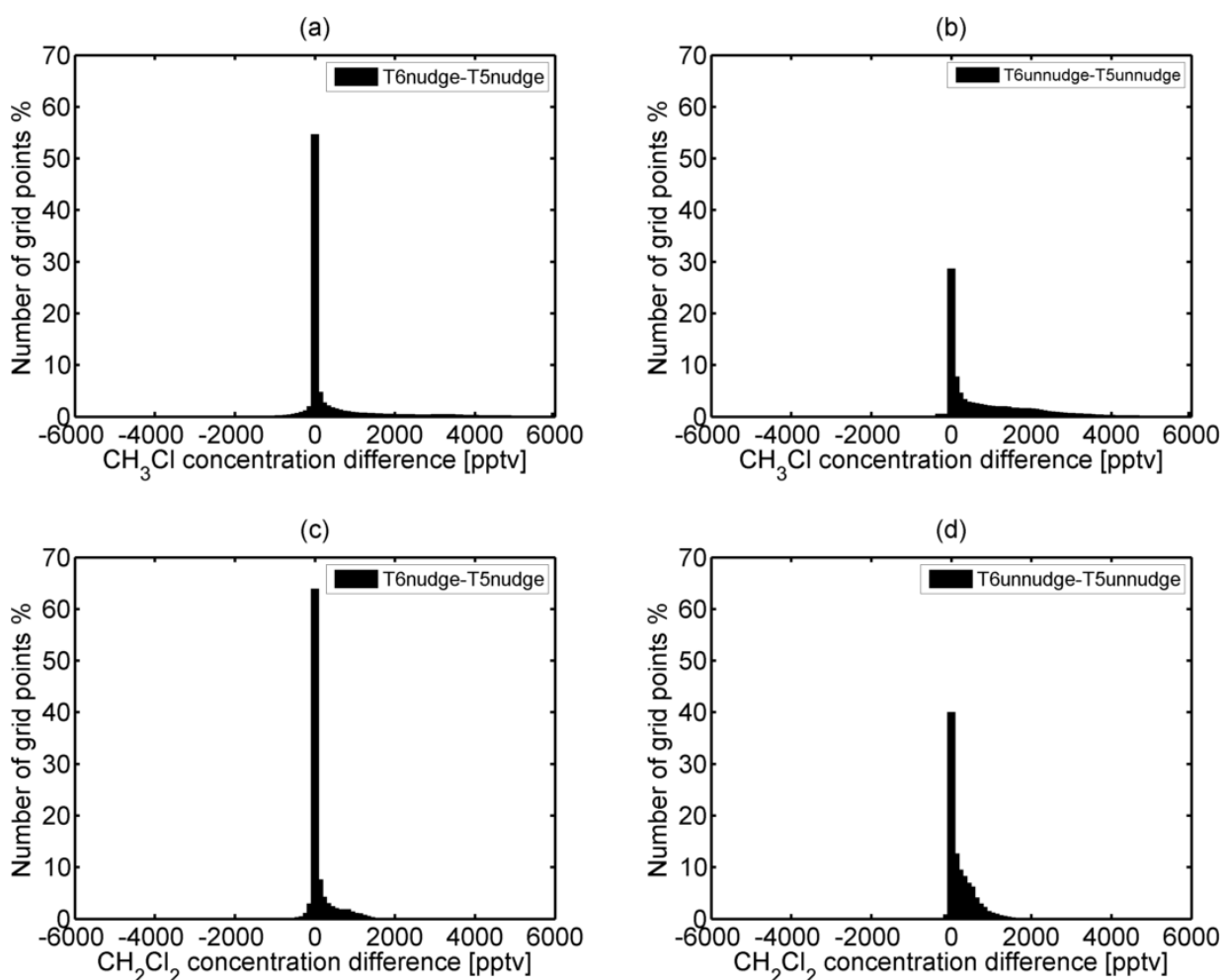


Figure 5.21 Frequency distribution of methyl halide concentration difference for different emission function with constant meteorology for the water source region.

The 50<sup>th</sup> percentile of constant and time dependent concentration differences of  $\text{CH}_3\text{Cl}$  and  $\text{CH}_2\text{Cl}_2$  is 0. METRAS (unnudge) case larger differences are seen. Overall, the 99<sup>th</sup> percentile shows a large difference in the concentrations. These large concentration differences are not seen in the mangrove source region. One shall note, however, that we do not have real observations for the ocean and the whole calculation implicitly assumes that the values at the two measurement sites are only impacted by emissions from water. If this were the case, then the type of emission functions is also playing an important role in the concentrations originating from a water source region.

Table 5.5 Percentiles of concentration difference between different emission functions for CH<sub>3</sub>Cl and CH<sub>2</sub>Cl<sub>2</sub> in pptv for water source region.

Percentiles	1	5	50	95	99
T6n-T5nCH <sub>3</sub> Cl	-1182	-237	0	3810	5659
T6un-T5unCH <sub>3</sub> Cl	-181	0	492	3853	5851
T6n-T5nCH <sub>2</sub> Cl <sub>2</sub>	-282	-56	0	911	1353
T6un-T5unCH <sub>2</sub> Cl <sub>2</sub>	-43	0	117	922	1399

## 5.5 Determination of methyl halide emissions from mangroves

In this section the up-scaled emission of methyl halides are presented using the model results and observations in the mangrove forest region. From eq. (5.3) one can calculate the measured emission using the ratio of concentration differences between upwind and downwind from the model to the observed values (Table 5.1).

The global mangrove area is slightly reduced at present (Giri et al., 2011) compared to the previous study by Duarte et al. (2005). Manley et al. (2007) used laboratory measurements of a single grown mangrove in a green house experiment to up-scale the CH<sub>3</sub>Cl contribution. Using a global area of  $2 \times 10^5$  km<sup>2</sup>, they estimated a CH<sub>3</sub>Cl emission of 12 Gg yr<sup>-1</sup>. In the present study the average CH<sub>3</sub>Cl global mangrove emission using different emission functions and with different meteorology yielded 4-7 Gg yr<sup>-1</sup> and 6-10 Gg yr<sup>-1</sup> for the updated mangrove area and the previously quantified area, respectively (Table 5.6).

Our estimated values are thus lower to slightly lower than the laboratory measurements by Manley et al. (2007). This suggests that we estimate a little less emission than the laboratory study. Using the CH<sub>3</sub>Cl global sink strength of 4106 Gg yr<sup>-1</sup> (Chapter 1), the mangrove production estimated range in the present study is 0.2 percent to 0.3 percent (global mangrove area of  $2 \times 10^5$  km<sup>2</sup>). The mangrove production estimated range is 0.1 percent to 0.2 percent with newly available global mangrove area of  $1.3776 \times 10^5$  km<sup>2</sup>. The observational error in the concentration is about  $\pm 9$  percent (Chapter 2). The maximum observational error in the mangrove emission is about  $\pm 18$  percent using the gradient method.

Table 5.6 Calculated global emission of  $\text{CH}_3\text{Cl}$  and  $\text{CH}_2\text{Cl}_2$  from the mangrove forest.

Tracer	$E_{\text{measured}}$ using global mangrove area of $1.3776 \times 10^5 \text{ km}^2$ ( $\text{Gg yr}^{-1}$ )	$E_{\text{measured}}$ using global mangrove area of $2 \times 10^5 \text{ km}^2$ ( $\text{Gg yr}^{-1}$ )	Observational error (%)
T3 $\text{CH}_3\text{Cl}_n$	6	9	$\pm 18$
T4 $\text{CH}_3\text{Cl}_n$	5	8	$\pm 18$
T3 $\text{CH}_3\text{Cl}_{un}$	7	10	$\pm 18$
T4 $\text{CH}_3\text{Cl}_{un}$	4	6	$\pm 18$
T3 $\text{CH}_2\text{Cl}_2_n$	2	2	$\pm 18$
T4 $\text{CH}_2\text{Cl}_2_n$	1	2	$\pm 18$
T3 $\text{CH}_2\text{Cl}_2_{un}$	2	3	$\pm 18$
T4 $\text{CH}_2\text{Cl}_2_{un}$	1	2	$\pm 18$

The estimated  $\text{CH}_2\text{Cl}_2$  global mangrove contribution is in the range of 1 – 2  $\text{Gg yr}^{-1}$  using the updated mangrove area (2 – 3  $\text{Gg yr}^{-1}$  for the older estimate for mangrove areas). We do not have any other observed values of  $\text{CH}_2\text{Cl}_2$  emission from mangroves from the literature. It has been concluded that mangroves emit  $\text{CH}_2\text{Cl}_2$  as well. Since the value for  $\text{CH}_3\text{Cl}$  is a reasonable range one might assume that this new value for  $\text{CH}_2\text{Cl}_2$  might also be reliable. The estimated annual emission of  $\text{CH}_2\text{Cl}_2$  from the industrial, biomass burning and oceans is  $604 \pm 251 \text{ Gg yr}^{-1}$  (Keene et al., 1999). Similarly Xiao (2008) estimated annual emission of  $\text{CH}_2\text{Cl}_2$  at  $629 \pm 44 \text{ Gg yr}^{-1}$ . Based on the present study the mangroves contribute 0.3 percent of  $\text{CH}_2\text{Cl}_2$  in the global emission budget.

In the case of methyl halide emissions from a water tracer, the model simulated concentrations were not up-scaled due to a lack of observational data. We scaled the water tracers also with the land measurements, which only gave a hint on impact parameters found in measurements. Hence, we could not use the “bottom-up” approach to up-scale the model concentrations.

## 5.6 Conclusions

This chapter presents the transport of concentrations of methyl halides for two different source regions. In order to understand the impact of meteorology on concentrations, we conducted two experiments with the METRAS mesoscale model. One experiment is METRAS driven by the large-scale forcing of the MBAR model (nudge). Another simulation is without any large-scale forcing (unnudge) of meteorology in the METRAS model. Then the model simulated concentrations are normalized using the observed  $\text{CH}_3\text{Cl}$  and  $\text{CH}_2\text{Cl}_2$

concentration in the mangrove forest region. We take advantage of land measurements to normalize the water source region as well, assuming the observed values are affected by sources in the water region. The Lagrangian approach is only recommended if the measurements were collected continuously in the field.

Our analysis suggests that we cannot derive and conclude on emission functions with the help of limited observational data. It has been noted that continuous observational measurements are required to reliably determine different emission functions. Hence it is impossible to derive the constant and time dependent emission functions of methyl halides using two observational data points.

In the case of the mangrove source region, meteorology has shown a larger impact on concentrations than the different emission functions used in the model METRAS. Emission functions do show a little influence in the concentrations. On the other hand, the METRAS model simulated concentrations resulting from emissions over the water show both meteorology and emission functions' role in the concentration.

The combination of measured air concentrations and simulated tracer transport with different types of emission functions allows the calculation of methyl halide emissions and, thus, an estimation of the source strength from mangrove forests.

The mean annual emission of methyl halides using different emission functions with different meteorology are 6-10 Gg yr<sup>-1</sup> for CH<sub>3</sub>Cl and 2-3 Gg yr<sup>-1</sup> for CH<sub>2</sub>Cl<sub>2</sub> using the larger mangrove area as used in previous estimates. In this study we have not quantified for the water source region due to lack of real observations from the ocean region.

## 6. Conclusions and future work

This study presents the observational and modeling application of two halogenated compounds, namely methyl chloride ( $\text{CH}_3\text{Cl}$ ) and methylene chloride ( $\text{CH}_2\text{Cl}_2$ ). The main aim of the thesis is to quantify the natural emission of methyl halides from the ocean and mangrove source region. This study presents first field data on methyl halide emissions in a tropical mangrove forest region. In this section, the thesis' main results found in the preceding chapters are briefly summarized.

$\text{CH}_3\text{Cl}$  and  $\text{CH}_2\text{Cl}_2$  are known to have natural and anthropogenic sources of emissions into the atmosphere including tropical and subtropical plants (Chapter 1).  $\text{CH}_2\text{Cl}_2$  emissions into the atmosphere can be largely attributed to anthropogenic sources with little emission from ocean and biomass burning.  $\text{CH}_3\text{Cl}$  and  $\text{CH}_2\text{Cl}_2$  have long lifetimes of about 1 year and 0.6 year, respectively (WMO, 2010). With these long lifetimes these compounds are transported into the stratosphere and impact the atmospheric chemistry in the atmosphere. These compounds destroy the ozone in the stratosphere and are involved in several chemical reactions. Despite all these hazardous effects, the quantification of emissions of  $\text{CH}_3\text{Cl}$  and  $\text{CH}_2\text{Cl}_2$  is uncertain. Chapter 1 summarizes the different source and sinks of methyl halides in the atmosphere. Chapter 1 also suggests that there is a global imbalance, i.e. known sinks are larger than the known sources.

Chapter 2 presents the background concentrations of  $\text{CH}_3\text{Cl}$  and  $\text{CH}_2\text{Cl}_2$  measured during the Meteor cruise M78/2. The combination of meteorological variables such as wind speed, air temperature and wind direction supplemented by concentration measurements in air and water allows for the quantification of oceanic emission of methyl halides. The methyl halide oceanic source strengths are  $150 \pm 150 \text{ nmol m}^{-2} \text{ d}^{-1}$  for  $\text{CH}_3\text{Cl}$ ,  $81 \pm 81 \text{ nmol m}^{-2} \text{ d}^{-1}$  for  $\text{CH}_2\text{Cl}_2$ . In addition to this we studied the diurnal cycle of the methyl halide fluxes and concentrations in the seawater and in the air. The diurnal variation of fluxes and concentrations reveals that slightly higher concentrations of  $\text{CH}_3\text{Cl}$  and  $\text{CH}_2\text{Cl}_2$  in seawater and higher fluxes of  $\text{CH}_3\text{Cl}$ ,  $\text{CH}_2\text{Cl}_2$  during the night-time may be due to the biological processes in the tropical Atlantic Ocean. However, the reason for high fluxes at night-time remains unknown. Moreover, we also found possible remote source regions of methyl halide using the backward trajectory calculation of the HYSPLIT model. The backward trajectories revealed that the tropical Atlantic Ocean and the African coast (also inland) were the primary and secondary source regions for methyl halides during the Meteor cruise. High concentration found nearer to the

South America coast with an (inland) air mass source region, which suggests that the (maybe mangrove) forest is most likely to be a source of methyl halides.

This study conducted field work in the tropical mangrove forest region as a first step. The results were presented in Chapter 3. The Lagrangian approach is used to measure concentrations at the upwind and downwind locations. The gradient method was applied to determine the mangrove forest region emission of  $\text{CH}_3\text{Cl}$  and  $\text{CH}_2\text{Cl}_2$ . We had limited instruments for the measurements due to technical problems in transporting the instruments into the Brazil. Despite all these problems, we were successful in obtaining measurement data from the mangrove forest. Using the gradient approach the mangrove forest concentrations difference between downwind and upwind are 744 pptv for  $\text{CH}_3\text{Cl}$  and 178 pptv for  $\text{CH}_2\text{Cl}_2$ . In addition to concentration data we also obtained the  $\text{CH}_3\text{Cl}$  stable carbon isotopic ratio. The stable carbon isotopic data supports the biogenic emission of methyl halides from the forest. Hence, we conclude that mangroves emit  $\text{CH}_3\text{Cl}$  and  $\text{CH}_2\text{Cl}_2$  compounds into the atmosphere. Our measured concentrations have a  $\pm 9$  percent observational error.

In order to quantify the mangrove emission of methyl halides, we used a mesoscale atmospheric model METRAS in this study. The adaptation of the METRAS model to the tropical Braganca region was presented in Chapter 4. The adaptation of the METRAS model was carried out by changing model surface parameters. The newly obtained surface parameters are summarized in Chapter 4. The model METRAS was applied to the Braganca model domain in a nudged and unnudged set-up, and the results were compared with available observational data. The nudged model simulated diurnal cycles of temperature and wind speed and wind direction well. The model METRAS is able to simulate air-sea breeze circulation in the tropical Braganca coast region.

In addition to the quantification of natural sources of methyl halides into the atmosphere, the important role of meteorology in concentrations was also studied. This shall also help to decide if a Lagrangian measurement set-up as done in the field campaign can help to determine emissions from plants. Chapter 5 is dedicated to determining (1) the impact of meteorology on concentrations, (2) the impact of the type of emission functions on concentrations, (3) whether time dependent emission functions can be determined from measured data. From detailed analysis in Chapter 5 it can be concluded that meteorology has a very large influence. Compared to the meteorology, emission functions have little impact on the concentrations of methyl halides in the coastal mangrove and water source regions. It

was also found that continuous meteorological and concentrations data are required to determine the time dependent emission function. In this study, given the limited observations, we cannot determine any type of emission functions. However, with the help of the model METRAS and observed field data, the estimated mangrove source strength ranges from (using a global area of  $1.3776 \times 10^5 \text{ km}^2$ ) of  $\text{CH}_3\text{Cl}$  and  $\text{CH}_2\text{Cl}_2$  are  $4\text{-}7 \text{ Gg yr}^{-1}$ ,  $1\text{-}2 \text{ Gg yr}^{-1}$ , respectively.

It will be more helpful to have continuous measurements for a more accurate quantification of source strength. Nonetheless, we successfully derived a range for methyl halide emissions from the mangroves. The calculated mangrove emissions are within the range of other estimates, but our concentration data are only based on a small period of time. The annual variation of mangrove emission over the tropical equatorial region may be small due to limited seasonal changes in the tropical equatorial region. These derived emissions can be used in global climate models to understand the impact of mangroves on the global chemistry. Furthermore, the change in mangrove area needs to be considered for global emissions. The change in mangrove area is to be expected due to anthropogenic activities, sea level rise and global warming; all this will directly have an impact on emission of methyl halides into the atmosphere.

The determined emissions can be used for the implementation of any global chemical climate model. The global model simulated chemistry will be interesting to see the type of source region emission changes in the concentrations pattern. In this study concentrations are measured during the dry season in the tropical equatorial region. It is also interesting to see the emissions in different seasons and in different forest regions such as India, Indonesia and Australia. From these results one can continue study of the seasonal biogenic emissions from the mangrove plant community. There is an opportunity for future work on important and not yet considered sources of methyl halides.

## **Acknowledgements**

I would like to pay my profound gratitude to my supervisor Prof. Dr. K. Heinke Schlünzen for her continuous guidance and for the invaluable discussions during the course. I thank a lot for understanding me and kindly helping me through out my dissertation period. I would also thank to my co-supervisor Dr. Richard Seifert for his excellent guidance.

My Ph.D advisory panel chair Prof. Dr. Felix Ament is greatly acknowledged for his continuous monitoring and suggestions throughout the course.

I am thankful to David Grawe for his continuous support and guidance along with my supervisors during the course. I would also thank to Dr. habil. Frank Laturus for his support during the field trip in the mangroves forest, Brazil and chemistry analysis. I also would like to thank Dr. Enno Bahlmann for reviewing chemistry data and discussing the chemistry results. Here, I would like to thank all the people, who helped me in the field work in Hamburg and Brazil. I also thank Prof. Dr. Nils Edvin Asp for sharing his lab and help during the field work in Braganca, Brazil.

Sincere acknowledgements go to all members of the MeMi working group for the great team work, and discussions in the group meetings. I personally thank Malte Uphoff for sharing the office in a friendly atmosphere. I also thank to Volker Reinhardt for his technical help.

I also would like to thank the School of Integrated Climate System Sciences former and current committee members for their continuous support and financial support during my study. The present work is supported through the Cluster of Excellence “CliSAP” (EXC177), University of Hamburg, funded through the German Science Foundation (DFG).

Here, I would like to acknowledge data sources used in my thesis. Firstly, I would like to thank INMET for providing MBAR model forecast data and automatic weather stations data for the study region. I also acknowledge NASA and NOAA data downloaded (<http://www.ncdc.noaa.gov/cdo-web/>).

I also acknowledge the TRMM data obtained from NASA, USA (<http://mirador.gsfc.nasa.gov/collections/T213RMM3B42daily-06.htm>). I acknowledge temperature data obtained from IBGE, Brazil site (<http://www.recor.org.br/index.php/banco-dados/dados-meteorologicos?id=269>).

I also thank my friends Suraj, Seethala, Suvarchal Kumar, Pankaj Kumar, Kameswar Rao, Ketan Kulkarni, Koteswara Rao, Neeraj Agarwal and Anurag for giving me friendly environment to work.

My special thankfulness is to my wife Nagalaksmi Kolusu for taking care of me and her continuous support to reach my new achievements. Finally, I would like to thank my parents, brother and sister who worked very hard to help me grow and brought me up to this stage. Without their support and hard work, I would not be in this stage. Hereby, I dedicate my thesis to my parents.

## Acronyms

AGAGE	Advanced Global Atmospheric Gases Experiment
AGL	Above the Ground Level
ARL	Air Resources Laboratory
BRT	Brazil local time
CFCs	Chlorofluorocarbons
EEZ	Exclusive Economic Zone
FAO	Food and Agricultural Organization
GC	Gas Chromatography
GDAS	Global Data Assimilation System
GEOS-Chem	Goddard Earth Observing System chemistry model
GH	Ground heat Flux
GLS	Global Land Survey
GUI	Graphical User Interface
HYSPLIT	Hybrid Single Particle Lagrangian Integrated Trajectory Model
IBGE	Brazilian Institute for Geography and Statistics
IfBM	Institute for Biogeochemistry and Marine Chemistry
INMET	National Institute of Meteorology
IPCC	Intergovernmental Panel on Climate Change
ITCZ	Inter Tropical Convergence Zone
LAI	Leaf Area Index
LH	Latent heat Flux
LW	Long wave Radiation
M78/2	Meteor cruise
MBAR	High resolution mesoscale model
METRAS	MEsocale TRANsport and fluid (Stream) model
MODIS	Moderate Resolution Imaging Spectroradiometer
MSYS	Multiscale Model System
NASA	National Aeronautics and Space Administration
NCEP	National Centers for Environmental Prediction
NH	Northern Hemisphere
NOAA	National Oceanic and Atmospheric Administration
NOAA/ESRL	NOAA Earth System Research Laboratory
ODS	Ozone Depleting Substance
PC	Personal computer

SH	Sensible heat Flux
SH	Southern Hemisphere
SNWR	Sevilleta National Wildlife Refuge
SRTM	Shuttle Radar Topography Mission
SST	Sea Surface Temperature
SW	Shortwave Radiation
TRMM	Tropical Rainfall Measuring Mission
UFPA	Federal University of Pará
UNEP	United Nations Environment Programme
UTC	Coordinated Universal Time
WMO	World Meteorological Organization

## References

- Abreu Sá, L. D., Viswanadham, Y., and Manzi, A.O. (1988):** Energy flux partitioning over the Amazon forest. *Theoretical and applied climatology*, 39(1), 1-16.
- Bahlmann, E., Weinberg, I., Seifert, R., Tubbesing, C., and Michaelis, W. (2011):** A high volume sampling system for isotope determination of volatile halocarbons and hydrocarbons. *Atmospheric Measurement Techniques*, 4(10), 2073-2086.
- Baker, J.M., Reeves, C.E., Nightingale, P.D., Penkett, S.A., Gibb, S.W., Hatton, A.D. (1999):** Biological production of methyl bromide in the coastal waters of the North Sea and open ocean of the Northeast Atlantic. *Mar. Chem.*, 64, 267-285.
- Blei, E., Hardacre, C.J., Mills, G.P., Heal, K.V., and Heal, M.R. (2010):** Identification and quantification of methyl halide sources in a lowland tropical rainforest. *Atmos. Environ.*, 44(8), 1005-1010.
- Burba, G. G., Verma, S. B., and Kim, J. (1999):** Surface energy fluxes of Phragmites australis in a prairie wetland. *Agricultural and Forest Meteorology*, 94:31–51.
- Butler, J. H. (2000):** Atmospheric chemistry – Better budgets for methyl halides? *Nature*, 403, 260–261.
- Carpenter, L. J. (2003):** Iodine in the marine boundary layer. *Chemical reviews*, 103(12), 4953-4962.
- Clerbaux, C., and Cunnold D.M. (Lead Authors), Anderson, J., Engel, A., Fraser, P.J., Mahieu, E., Manning, A., Miller, J., Montzka, S.A., Nassar, R., Prinn, R., Reimann, S., Rinsland, C.P., Simmonds, P., Verdonik, D., Weiss, R., Wuebbles, D., and Yokouchi, Y., Long-lived compounds, Chapter 1 in Scientific Assessment of Ozone Depletion: (2007):** Global Ozone Research and Monitoring Project—Report No. 50, 572 pp., *World Meteorological Organization, Geneva, Switzerland*.
- Cox, M. L., Sturrock, G. A., Fraser, P. J., Siems, S., Krummel, P., and O’Doherty, S. (2003):** Regional sources of methyl chloride, chloroform and dichloromethane identified from AGAGE observations at Cape Grim, Tasmania, 1998–2000. *J. Atmos. Chem.*, 45, 79–99.
- Cox, R. A., Derwent, R. G., Eggleton, A. E. J., and Lovelock, J. E. (1976):** Photochemical oxidation of halocarbons in the troposphere. *Atmospheric Environment (1967)*, 10(4), 305-308.
- Crutzen, P. (1974):** A review of upper atmospheric photochemistry. *Canadian Journal of Chemistry*, 52(8), 1569-1581.
- Dennison, M.S., Berry, J.F. (1989):** Wetlands. Guide to science, law, and technology. *Noyes publications*, Park Ridge, NJ, USA, 439 pp.
- Dierer, S., Schlünzen, K. H., Birnbaum, G., Brümmer, B., and Müller, G. (2005):** Atmosphere-sea ice interactions during a cyclone passage investigated by using model simulations and measurements. *Monthly Weather Review*, 133, 3678 – 3692.

- Dimmer, C. H., Simmonds, P. G., Nickless, G. N., and Bassford, M. R. (2001):** Biogenic fluxes of halomethanes from Irish peatland ecosystems. *Atmos. Environ.*, 31, 321–330.
- Draxler, R. R. (2003):** Evaluation of an ensemble dispersion calculation. *Journal of Applied Meteorology*, 42(2), 308-317.
- Draxler, R.R., and Hess, G.D. (1997):** Description of the HYSPLIT\_4 modeling system. NOAA Tech. Memo. ERL ARL-224, *NOAA Air Resources Laboratory*, Silver Spring, MD, 24 pp.
- Duarte, C. M., Middelburg, J. J., and Caraco, N. (2005):** Major role of marine vegetation on the oceanic carbon cycle. *Biogeosciences*, 2(1), 1-8.
- Fahey, D.W., and Hegglin M.I. (2011) (Coordinating Lead Authors):** Twenty Questions and Answers About the Ozone Layer: 2010 Update, Scientific Assessment of Ozone Depletion: 2010, 72 pp., World Meteorological Organization, Geneva, Switzerland, 2011. [Reprinted from *Scientific Assessment of Ozone Depletion: 2010, Global Ozone Research and Monitoring Project-Report No. 52, 516 pp., World Meteorological Organization, Geneva, Switzerland.*].
- FAO (Food and Agriculture Organization of the United Nations) (2005):** The world's mangroves 1980-2005. FAO Forestry Paper 153. FAO, Rome.
- Gebhardt, S., Colomb, A., Hofmann, R., Williams, J., and Lelieveld, J. (2008):** Halogenated organic species over the tropical South American rainforest. *Atmos. Chem. Phys*, 8(12), 3185-3197.
- Giambelluca, T. W., Scholz, F. G., Bucci, S. J., Meinzer, F. C., Goldstein, G., Hoffmann, W. A., Franco, A. C., and Buchert, M. P. (2009):** Evapotranspiration and energy balance of Brazilian savannas with contrasting tree density. *Agricultural and forest meteorology*, 149(8), 1365-1376.
- Giri, C., Ochieng, E., Tieszen, L L., Zhu, Z., Singh, A., Loveland, T., Masek, J., and Duke, N. (2011):** Status and distribution of mangrove forests of the world using earth observation satellite data. *Global Ecology and Biogeography*, 11:154–159.
- Groszko, W., and Moore, R. (1998):** Ocean-atmosphere exchange of methyl bromide: NW Atlantic and Pacific Ocean studies. *J. Geophys. Res.*, 103(D13) Issn: 0148-0227.
- Harper, D.B., and Hamilton, J.T.G. (2003):** The global cycles of the naturally occurring monohalomethanes. In: Gribble, G.W. (Ed.), *The Handbook of Environmental Chemistry: The Natural Production of Organohalogen Compounds*. Springer Verlag, Heidelberg, pp. 17–41.
- Hemakumara, H. M., Chandrapala, L., and Moene A. F. (2003):** Evapotranspiration fluxes over mixed vegetation areas measured from large aperture scintillometer. *Agricultural water management*, 58(2), 109-122.
- Hu, L., S.A., Yvon-Lewis, Y., Liu, J.E., Salisbury, and O'Hern, J.E. (2010):** Coastal emissions of methyl bromide and methyl chloride along the eastern Gulf of Mexico and the east coast of the United States. *Global Biogeochem. Cycles*, 24, GB1007.

- Hughes, C., Chuck, A. L., Rossetti, H., Mann, P. J., Turner, S. M., Clarke, A., and Liss, P. S. (2009):** Seasonal cycle of seawater bromoform and dibromomethane concentrations in a coastal bay on the western Antarctic Peninsula. *Global Biogeochemical Cycles*, 23(2).
- IPCC (2007):** Fourth Assessment Report: *Climate Change 2007 (AR4)*.
- Jarvis, A., Reuter, H.I., Nelson, A., Guevara, E. (2008):** Hole-filled SRTM for the globe Version 4, available from the CGIAR-CSI SRTM 90m *Database*: <http://srtm.csi.cgiar.org>.
- Jarvis, P. G., James, G. B., and Landsberg, J. J. (1976):** ‘Coniferous Forests’, in J. L. Monteith (ed.), *Vegetation and the Atmosphere*, Academic Press, New York. pp. 171-240.
- Keene, W., Khalil, M. A. K., Erickson, D., McCulloch, A., Graedel, T. E., Lobert, J. M., and Li, Y. F. (1999):** Composite global emissions of reactive chlorine from anthropogenic and natural sources: Reactive Chlorine Emissions Inventory. *Journal of Geophysical Research: Atmospheres (1984–2012)*, 104(D7), 8429-8440.
- Keppler, F., Harper, D.B., Röckmann, T., Moore, R.M., and Hamilton J.T.G. (2005):** New insight into the atmospheric chloromethane budget gained using stable carbon isotope ratios. *Atmos. Chem. Phys.*, 5 (9), 2403-2411.
- Khalil, M. A. K. and Rasmussen, R. A (1999):** Atmospheric methyl chloride. *Atmos. Environ.*, 33 (8), 1305–1321.
- Khalil, M.A.K., Moore, R.M., Harper, D.B., Lobert, J.M., Erickson, D.J., Koropalov, V., Sturges, W.T., and Keene, W.C. (1999):** Natural emissions of chlorine-containing gases: Reactive Chlorine Emissions Inventory. *J. Geophys. Res.*, 104, 8,333–8,346.
- King, D. B., Butler, J. H., Montzka, S. A., Yvon-Lewis, S. A., and Elkins, J. W. (2000):** Implications of methyl bromide supersaturations in the temperate North Atlantic Ocean. *J. Geophys. Res.*, 105, 19,763 – 19,769.
- King, D. B., Butler, J. H., Yvon-Lewis, S. A., and Cotton, S. A. (2002):** Predicting oceanic methyl bromide saturation from SST. *Geophys. Res. Lett.*, 29(24), 2199.
- Kjerfve, B., Lacerda, L.D., and S. Diop. (1997):** Mangrove Ecosystem Studies in Latin America and Africa. *UNESCO*, Paris, pp.1-7.
- Koppmann, R., Johnen, F.J., Plassdulmer, C., and Rudolph, J. (1993):** Distribution of methylchloride, dichloromethane, trichloroethene and tetrachloroethene over the North and South-Atlantic. *J. Geophys. Res.*, 98, 20,517–20,526.
- Krause, G., Schories D., Glaser, M., and Diele, K. (2001):** Spatial patterns of mangrove ecosystems: The Bragantian mangroves of Notrh Brazil (Braganca,Para). *Ecotropica*, 7:93-107.
- Kurc, S. A., and Eric E. S. (2004):** Dynamics of evapotranspiration in semiarid grassland and shrubland ecosystems during the summer monsoon season, central New Mexico. *Water Resources Research*, 40 (9), W09305.

- Lafleur, P. M. (1990):** Evapotranspiration from sedge dominated wetland surfaces. *Aquatic Botany*, 37(4), 341-353.
- Large, W. G., and Pond, S. (1981):** Open ocean momentum flux measurements in moderate to strong winds. *J. Phys. Ocean.*, 11, 324-481.
- Lee-Taylor, J. M., Brasseur, G. P., and Yokouchi, Y. (2001):** A preliminary three-dimensional global model study of atmospheric methyl chloride distributions. *J. Geophys. Res.-Atmos.*, 106, 34 221–34, 233.
- Lee-Taylor, J. M., Doney, S. C., Brasseur, G. P., and Muller, J. F. (1998):** A global three-dimensional atmosphere-ocean model of methyl bromide distributions. *J. Geophys. Res.-Atmos.*, 103, 16 039–16 057.
- Li, H.-J., Yokouchi, Y., and Akimoto, H. (1999):** Measurements of methyl halides in the marine atmosphere. *Atmos. Environ.*, 33, 1881–1887.
- Liss P.S., and Merlivat L. (1986):** Air-sea gas exchange rates: introduction and synthesis. In the Role of Air-Sea Exchange in Geochemical Cycling, ed. P Buat-Menard, pp. 113–29. Boston, MA: Reidel.
- Liss, P. S., and Slater, P. G. (1974):** Flux of Gases across the Air-Sea Interface. *Nature*, 247, 181 – 184.
- Lobert, J. M., Keene, W. C., Logan, J. A., and Yevich, R. (1999):** Global chlorine emissions from biomass burning: Reactive chlorine emissions inventory. *J. Geophys. Res.*, 104, 8373– 8389.
- Lobert, J.M., Geller, L S., Yvon, S. A., Clarke, A. D., Butler, J. H., Montzka, S.A., Myers, R. C., and Elkins, J. W. (1996):** BLAST 94: Bromine Latitudinal Air/Sea Transect 1994. Report on Oceanic Measurements of Methyl Bromide and Other Compounds. *NOAA Technical Memorandum ERL CMDL-10*.
- Lobert, J.M., Yvon, S.A., Butler, J.H., Montzka, S. A., and Myers, R.C. (1997):** Under saturations of Methyl Bromide in the Southern Ocean. *Geophys. Res. Lett.*, 24, 171-172.
- Lu, X.-L., Yang, G.-P., Song, G.-S., and Zhang, L. (2010):** Distributions and fluxes of methyl chloride and methyl bromide in the East China Sea and the Southern Yellow Sea in autumn. *Mar. Chem.*, 118 (1-2), 75- 84.
- Lüpkes, C., and Schlünzen, K. H. (1996):** Modelling the Arctic convective boundary-layer with different turbulence parameterizations. *Boundary-Layer Meteorology*, 79, 107 – 130.
- MacDonald, S., and Moore, R.M. (2007):** Seasonal and spatial variations in methyl chloride in NW Atlantic waters. *J. Geophys. Res.*, 112, C05028.
- Majewski, D., Frank, H., and Liermann, D. (2010):** GME User’s Guide Version 2.23, corresponding to model version gmtri 2.23 and higher. *DWD, Offenbach*, 72.
- Manley, S.L., Wang, N.-Y., Walser, M.L., and Cicerone, R.J. (2006):** Coastal salt marshes as global methyl halide sources from determinations of intrinsic production by marsh plants. *Global Biogeochem. Cycles*, 20, GB3015.

- Manley, S.L., Wang, N.-Y., Walser, M.L., and Cicerone, R.J. (2007):** Methyl halide emissions from greenhouse grown mangroves. *Geophys. Res. Lett.*, 34, L01806.
- Mauder, M., Jegede, O. O., Okogbue, E. C., Wimmer, F., and Foken, T. (2007):** Surface energy balance measurements at a tropical site in West Africa during the transition from dry to wet season. *Theoretical and applied climatology*, 89(3), 171-183.
- McCaughey, J. H. (1985):** A radiation and energy balance study of mature forest and clear-cut sites. *Boundary-Layer Meteorology*, 32(1), 1-24.
- McCulloch, A., Aucott, M. L., Graedel, T. E., Kleiman, G., Midgley, P. M., and Li, Y.-F. (1999):** Industrial emissions of trichloroethene, tetrachloroethene, and dichloromethane: Reactive Chlorine Emissions Inventory. *J. Geophys. Res.*, 104, 8417–8427.
- McGillis, W. R., Edson, J. B., Ware, J. D., Dacey, J. W. H., Hare, J. E., Fairall, C. W., and Wanninkhof, R. (2001b):** Carbon dioxide flux techniques performed during GasEx 98. *Mar. Chem.*, 75, 267-280.
- McGillis, W.R., Edson, J.B., Hare, J.E. and Fairall, C.W. (2001a):** Direct covariance air-sea CO<sub>2</sub> fluxes. *J. Geophys. Res.*, 106(C8): Issn: 0148-0227.
- Menard, H. W., and Smith, S. M. (1966):** Hypsometry of ocean basin provinces, *J. Geophys. Res.*, 71(18), 4305–4325.
- Miranda, A.C., Miranda, H.S., Lloyd, J., Grace, J., Francey, R.J., McIntyre, J.A., Meir, P., Riggan, P., Lockwood, R., and Brass, J. (1997):** Fluxes of carbon, water and energy over Brazilian cerrado: an analysis using eddy covariance and stable isotopes. *Plant, Cell and Environment*, 20, 315– 328.
- Montzka, S. A. and Reimann, S. (2011):** Ozone-depleting substances (ODSs) and related chemicals, in: Scientific Assessment of Ozone Depletion: 2010, Global Ozone Research and Monitoring Project. Report No. 52, Chapt. 1, edited by: *World Meteorological Organization, Geneva, Switzerland, 2011.*
- Montzka, S. A., Butler, J. H., Hall, B. D., Mondeel, D. J., and Elkins, J. W. (2003):** A decline in tropospheric organic bromine. *Geophys. Res. Lett.*, 30(15), 1826.
- Moore, R. M. (2000):** The solubility of a suite of low molecular weight organochlorine compounds in seawater and implications for estimating the marine source of methyl chloride to the atmosphere. *Chemosphere Global Change Sci.*, 2, 95 – 99.
- Moore, R. M. (2004):** Dichloromethane in North Atlantic waters. *J. Geophys. Res.*, 109, C09004.
- Moore, R.M., Groszko, W., and Niven, S.J., (1996):** Ocean-atmosphere exchange of methyl chloride: results from N.W. Atlantic and Pacific studies. *J. Geophys. Res.*, 101, 28529–28538.
- Niemeier, U., and Schlünzen, K. H. (1993):** Modelling steep terrain influences on flow patterns at the Isle of Helgoland. *Beitraege zur Physik der Atmosphaere*, 66, 45 – 62.

- Nightingale, P. D., Malin, G., Law, C. S., Watson, A. J., Liss, P. S., Liddicoat, M. I., Boutin, J., and Upstill-Goddard, R. C. (2000):** In situ evaluation of air-sea gas exchange parameterizations using novel conservative and volatile tracers. *Global Biogeochem. Cycles*, 14, 373 – 387.
- Ooki, A., and Yokouchi, Y. (2011):** Dichloromethane in the Indian Ocean: Evidence for in-situ production in seawater. *Marine Chemistry*, 124 (1-4), pp.119-124.
- Ooki, A., Kameyama, S., Takeda, S., Itoh, S., Suga, T., and Yokouchi, Y. (2010):** Methyl halides in surface seawater and marine boundary layer of the northwest Pacific. *Journal of Geophysical Research: Oceans* (1978-2012), 115(C10).
- Prinn, R.G., Weiss, R.F., Fraser, P.J., Simmonds, P.G., Cunnold, D.M., Alyea, F.N., O'Doherty, S., Salameh, P., Miller, B.R., Huang, J., Wang, R., Hartley, D.E., Harth, C., Steele, L.P., Sturrock, G., Midgley, P.M. and McCulloch, A. (2000):** A history of chemically and radiatively important gases in air deduced from ALE/GAGE/AGAGE. *J. Geophys. Res.*, 105(D14).
- Rayner, N. A., Parker, D. E., Horton, E. B., Folland, C. K., Alexander, L. V., Rowell, D. P., Kent, E. C., and Kaplan, A. (2003):** Global analyses of SST, sea ice and night marine air temperature since the late nineteenth century. *J. Geophys. Res.*, 108, 4407.
- Reeves, C. E. (2003):** Atmospheric budget implications of the temporal and spatial trends in methyl bromide concentration. *J. Geophys. Res.-Atmos.*, 108, 4343.
- Rhew, R. C. (2011):** Sources and sinks of methyl bromide and methyl chloride in the tall grass prairie: Applying a stable isotope tracer technique over highly variable gross fluxes. *J. Geophys. Res.*, 116, G03026.
- Rhew, R. C., Miller, B. R., and Weiss, R. F. (2000):** Natural methyl bromide and methyl chloride emissions from coastal salt marshes. *Nature*, 403, 292–295,
- Rhew, R. C., Teh, Y. A., and Abel, T. (2007):** Methyl halide and methane fluxes in the northern Alaskan coastal tundra. *J. Geophys. Res.*, 112(G2), G02009.
- Rhew, R.C., Miller, B.R., and Weiss, R.F., (2000):** Natural methyl bromide and methyl chloride emissions from coastal salt marshes. *Nature*, 403, 292–295.
- Saito, T., and Yokouchi, Y. (2006):** Diurnal variation in methyl halide emission rates from tropical ferns. *Atmospheric environment*, 40(16), 2806-2811.
- Samson, F. B., and Knopf, F. L. (1994):** Prairie conservation in North America. *BioScience*, 44:418-421.
- Schlünzen K.H., Bigalke K., Lüpkes C., Niemeier U., and von Salzen K. (1996):** Concept and realization of the mesoscale transport and fluid model 'METRAS'. Meteorologisches Institut, Universität Hamburg, *METRAS Techn. Rep.*, 5, 156.
- Schlünzen, K. H., and Katzfey, J. J. (2003):** Relevance of subgrid-scale land-use effects for mesoscale models. *Tellus*, 55A, 232 – 246.

- Schlünzen, K.H., Flagg, D.D., Fock, B.H., Gierisch, A., Lüpkes, C., Reinhardt, V., Spensberger, C. (2012):** Scientific Documentation of the Multiscale Model System M-SYS (METRAS, MITRAS, MECTM, MICTM, MESIM) - Version: 2012-02-09. *MEMI Technical Report 4*. Meteorologisches Institut KlimaCampus Universität Hamburg. 138 p.
- Scholes, R.J., and Archer, S.R. (1997):** Tree-grass interactions in savannas. *Annual Review of Ecology and Systematics*, 28, 517–544.
- Schueler, S., and Schlünzen, K. H. (2006):** Modeling of oak pollen dispersal on the landscape level with a mesoscale atmospheric model. *Environmental Modeling and Assessment*, 11(3), 179-194.
- Shuttleworth, W. J. (1993):** Evaporation, in Handbook of Hydrology, edited by D. Maidement, pp. 4.1–4.53, *McGraw-Hill*, New York.
- Simmonds, P. G., Manning, A. J., Cunnold, D. M., McCulloch, A., O'Doherty, S., Derwent, R. G., and Prinn, R. G. (2006):** Global trends, seasonal cycles, and European emissions of dichloromethane, trichloroethene, and tetrachloroethene from the AGAGE observations at Mace Head, Ireland, and Cape Grim, Tasmania. *J. Geophys. Res.*, 111 (D18), D18304.
- Singh, H. B., Salas, L. J., and Stiles, R. E. (1983):** Methyl halides in and over the eastern Pacific (40 N–32 S). *J. Geophys. Res.*, 88, 3684 – 3690.
- Smid, P. (1975):** Evaporation from a reedswamp. *The Journal of Ecology*, 299-309.
- Swanson, A. L., Blake, N. J., Blake, D. R., Sherwood Rowland, F., Dibb, J. E., Lefer, B. L., and Atlas, E. (2007):** Are methyl halides produced on all ice surfaces? Observations from snow-laden field sites. *Atmos. Environ.*, 41(24), 5162-5177.
- Tait, V. K., and Moore, R. M. (1995):** Methyl chloride (CH<sub>3</sub>Cl) production in phytoplankton cultures. *Limnol. Oceanogr.*, 40: 189-195.
- Teh, Y. A., Mazéas, O., Atwood, A. R., Abel, T., and Rhew, R. C., (2009):** Hydrologic regulation of gross methyl chloride and methyl bromide uptake from Alaskan Arctic tundra. *Global Change Biol.*, 15: 330- 345.
- Tiedtke, M., and Geleyn, J.F. (1975):** The DWD general circulation model-description of its main features. *Beitr. Phys. Atmosph.*, 48, 255-277.
- Tokarczyk, R. and Moore, R. (2006):** A seasonal study of methyl bromide concentrations in the North Atlantic (35°-60°N). *J. Geophys. Res.*, 111(D8), Issn: 0148-0227.
- Torres, O., Chen, Z., Jethva, H., Ahn, C., Freitas, S. R., and Bhartia, P. K (2010):** OMI and MODIS observations of the anomalous 2008– 2009 Southern Hemisphere biomass burning seasons. *Atmos. Chem. Phys.*, 10, 3505–3513.
- UNEP (1995):** Global Biodiversity Assessment. Cambridge, Cambridge University Press.
- Wanninkhof, R. (1992):** Relationship between wind-speed and gas-exchange over the ocean. *J. Geophys. Res.*, 97, 7,373–7,382.
- Warneck, P (1988):** Chemistry of the Natural Atmosphere, Academic Press, New York, 1988. Historical survey, photochemistry of O<sub>2</sub> and O<sub>3</sub>.

- Warwick, N. J., Pyle, J. A., and Shallcross, D. E (2006):** Global modelling of the atmospheric methyl bromide budget. *J. Atmos. Chem.*, 54, 133–159.
- Warwick, N. J., Pyle, J. A., Carver, G. D., Yang, X., Savage, N. H., Connor, F. M. O., and Cox, R. A. (2006):** Global modeling of biogenic bromocarbons. *J. Geophys. Res.*, 111(D24), D24305.
- WMO (World Meteorological Organization), Scientific Assessment of Ozone Depletion: (2010):** Global Ozone Research and Monitoring Project-Report No. 52, 516 pp., Geneva, Switzerland, 2011.
- WMO (World Meteorological Organization), Scientific Assessment of Ozone Depletion: (2007):** Global Ozone Research and Monitoring Project-Report No. 50, 572 pp., Geneva, Switzerland, 2007.
- Xiao, X. (2008):** Optimal estimation of the surface fluxes of chloromethanes using a 3-D global atmospheric chemical transport model. *PhD thesis*, MIT, Cambridge.
- Xiao, X., Prinn, R. G., Fraser, P. J., Simmonds, P. G., Weiss, R. F., O'Doherty, S., Miller, B. R., Salameh, P. K., Harth, C. M., Krummel, P. B., Porter, L. W., Mühle, J., Grealley, B. R., Cunnold, D., Wang, R., Montzka, S. A., Elkins, J. W., Dutton, G. S., Thompson, T. M., Butler, J. H., Hall, B. D., Reimann, S., Vollmer, M. K., Stordal, F., Lunder, C., Maione, M., Arduini, J., and Yokouchi, Y (2010a):** Optimal estimation of the surface fluxes of methyl chloride using a 3-D global chemical transport model. *Atmos. Chem. Phys.*, 10, 5515-5533.
- Yokouchi, Y., Ikeda, M., Inuzuka, Y., and Yukawa, T. (2002):** Strong emission of methyl chloride from tropical plants. *Nature*, 416(6877), 163-165.
- Yokouchi, Y., Nojiri, Y., Barrie, L. A., Toom-Sauntry, D., Machida, T., Inuzuka, Y., Akimoto, H., Li, H.-J., Fuginuma, Y., and Aoki, S. (2000):** A strong source of methyl chloride to the atmosphere from tropical coastal land. *Nature*, 403, 295-298.
- Yokouchi, Y., Nojiri, Y., Barrie, L. A., Toom-Sauntry, D., and Fujinuma, Y. (2001):** Atmospheric methyl iodide: High correlation with surface seawater temperature and its implications on the sea-to-air flux. *J. Geophys. Res.*, 106(D12), 12,661– 12,668.
- Yokouchi, Y., Toom-Sauntry, D., Yazawa, K., Inagaki, T. and Tamaru, T. (2002b)** Recent decline of methyl bromide in the troposphere in accordance with the Montreal Protocol phase-out schedule. *Atmos. Environ.*, 36, 4985–4989.
- Yoshida, Y., Wang, Y., and Zeng, T. (2004):** A three-dimensional global model study of atmospheric methyl chloride budget and distributions. *J. Geophys. Res.*, 109, D24309.
- Yvon-Lewis, S. A., King, D. B., Tokarczyk, R., Goodwin, K. D., Saltzman, E. S., and Butler, J. H. (2004):** Methyl bromide and methyl chloride in the Southern Ocean. *J. Geophys. Res.*, 109, C02008.
- Yvon-Lewis, S. A., Saltzman, E. S., and Montzka, S. A. (2009):** Recent trends in atmospheric methyl bromide: analysis of post-Montreal Protocol variability. *Atmos. Chem. Phys.*, 9, 5963–5974.